WAD R-572Q1

First Quarterly Report

For

THE DEVELOPMENT OF A SEGMENTED, AXIALLY CONDUCTING, PYROLYTIC GRAPHITE REACTION CONTROL ENGINE

Contract No. NAS 9-5424

December 15, 1965 - March 14, 1966

Submitted To

NASA - Manned Spacecraft Center
Houston, Texas 77058

Prepared By

Curtiss-Wright Corporation
Wright Aeronautical Division
Wood-Ridge, New Jersey 07075

WAD R-572Q1

Copy No.___

First Quarterly Report

For

THE DEVELOPMENT OF A SEGMENTED, AXIALLY CONDUCTING, PYROLYTIC GRAPHITE REACTION CONTROL ENGINE

Contract No. NAS 9-5424

December 15, 1965 - March 14, 1966

Submitted To

NASA - Manned Spacecraft Center
Houston, Texas 77058

Prepared By

Curtiss-Wright Corporation
Wright Aeronautical Division
Wood-Ridge, New Jersey 07075

WRIGHT AERONAUTICAL DIVISION • CURTISS-WRIGHT CORPORATION • WOOD-RIDGE, N. J., U. S. A.

ABSTRACT

This is the first quarterly report covering the work performed under NASA contract NAS-9-5424 during the period from December 15, 1965 through March 14, 1966. The objective of this program is to demonstrate a flight type configuration of an Axially Conducting Engine (ACE) in which pyrolytic graphite (PG) wedges, restrained by an elastic structure, form the combustion chamber and nozzle of the engine.

During this quarter, the design of a rig engine, including thermal and structural analyses, was completed, and fabrication of parts for the first engine build was initiated.

Table of Contents

LIST OF ILLUSTRATIONS

LIST OF TABLES

I. INTRODUCTION

A. Program Scope and Objective

A thirteen month program is being conducted for the preliminary development of a segmented, axially conducting, 100 pound thrust pyrolytic graphite (PG) rocket engine. The program schedule is shown in Figure 1. The development plan includes thermal and structural analyses, design verification tests of two rig engines, two flight configuration engine tests for final design demonstration, and an examination of engine compatibility with advanced propellants. The delivery of a flight configuration engine to NASA Manned Spacecraft Center will occur at the end of the fourteenth month.

The objective of this program is to demonstrate the feasibility of the Axially Conducting Engine (ACE) concept for reaction control engine applications. Ultimately, the engine will be capable of buried and/or exposed installation on a spacecraft and will be capable of use with the fluorine family of advanced propellants.

The design conditions for the flight type ACE engine are as follows:

Vacuum Thrust:	100 lbs with 40:1 nozzle area ratio
Chamber Pressure:	100 psia
Propellant Inlet Pressure:	195 $\pm$ 5 psia
Fuel:	Monomethylhydrazine
Oxidizer:	Nitrogen Tetroxide
Oxidizer/Fuel Ratio:	1.6:1
Specific Impulse:	290 seconds when operating with 40:1 area ratio nozzle for pulses of 1.0 second duration or longer.

Minimum Impulse Bit:	0.5 lb-sec
Life:	1000 seconds total time including a 500 second continuous run.
Weight:	Not specified but all efforts shall be made to attain a minimum value.

The Curtiss-Wright designation for the engine being developed under this contract is WLR-23.

B. Engine Concept

The axially conducting engine, Figure 2, consists of a number of pyrolytic graphite wedges, radially insulated, and restrained by an elastic watchband structure. The face of each wedge is undercut to form a land which serves as the inner portion of the chamber. The watchband, a relatively stiff circumferential spring, holds the wedge in compressive contact only along the land surface. In addition, the watchband allows enough thermal growth of the wedges (primarily in a circumferential direction) to maintain reasonable land stresses. The undercutting of the wedges also minimizes the amount of circumferential thermal growth that must be handled by the watchband structure.

A pyrolytic graphite sleeve assembly insulates the watchband from the heat sink formed by the wedges. These sleeves are split longitudinally into sectors to eliminate hoop restraint and assure uniform transmission of the watchband load to the wedges. Pyrolytic graphite insulating washers are provided at both ends of the wedge assembly to minimize heat conduction into the injector, and into the rear housing flange.

The high thermal conductivity of the PG in the plane of the wedge is used to conduct heat from the inner chamber surface to the cooler portions of the chamber. During the shut down periods following engine operation the heat is radiated to space. An internal spray cooling concept is provided to further extend engine durability. A portion of the fuel from the injector is

introduced tangentially on the chamber wall adjacent to the injector. Use of this spray results in lower chamber and throat temperatures and restricts onset of erosion.

A sixteen port swirl cup injector is used with the ACE chamber. Alternating fuel and oxidizer ports are tangent to the swirl cup circumference, with a nine degree cant toward the cup outlet. This swirl cup serves as a pre-mix chamber where initial burning of the propellants takes place.

C. Summary of Program Status

Figure 1 shows the program schedule. Phase I of the program has been completed and the layout design of the rig engine configuration is shown in Figure 4. Hot firing tests of the rig engine will verify the design which differs from the flight configuration in three major areas, as shown on the preliminary layout, Figure 2:

1. The spray cooling orifices are contained in individual pintles mounted in a separate housing on the rig engine. This flexibility provides an easy means of adjusting the spray direction, penetration, and velocity should testing indicate changes are required. In the flight configuration, the spray orifices are an integral part of the injector.

2. Because of the individual pintle arrangement in the rig engine, the Belleville washers are relocated to the exhaust nozzle exit. This arrangement is not used in the flight engine as it would interfere with the nozzle extension.

3. A heavy duty rig engine housing is provided to mount deflection probe instrumentation used to measure the radial deflections of the wedge and watchband assembly during test. Space is also provided between the rig housing and the watchband to allow for modifications to the wedge retention loading if required.

Detailed drawings for all rig engine parts for use in fabrication have been completed.

Thermal and stress analyses were conducted to support the mechanical design activity. A thermal model for the WLR-23 rig engine was prepared and computer runs were made to establish the time-temperature history for a 500 second firing. Overall results, shown in Figure 3, indicate a pyrolytic graphite throat temperature of 2370°F which is below the temperature at which erosion occurs. The computed watchband temperature of 1460°F at the end of the run led to the selection of Rene' 41 as the best watchband material.

An important part of the thermal analysis program was to establish the heat transfer coefficients to be used. Engine firings were made with a sixteen port swirl cup injector similar to the one to be used on the ACE rig engine tests and an instrumented copper chamber. The temperature data from these tests was used in a correlation procedure to establish the heat transfer coefficients.

The temperature profiles established during the thermal analysis were utilized in the structural analysis of the watchband and wedge assembly. Restraint must be provided by the watchband to insure proper contact of the wedge lands under all conditions, but this loading must be within the capabilities of the pyrolytic graphite and the watchband material. An iteration procedure was used to arrive at a satisfactory watchband design.

All detailed drawings for fabrication have been released and the current status of manufacture of these parts places the initial test of the ACE rig engine in early April 1966, somewhat ahead of schedule.

Section II of this report contains detailed discussions of the rig engine design and analyses, results of the analyses, and descriptions of the fabrication process of pertinent rig engine parts.

II. DISCUSSION

A. Rig Engine Design

1. Objectives

The broad objectives for the rig engine design were to:

a) Retain the basic features of the Curtiss-Wright WLR-21 configuration and thus rely heavily on our previous experience.

b) Maintain interchangeability of the combustion chamber between the WLR-23 rig and flight configurations.

The major change in the WLR-23 rig engine from the WLR-21 configuration was decreasing the size from a 5.5 inch OD to a 4.0 inch nominal outside diameter to reduce weight and envelope.

In addition, interchangeability of the rig engine and the flight engine combustion chamber was provided so that the analytical studies, fabrication and test experience are directly applicable to the final design.

2. Engine Performance

The performance targets for the engine, under vacuum conditions, are 100 pounds of thrust at a minimum specific impulse of 290 seconds assuming a 40:1 nozzle expansion ratio. Based on these requirements, the following pertinent engine parameters, assumed and calculated, were established:

Nozzle Efficiency (C_F)	98%
C* Efficiency	96%
Heat Loss to the Chamber	1.5%
Chamber Pressure	100 psia
Total Propellant Flow	0.333 lb/sec
Oxidizer/Fuel Ratio	2.0
Nozzle Throat Area	0.547 in^2
Chamber Contraction Ratio	5.0:1

3. Component Designs

The overall WLR-23 engine design is illustrated in Figure 4. The chamber assembly consists of eighteen circumferentially oriented pyrolytic graphite wedges with radial insulating sleeves restrained by an external elastic hoop, or watchband. The assembly is supported in the heavy duty rig housing by means of the insulating sleeve overhang and the end sealing and insulating washers. At the injector end, this washer pilots in the pintle housing, which in turn, is doweled to the external housing. At the nozzle, the sealing washer pilots in the spring shoe which fits within the housing inside diameter. An axial sealing load is applied to the end washer faces by four parallel Belleville springs located at the aft end of the engine. These springs are loaded by a shim integral with the aft flange.

The pintle housing contains sixteen individual and adjustable pintles with spray orifices that provide fuel spray coolant on the combustion chamber to extend engine durability. Both angular and radial pintle adjustments are possible. Fuel is supplied to the orifices by means of a common manifold through a single inlet fitting.

The injector is a 16-port, single plane, swirl cup mounted in the center of the pintle housing and held in place by a clamp ring. Two internal propellant manifolds (fuel and oxidizer) are connected to the orifices by a series of drilled passages. The orifices enter the swirl cup tangentially with a nine degree cant toward the cup outlet. An inlet fitting close couples each manifold to the propellant valves.

A detailed discussion of pertinent features follows.

Wedge Chamber Assembly

A sketch of the chamber internal contour is shown in Figure 5. The combustion chamber size was established from in-house performance optimization tests where various chamber lengths and contraction ratios were tested to provide trends of size versus performance.

Wedge depth as it affects stiffness was also considered in establishing the internal dimensions of the engine since the watchband and insulating sleeves occupy much of the radial depth of the chamber. Adjustment of the chamber ID was required to provide sufficient wedge stiffness in bending.

Another advantage of the contraction ratio selected (5.0:1) is a reduced differential thermal expansion due to differences in diameter between the chamber and throat sections.

The divergent portion of the wedges provides an exit cone expansion ratio of 4.5:1. The expansion ratio and cone half-angle are the same as used on the WLR-21 engine. Several other angles were studied to obtain a contour and divergence with no abrupt curvature change after the throat section.

The selected 4.5:1 wedge expansion ratio provides an exit diameter nearly the same as the chamber diameter for structural reasons, minimum external watchband containment load requirements, and a light weight configuration.

Provisions for an exit cone extension could be made to the aft end of the flight engine to achieve the specified vacuum performance at full expansion. The exact bellmouth contour would be established by an aerodynamic study which is not within the scope of this program.

A C_F efficiency of 0.98 was used for design calculation, which includes nozzle contour and friction losses.

Heavy Duty Rig Housing

The rig housing is the heavy duty structure into which the thrust chamber assembly is mounted for testing. Space is provided to supplement the watchband restraining load on the wedge assembly with circumferential leaf springs.

A pair of deflection probes 180 degrees apart, will be installed at each of four locations along the chamber length. These probes measure radial growth of the watchband and wedge assembly during test.

Four short thermocouple wire clearance grooves are located on the inner diameter at the back end of the housing. A fitting to measure cavity pressure is located behind the rearmost deflection probe.

Shoe

The shoe transmits the axial Belleville spring load to the sealing washers and the wedge assembly. It supports the aft end of the thrust chamber assembly within the inside diameter of the heavy duty housing by means of the pilot provisions with the rear sealing washer. A sprayed coating of Rokide Z insulation on the inner conical surface shields the shoe from the exhaust gas stream. The Belleville springs, which are housed in the shoe, are also protected by the conical extension on the inside diameter.

Belleville Springs

Four stacked Belleville springs are installed at the aft end of the engine. They are partially deflected to exert an axial load to maintain a leakproof seal at the ends of the thrust chamber assembly. During test, the springs will compensate for the differential thermal expansion between the chamber assembly and the external housing.

Figure 6 shows the load-deflection and the stress-deflection curves of the Belleville spring set. Values are plotted for conditions at both room temperature and 600°F (the operating range during the 500 second test run). The dashed line drawn between these curves represents the load/stress values at intermediate temperatures during the test. Although only moderate operating temperatures will occur, Rene 41, a nickel-base high temperature corrosion resistant alloy is used to insure satisfactory results.

The initial preload of the springs is 2500 pounds. This is 25% higher than the pressure area term over the inside cross-section of the housing. At the end of 500 seconds of running, the net axial thermal growth is calculated as .025 inches. During the 500 second run the load-deflection rate will follow the dashed line path shown on Figure 6.

A summary of the engine bearing stresses is presented below:

	Bearing Stress - Psi	
Interface	t = 0	t = 500 sec
Pintle Housing - Front Sealing Washer	494	563
Front Sealing Washer - Wedge Assy.	1003	1170
Wedge Assy. - Rear Sealing Washer	958	1090
Rear Sealing Washer - Shoe	590	672

The bearing stresses remain nearly constant because of the flat load-deflection characteristic of the spring.

Pintle Housing and Pintle

The pintle housing contains sixteen pintles which spray cool the combustion chamber wall. The pintles are radially located in the housing and connected to a common manifold that is fed from a single external fitting.
The housing is the forward closure of the engine and supports the chamber assembly and an end seal.

Structually, the pintle housing is treated as a solid flat plate with a central hole. It is freely supported on the inside diameter and both fixed and simply supported on the outside diameter. The maximum edge stresses and deflections are increased by the reduction in cross-sectional stiffness due to the pintle holes and clearance grooves. The maximum stress and deflection occurs for the conservative case of a simply supported outside edge. The maximum stress was calculated as 14,720 psi with a deflection of .0026 inches.

The pintle is a hollow stepped bar with an orifice at one end and a cleaning plug at the other. A radial feed hole below the step connects with the common manifold in the pintle housing. Redundant O-ring seals are provided to prevent any external or internal propellant leakage. Indexing lines on the outer end allows each pintle to be precisely adjusted. A shimming arrangement provides an exact adjustment of the radial distance of the orifice from the chamber wall.

Injector

Figure 7 shows the rig injector design for the WLR-23 engine. The propellants are introduced tangentially into the 16-port swirl cup where the flow becomes rotational and mixing takes place around the wall. The centrifugal force of the swirling propellant maintains a liquid film on the wall which prevents the wall of the cup from becoming overheated. A low thermal shape factor also contributes to the injector durability and minimizes heat input to the valving.

The propellants enter the injector through an inlet fitting in the manifold. Within the manifold the flow divides in half and then branches via cross drillings to the orifice connecting holes. The metering orifices are tangent to the swirl cup at a 9 degree cant toward the cup outlet.

The manifolds are constructed with gradually decreasing steps. This maintains constant velocity and minimizes the internal losses caused by sudden decreases in flow volume at intersections with the branch holes.

The criteria for the design of the two injector configurations which have been fabricated are summarized below:

	ES156903N1		ES159903N2	
Oxidizer Flow (Injector) lbs/sec	.2050		.2050	
Fuel Flow (Injector) lbs/sec	.1025		.1025	
Injector O/F	2.0		2.0	
Overall Engine O/F	1.6		1.6	
% Spray Cooling	20		20	
Spray Fuel Flow (Pintles) lbs/sec	.0255		.0255	
Discharge Coefficient C_D	.85		.85	
	Oxid.	Fuel	Oxid.	Fuel
Orifice Pressure Drop - psi	40	78	45	50
Orifice Diameter - in.	.0310	.0209	.0300	.0234
Injection Velocity - ft/sec	54.5	97.7	57.8	78.3

A summary of the internal passage flow velocities is given below:

INTERNAL FLOW VELOCITIES
16 PORT INJECTOR

	OX	FUEL
INLET FITTING		
Hole Dia - in.	.156	.156
Velocity - ft/sec	17.5	17.5

MANIFOLD								
Flow Fraction	1/2	3/8	1/4	1/8	1/2	3/8	1/4	1/8
Passage Width - in.	.25	.188	.125	.0625	.25	.188	.125	.125
Passage Depth - in.	.116	.116	.116	.116	.25	.25	.25	.125
Velocity - ft/sec	5.75				2.15			

FEED HOLES TO ORIFICES	Dia - in	Vel ft/sec	Dia - in	Vel ft/sec
Axial Connecting	.086	7.0	.086	5.7
Radial Connecting (Body)	.086	7.0	.086	5.7
Radial Connecting (Insert)	.073	9.8	.073	7.9

The overall response time (signal to 90% thrust) for these injectors is estimated to be 50 milliseconds.

A summary of the response times for both injectors is shown below:

TIME IN MILLISECONDS

	OXIDIZER	FUEL
Signal to Valve Open	12.0	12.0
Injector Fill Time	19.0	29.0
Ignition Delay Time	4.0	4.0
Pressure Rise to 90% Max. Thrust	5.0	5.0
	40.0	50.0

4. Instrumentation

The instrumentation drawing, Figure 8, indicates the location of temperature, pressure, and deflection instrumentation to be used during rig engine testing. This instrumentation is required to monitor test progress, and to provide data for evaluation of the design.

Thermocouples

A thermocouple in the injector will measure the swirl cup inner wall temperature to evaluate long duration firing effects. Four thermocouples, attached to the rig housing outside surface, are used to provide thermal corrections of the deflection readings to account for housing growth. Thermocouples are attached to two deflection probe rods inside the housing cavity to measure temperature due to contact with the watchband. This temperature will be used to correct for thermal expansion in the deflection readings. Two thermocouples are welded to the watchband outside diameter in the housing cavity to monitor this temperature during the test runs for comparison with analytical heat transfer results.

Pressures

Pressure fittings are provided to measure static pressure at various locations in the engine. The pressure in the back wall of the injector swirl cup and combustion chamber pressure at two locations at the lip of the swirl cup are measured. In addition a fitting is provided in the heavy duty housing for measuring cavity pressure. This provides an indication of the thrust chamber wedge land seal or end seal leakage and is monitored during test.

Deflection

Deflection probes are used to measure the radial deflection of the watchband due to the thermal growth of the wedge assembly. The probe is a slender guided rod that rests on the outside diameter of the thrust chamber assembly (watchband). An O-ring seal prevents gas leakage and a loading spring holds it in place against gas pressure.

Deflections are measured by translating the radial movement of the rod into an electrical signal using a Linear Variable Differential Transformer (LVDT) mounted on the probe body. This electrical signal is recorded on strip charts and is directly proportional to the direction and displacement of the probe.

Eight deflection probes are arranged in pairs located 180 degrees apart, and positioned axially at stations which correspond to the analytical sections used in the computer program.

Each pair of readings will be averaged and compared with the predicted analytical value at that section. Discrepancies are due mainly to a difference between the predicted and analytical temperatures on the inner wall of the thrust chamber. An iterative process is conducted in which a nozzle inner wall temperature is assumed as well as a thermal gradient to the measured temperature of the watchband. The radial thermal expansion of each element is calculated, as is the radial deformation due to the compressive load in the land. These displacements are combined to give a net radial deflection. The procedure is repeated until the calculated deflection agrees with the measured value.

The calculation is repeated for several firing times at the chamber and throat probe locations and the actual inner wall temperature distribution determined. These results are then used for correlating the heat transfer analysis, and for adjusting the retention loads, if required.

The effects of axial bending are not included in the iterative method. To determine whether the effects of axial bending are significant in the correlation procedure, the ring analysis is used and results compared with the combined ring and bending analysis.

II. DISCUSSION

B. Thermal Analysis

Temperature profiles in the WLR-23 rig engine configuration were calculated at several chamber locations for a 500 second firing (plus a 100 second soak period) by means of a thermal computer program. This temperature data was required to properly establish the mechanical and structural design of the engine. A thermal model for the engine was constructed based on the preliminary layout, Figure 2. The film coefficients used were calculated from data obtained during instrumented copper engine tests.

1. Method of Analysis

The analytical temperature-time relationships for the copper engine and rig engine were obtained using a Thermal Analyzer Digital Computer Program. This program uses the general heat conduction equation and an equivalent resistance capacitance network to provide solutions for transient or steady-state analysis of a number of materials having variable thermophysical properties. The analysis considers heat transfer by conduction, convection, and radiation. Ablation, deposition, mass transfer, change of phase and various combinations of these factors with a wide variety of boundary conditions are also easily handled.

The time-temperature data from a copper chamber hot firing test without spray cooling was used to first determine the heat flux (Q) to the inner wall and the film coefficient (h) representing the boundary conditions of a dry wall. The film coefficient is primarily a function of two parameters which are normally constant during a test run: total temperature of the gas and chamber pressure. During the initial few seconds of firing, the time-temperature curve (slope) is almost entirely dependent on the heat entering the inner wall. Only a negligible amount of heat leaves the backside of the engine during this initial period. A thermal model was constructed, incorporating the calculated film coefficient at each chamber location and the resulting time-temperature histories were then compared to the test results.

The same copper engine was also hot fired using propellant spray cooling on the inner wall. The liquid on the wall is converted to vapor within a short axial distance from the point of injection. Reference (1),p.17, presents a method of thermal analysis which assumes the layer remains along the entire chamber wall. This analysis, used with the WLR-21 test results, showed a close correlation which indicates that this coolant vapor persists to the throat of the nozzle.

Using Reference (1), adiabatic wall temperatures were calculated. These calculated temperatures were then used as the driving temperatures in a thermal model with the film coefficients calculated from the dry copper engine run, to estimate the effect (time-temperature history) of spray cooling. The time-temperature history thus produced is compared to the spray cooled copper chamber test data.

Finally, a thermal model for the ACE rig configuration was constructed using the film coefficients from the copper engine studies. The adiabatic film temperature used in the copper engine correlation was corrected for the slightly longer axial cooling path in the ACE rig configuration. Another refinement to the thermal model concerned the amount of physical contact between certain components. WLR-21 engine test experience showed that the thermal contact between the pyrolytic graphite sleeves and the wedges plays an important role in predicting their temperatures. The thermal contact was found to be time dependent; as the wedge temperature rises the contact loading increases. This factor was also considered in establishing the WLR-23 thermal model.

2. Copper Chamber Test Configuration

A drawing of the copper chamber, rig injector, and spray pintle arrangement is shown in Figure 9. The injector (ES156732) is heavy duty rig type hardware developed during an in-house program and approximates the injector configuration that will be used during the ACE rig engine testing.

The spray cooling configuration contained sixteen individual pintles equally spaced and positioned radially about the pintle housing. The pintle

protrusion into the chamber and angular position are adjustable. Based on WLR-21 experience, the pintle orifice centerline was positioned 0.025 inches into the chamber and at an angle of 20° with respect to the engine centerline. The spray direction was in an opposite rotational direction to that of the propellant from the swirl cup. For test runs where spray cooling is not required, the pintle and housing assembly is replaced with a copper spacer of equivalent thickness.

The copper combustion chamber was instrumented with chromel-alumel thermocouples, a flush mounted high frequency Kistler pressure transducer, and a Wianko pressure transducer for steady-state pressure measurements. Details of the thermocouple positioning is given in Figure 10. The thermocouples were spring loaded to insure contact throughout the firing cycle.

Design point conditions for this hardware are as follows:

	Oxidizer	Fuel	Spray
Propellant weight flow - lbs/sec.	C.205	0.1025	0.0255
Propellant orifice pressure drop - psi	35	78	52
Propellant orifice exit velocity - ft/sec	51	98	28

3. Copper Chamber Test Results and Correlation

Spray cooled and non-spray cooled hot firing engine tests were made to provide data for correlating with the analytical computer program. The tests were terminated when combustion chamber temperature reached approximately 1000°F. The effectiveness of the cooling device is indicated in Figure 11. The time to reach the 1000°F temperature increased by a factor of two when spray cooling was used. The engine performance during these runs is given in Tables I and II and indicates no change in performance between the dry and spray cooled tests. In addition, transient pressure traces taken during the two tests, Figures 12 and 13, indicate comparable stability characteristics.

The temperature data for the dry run is presented in Figures 14 to 22. The dotted line on each curve indicates the analytical correlation with the assumed heat transfer coefficient (h) noted. Although the correlation at

some locations in the nozzle portion of the chamber is not in complete agreement, it was considered prudent to use the higher "h" in order to achieve a somewhat conservative rig engine analysis. In a similar manner the tempera- data for the spray cooled run is presented in Figures 23 to 31.

4. Results of Rig Engine Computer Analysis

The results of the computer run on the WLR-23 rig engine model are shown in Figures 32 through 38. Figure 3 is a plot of the temperature at various strategic locations in the engine versus time for a continuous firing of 500 seconds. The 500 seconds following shut down are also shown to indicate the temperature prediction for the soak period. Throat temperature at the end of the firing is predicted to be 2375°F. This value is substantially below the temperature at which erosion of the PG material takes place. The maximum watchband temperature during firing is 1460°F and indicates the need for a good high temperature material. Based on this temperature prediction, Rene' 41 material was selected for the watchband.

Figures 32 through 38 show the temperature profile at 140 locations in the rig engine for firing times of 50, 100, 200, 300, 400 and 500 seconds of operation and for 100 seconds of soak. This temperature data was used for the structural analysis of the engine to insure proper watchband restraint and the structural integrity of the engine materials.

Reference

1. C.F. Warner and D.L. Emmons, Effects of Selected Gas Stream Parameters and Coolant Properties on Liquid Film Cooling - Journal of Heat Transfer Vol. 86 Number 2, May 1964.

II. DISCUSSION

C. Structural Analysis

Analyses were made to determine the watchband configuration and its structural adequacy. Additional analyses, using the IBM 704 computer, were made to establish the hoop and bending stress profiles for the pyrolytic graphite wedges. Since the behavior of the watchband and wedges are intimately related, their solutions must be compatible at all times. The watchband must be flexible enough to permit thermal growth of the wedges yet restrictive enough to maintain a compressive hoop stress on the wedge lands. Particular attention must be paid to the watchband and wedge stresses during the initial 100 seconds of firing. During this time the maximum differential thermal expansion between the wedge lands and the watchband occurs. Maximum differential thermal expansion is coincident with maximum stresses in the wedges and maximum stress in the watchband.

1. Method of Analysis

Watchband

The design of the flexible watchband housing permits the housing loads to be carried in bending rather than in hoop. The watchband consists of a number of rows of tapered, interconnected cantilever beams circumferentially stacked to form a flexible cylindrical shell. The beams have a taper ratio (root width to tip width) of 2.75. This taper ratio, applied to a beam of constant (watchband) thickness, results in a tip deflection twice that of a non-tapered beam. This results in a beam of optimum design having constant stress throughout the material.

The equations for determining the watchband stress level and deflection are modified to account for the physical differences between the theoretical model and the actual beam. These adjustments include the effect of the longitudinal stringers upon the length of the beam and the distortion of the beam root width from setting the tapered beam at an angle with respect to the longitudinal axis. The correction factor used in this analysis was based on the results of the watchband tensile test for the 5.5 inch O.D. WLR-21

engine program. A tensile test of the new watchband design was conducted and indicated that the correction factor was not required. The tensile test data and the changes that were made are discussed in Section II-D.

Initial sizing of the watchband was made by hand calculations based on thermal growth through the throat section and through the chamber section of the engine at the end of a long duration firing. The configuration was then checked at room temperature conditions to insure adequate preload at installation. This simplified ring analysis assumes average land stresses, and internal deformation in the land only. Axial compatibility is neglected due to added complexity. An equivalent modulus of elasticity for the watchband is used based on the comparable behavior of a solid shell of equal thickness. The equivalent watchband modulus is required as input data for the analysis of the pyrolytic graphite wedges.

Pyrolytic Graphite Wedges

A computer program (Log 918-927) which determines hoop and bending stresses throughout the engine for any particular instant of time is used for the structural analysis of the pyrolytic graphite wedges. Deflections and interface pressures are also computed.

Basically, the analysis is made in two parts. The first part is a ring analysis which assumes the engine divided into axial sectors (maximum of seven) with each sector composed of a series of concentric longitudinally cut rings surrounding the wedge and land ring with a watchband completing the assembly. The geometry and temperature of each element is then defined. The interaction analysis between the radial elements includes the effect of the watchband interference fit and the anisotropic properties of pyrolytic graphite. Since each sector is subject to different thermal gradients, compatibility of deflection in the axial direction is necessary. Hence, the second part of the analysis is a longitudinal bending analysis which insures axial compatibility. The final stresses, deflections and interface pressures are solved for the combined ring and bending analysis.

2. Design Criteria

Design criteria for the watchband are based on previous experience and are listed below:

Limit the watchband stress level to below 120,000 psi based on the use of Rene' 41 material.

Provide a constant interference fit between the watchband and wedges along the entire length of the engine at installation.

Provide watchband support over the full length of the wedges consistent with minimum watchband overhang.

Attempt to maintain a constant thickness watchband.

The design criteria for the pyrolytic graphite wedges is similarly based on previous experience with the WLR-21 rig engine. These requirements are as follows:

Provide Compressive hoop stress at the inner and outer surfaces of the land throughout engine firing.

Do not exceed approximately 17,000 psi combined tensile bending stresses in the axial direction at the outer surface of the land.

Maintain uniform stress levels along the length of the wedge land, in both hoop and bending.

Maintain uniform watchband deflections along the length of the engine.

Minimize throat area change by providing adequate restraint.

3. Analytic Results

The results of the analyses conducted for the final watchband and wedge configurations are presented in both tabular and graphical form. The data covers conditions from startup to the end of a 500 second firing. Computations were made at 0, 50, 100, 400, 500 and 600 seconds (end of firing plus

100 seconds of soak). Watchband design thickness was constant at 0.265 inches and the wedge land height was constant at 0.11 inches. Radial interference fits of .010, .011 and .012 inches were included in these analyses.

Tables III through V tabulate the hoop stresses at the inner and outer surfaces of the wedge land as a function of time and interference fit. The location of the various sections is defined in Figure 39. Uniformity of stress levels at each increment of time is readily apparent. The maximum compressive hoop stress occurs at approximately 100 seconds at Section D and ranges from 16,760 psi to 17,790 psi for the variations of interference fits. At the end of firing (500 seconds) the range of compressive hoop stress at the inner surface of the throat is from 480 psi to 2080 psi. After 100 seconds of soak, the hoop stress at the inner surface of the throat is in tension ranging from 1740 psi to 115 psi. Hence, the throat will remain closed during firing but will tend to open slightly at the land I.D. after engine shutdown. This is not considered significant since much of the surface of the land at the throat will remain in compression thereby maintaining the seal across the wedge land. The engine test will confirm this assumption.

Tables VI through VIII are of particular importance since they define the combined axial tensile bending stresses at the outer surface of the land. Experience has indicated that 16,000 - 17,000 psi should be considered as the maximum allowable tensile stress. Bend tests of the pyrolytic graphite plates are made during the fabrication process to insure the material is well above this value. Maximum bending stress occurs at Section E at 100 seconds for each interference fit considered. The peak values are 16,150 psi at .010 in. interference, 16,680 psi at .011 in. interference and 17,220 psi at .012 in. interference. The design was set to .011 in. maximum radial interference.

Watchband bending stresses as a function of time and interference fit is presented in Table IX and graphically in Figure 40. Data is given for the throat and a typical chamber section. Stresses at other sections would be of the same order of magnitude. The stress level is maximum for the throat section at 50 seconds of firing. At .011 in. interference the stress is

100,000 psi resulting in a margin of safety of 20%. The margins of safety at all other times are higher. As expected, the watchband stresses increase with interference fit, running about 2000 - 4000 psi higher per .001 inch additional interference.

Tables X through XII show the uniformity of deflection of the watchband from section to section as a function of time. Maximum deviation from section to section appears to be about .001 inch. However, the deviation at the majority of adjacent sections is less than .0005 inch. There are no sharp discontinuities of deflection in the engine.

Figure 41 shows in graphical form the change in the engine throat area with respect to time. The throat area increases about 7.4% at 500 seconds due to thermal expansion.

Two other significant illustrations are Figure 42 which defines the weight of the watchband as a function of its thickness, and Figure 43 which defines the flight engine envelope as a function of watchband thickness. For the design thickness of 0.265 inch the watchband weight is 3.43 lbs, and the engine OD is 4.275 in. An improved radial insulator design would considerably reduce the watchband thickness and weight.

Due to the range of temperatures predicted for the watchband (up to 1500°F) by the thermal analysis, it was necessary to select a material having high temperature capability. The material chosen for the watchband is forged Rene' 41 heat treated and aged to Rockwell C36 minimum hardness and 130,000 psi 0.2% offset yield strength at room temperature. Other watchband materials such as maraging steel and titanium were considered but were rejected at this time due to the high temperature requirements. While both of these materials have strength-to-weight ratios greater than Rene' 41 at moderate temperatures, both have upper temperature limitations of about 800°F. The use of an improved radial insulator would reduce the watchband temperature and permit use of a material other than Rene' 41. This would result in a reduced watchband thickness and weight. Improved insulation development is not, however, within the scope of this program.

Numerous computer runs were conducted prior to the selection of the 0.265 in. watchband design thickness. Thicknesses ranging from 0.180 inches to 0.400 inches were investigated. Stepped thickness and interference fits from 0.008 to 0.012 inches were also included. The final solution is the result of 44 computer runs. Of these, 18 runs were for the final design at six instances of time and three interference fits each. Of the remaining 26 runs, 10 were to determine the effect of interference fit and 16 runs to establish the watchband thickness and beam angle. These computer runs included conditions at installation and at elevated temperature.

In order to minimize the watchband overhang, it is desirable to have a large a beam angle as possible consistent with all other wedge and watchband requirements. Beam angles ranging from 25° to 41° were investigated. The final design incorporates a beam angle of 32°30' at a pitch of 0.43 inches. The positioning of the watchband with respect to the wedges is shown in Figure 44 which shows that the wedges are fully supported for almost their entire length.

4. Summary

The following items summarize the results of the watchband and the pyrolytic graphite wedge analyses for the WLR-23 rig engine:

The WLR-23 rig engine should operate for a continuous firing of 500 seconds provided the measured watchband temperature is within 15% of the theoretical watchband temperature throughout the run.

The rig engine should be built with a watchband radial interference of 0.010 - 0.011 inches.

Peak watchband stresses occur at about 50 seconds of firing, reaching a level of 100,000 psi over the throat section.

Peak compressive hoop stress and tensile bending stress in the wedges occur at about 100 seconds, reaching a level of 16,560 psi and 16,690 psi respectively at the convergent section of the throat.

The maximum radial deflection of the watchband should not exceed 0.025 inches at 500 seconds.

The theoretical throat area increase is 7.4% after 500 seconds.

Note that some of these results have been modified, based on the watchband tensile specimen test. The revisions in configuration and minor changes in stress level are discussed in the following section, II-D.

II. DISCUSSION

D. Watchband Tensile Specimen

A watchband tensile specimen, Figure 45, was fabricated to test a sample section of the watchband beam configuration. This test was made to determine the actual spring rate of the watchband design, compare it with the analytical prediction, and then determine the design adjustments needed to obtain the desired loading. Final machining (OD and ID) of the watchband was delayed until the results of this procedure were known.

The tensile specimen test configuration is shown in Figure 46. The load-deflection curve obtained from the test data and the analytical prediction are given in Figure 47. As discussed in the previous section (II-C), the analysis included a correction factor for the effective length of the beam, and beam root distortions. From the test results it appears that only minor corrections were required and actually could have been disregarded.

Investigation was made to determine means of modifying the design to obtain the required loading schedule within the dimensions of the partially fabricated watchband. The watchband was complete except for final grinding of the inside and outside diameters with approximately .040 inch excess stock on each of these surfaces.

Hand calculations and some preliminary computer runs indicated that a watchband with reduced stiffness would be satisfactory if the initial interference fit were increased. In addition, the thickness of the part could be increased within the limits of the available material to gain some increase of stiffness over the test results. Thus, the nominal radial interference fit was increased from 0.011 inches to 0.025 inches, and the wall thickness was increased from 0.265 inches to 0.290 inches.

Structural analyses of this configuration were made and the results are summarized in Figure 48 and in Tables XIII through XVI. Figure 48 presents a plot of watchband stresses at the throat and chamber sections as a function of run time. The maximum stress, which occurs at 50 seconds, is increased by approximately 9% over the original design but is still well within the limitations of the material.

Tables XIII and XIV show the hoop stress, and combined bending stress in the wedge land. The higher interference fit results in an improved overall stress picture. The installation stresses are somewhat higher; however, the maximum stress at 100 seconds is now lower. At 500 seconds the slightly higher stress improves the land loading condition in the throat; after 100 seconds of soak the throat inner land surface is still closed. In the original design it was in slight tension.

Table XV shows no appreciable change from the original analysis of the watchband radial deflection history as measured from the installed position. The radial installation stretch is increased from about .007 to .020 inches.

No appreciable throat area variation occurs between the initial and final designs. Table XVI shows the theoretical percent throat area change. At 50 seconds the change increased from 2.2 percent in the original design to 2.8 percent. At 500 seconds it increased from 7.32 percent to 7.8 percent.

In summary, the watchband design revisions provide a completely satisfactory configuration which in some respects is an improvement over the original design.

II. DISCUSSION

E. Rig Engine Fabrication

Fabrication of all parts required for the initial rig engine build is well underway and somewhat ahead of schedule. The current status of fabrication should allow the initial test to start during the first week in April 1966. The manufacture of pertinent rig engine parts is discussed in the following paragraphs.

Pyrolytic graphite plates for the wedges were purchased to WAD Specification 5839 (Appendix I). The material was subjected to the quality control and fabrication procedure outlined in Figure 49. Visual inspection was made for surface flaws and gross delaminations. Nodules were measured for conformance to the specification requirements.

A template made to the shape of the detail wedge was positioned on each plate to establish an optimum location which had no large nodules in the wedge land. A flexure test specimen was sectioned from each plate as shown in Figure 50 to insure that the structural properties of each plate were satisfactory. A schematic of the flexure test configuration is shown in Figures 51 and 52. Testing was performed on an Instron Tensile machine using a cross head movement rate of 0.02 inches/minute. The test results for wedges to be used in the first engine build are tabulated in Table XVII and are well above the stress levels that are predicted during test.

The rough wedge outline was cut from each plate and the angles on the sides were rough milled leaving .006 inch excess stock on each side. One side of the wedge was finish ground. Positioning on this ground side, the undercut that forms the land was then milled on the opposite side using a Hydrotel machine. The land surface on the relieved side of the wedge was then finish ground completing the wedge detail as shown in Figure 53. Prior to assembly the wedges were inspected for delamination and/or surface flaws by a dye penetrant (Zyglo - post emulsification) process in accordance with specifications AMS2645 and AMS3156.

The eighteen wedges that form the chamber were assembled and retained by a split sleeve tool as shown in Figure 54. The ends were ground to establish overall length and a chamfer was machined on both ends. These chamfers provided a surface upon which end clamping discs rode while holding the assembly during finish grinding of the outside diameter.

With the outside diameter finished machined, the PG cylinder segments and the sheaths will be placed around the wedge assembly. The watchband will then be expanded over the wedge assembly by use of a tapered plug. The wedge assembly inner diameter will be ground to produce the proper contour. The wedge assembly, PG inlet and exit washers, Belleville springs, the shoe, and the exit flange will then be assembled into the housing.

The Belleville springs, were fabricated from 0.233 inch Rene' 41 sheet material. The springs were treepaned from the sheet and machined to size. After machining, the springs were heat treated in stacks of four to produce the final spring assembly. The springs were aged at 1400°F $\pm$ 15°F for 16 hours and air cooled. After aging, the springs were inspected for the minimum desired hardness of R_c 36.

A Rene' 41 forging was purchased for the watchband and turned on both the outer and inner diameters leaving .050 inch excess stock on each surface. This cylinder was then aged at 1400° $\pm$ 15°F for 16 hours and air cooled. After aging the cylinder was checked for hardness and a reading of R_c 38 was obtained. This value is within the drawing requirements. The watchband slots are being produced by an elox method. Electrodes, fabricated from graphite to the shape of the slot, are arranged in banks of fifteen and are used to burn the slots in the cylinder.

II. DISCUSSION

F. Injector Development

The WLR-23 injector has to pass the necessary propellant weight flow to produce 100 lbs. of thrust at a pressure drop consistent with a feed pressure target of 195 ± 5 psia.

An in-house program was initiated prior to receipt of contract to upgrade the WLR-21 injector from 85 to 100 lb. thrust level. In addition, to further insure good distribution (from the standpoint of chamber durability) the total number of ports was increased from 8 to 16. Heavy duty injectors with manifolding requiring long fill times, were used. This program produced an injector configuration shown in Figure 9, having good stability characteristics (reference Figures 12 and 13). However, the fuel feed pressure schedule was somewhat above the desired value, as shown in Table XVIII.

Two low fill time injectors having a calculated response time (signal to 90% thrust) of 50ms have been designed, Figure 7, and fabricated for use with the WLR-23 rig engine.

One of these injectors, (ES 156903N1) incorporates orifices sized to produce pressure drops of 40 psi for the oxidizer and 78 psi for the fuel. This injector is similar to that run during the copper engine tests (except for reduced manifold volume to reduce fill time and response time) and should produce fully stable combustion. However, the fuel feed pressure requirement would be approximately 30 psi over target. A variation of this design (ES156903N2) reduces the fuel orifice pressure drop to meet the target feed pressure.

Both of these injector designs have been fabricated. The cold flow calibration curves of the injector inserts are shown in Figures 55 and 56. The low pressure drop injector orifice calibration indicates that design flow is attained at 40 psi pressure drop for both propellants. This pressure drop is lower than design values and is thought to be due to a slightly rounded orifice entry which resulted in a mean coefficient of discharge of 0.91 for the oxidizer and 0.95 for the fuel orifices. The discharge coefficient used in

design of the orifices was 0.85. The spread in orifice-to-orifice calibration is satisfactory and no attempt was made to change the pressure drops to match the design conditions.

The higher pressure drop injector calibration, Figure 56, shows that the oxidizer weight flow is obtained at 37 psia pressure drop and fuel weight-flow at 80 psi pressure drop. These values are close to the design estimates. The spread in flow between orifices is also quite satisfactory.

Both of these injectors will be tested early in the second quarter to determine which will be used for the ACE rig engine test series.

III. PLANNED FUTURE ACTIVITY

The activity planned for the second quarter of the program is outlined in Figure 1 and is briefly described below.

Rig Engine Fabrication

All detail parts for the first rig engine build are available with the exception of the watchband. Final machining of the watchband is in process and is scheduled for completion the last week of March. Completion of the engine assembly is scheduled for the first week of April.

Evaluation Testing (Rig Engine)

Start of rig engine evaluation testing is now scheduled for early April. A test plan has been submitted to NASA for approval. The test series on the first engine will be completed during the second quarter.

Flight Configuration Design

Design of the flight configuration will be initiated based on the results of the first test series on the rig engine.

Injector Development

Evaluation of two injector configurations, designed for use with the rig engine, will be completed by the end of March and one configuration will be selected. Activity on the integral spray injector will be based on these results and will be initiated in the second quarter.

SPECIFICATION

CURTISS-WRIGHT CORPORATION
WRIGHT AERONAUTICAL DIVISION
WOOD-RIDGE, N.J.

5839

4 Pages

ISSUED 3-22-63
REVISED
REVISED
PREPARED BY Engrg. DEPT.

SPECIFICATION CLASSIFICATION
MATERIAL SPECIFICATION

TITLE
PYROLYTIC GRAPHITE PLATE

1. ACKNOWLEDGMENT: A vendor shall mention this specification number in all quotations and when acknowledging purchase orders.

2. FORM: Flat plates.

3. APPLICATION: Primarily for use in the fabrication of various components where anisotropic properties of thermal conductivity and/or resistivity are necessary at approximately 5000 F.

4. MATERIAL: A polycrystalline form of graphite having a high degree of orientation and purity. Material shall be produced by the deposition of carbon from a vapor phase onto a substrate at an elevated temperature.

5. TECHNICAL REQUIREMENTS:

5.1 Properties: Unless otherwise specified, the material shall conform to the following requirements:

5.1.1	Density, g per cc at 77 F ± 5	2.18 - 2.20
5.1.2	Decomposition, Total Ash, Wgt, %	0.1
5.1.3	Degree of Preferred Orientation, n value	Greater than 7 but less than 50 (See Note 1)
5.1.4	Flexural Strength, "a" direction (in the plane, parallel to surface of deposition), psi, min, at 77 F ± 5	15,000 (See Note 2)
5.1.5	Tensile Strength, "a" direction (in the plane, parallel to surface of deposition), psi, min, at 77 F ± 5	8,000

5.1.6	Thermal Expansion (if determined), "a" direction, in./in./deg F. from 100 - 1500 F	Less than 0.00[illegible]
5.1.7	Curvature, deflection, max	Not to exceed 0.035R (See Note 3)

Note 1. The n value, as determined by x-ray diffraction, is the slope of log I/Im vs log cos w, where $I/Im = \cos^{n}w$ and w is the angle between the reflection plane and the texture direction.

Note 2. The specimen shall have the same width as its thickness and a minimum length of 3 inches. It shall be loaded perpendicularly to the basal plane.

Note 3. The curvature of all plates shall be measured before grinding. R is the distance from the edge of the plate to the point of maximum deflection when measured on the concave surface.

6. QUALITY:

6.1 Material shall be uniform in quality and condition, clean, and free from imperfections detrimental to its performance.

6.2 Conical Growth Defects (Nodules):

6.2.1 Discontinuously Nucleated: No nodule or cluster of nodules (nodules touching each other) shall be larger in diameter than one-half the thickness of the plate for all thicknesses up to and including 3/8 inch. For plates thicker than 3/8 inch, no nodule shall be larger than 3/16 inch in diameter. There shall be at least one inch between any two nodules of the largest size allowed for the thickness of the plate and there shall be not more than 15 nodules in an area of 25 square inches.

6.2.2 Continuously Nucleated: The material shall be free from nodules. A microstructural examination shall be performed to verify that the material is continously nucleated.

6.3 Surface Flaws: The exposed surfaces of the plate shall not have any cracks when examined visually nor shall the surfaces be visibly marked (grooved or gouged) by measuring instruments. Final inspection for cracks shall be made by a penetrant dye check. Plates having surface flaws shall be rejected.

6.4 Delaminations: Edges of the plate shall be examined visually for delaminations parallel to the deposition surface. Final inspection for delaminations shall be made by a penetrant dye check after finish machining. Delaminated material shall be rejected.

7. REPORTS:

7.1 Unless otherwise specified, the vendor of the product shall furnish with each shipment three copies of a report stating that the product conforms to the requirements of this specification. This report shall include the purchase order number, material specification number, vendor's material designation, form or part number, quantity, and process records showing outgassing and furnace cooling time, deposition time and temperature, and total cubic feet and specific type of hydrocarbon gas used for each furnace lot of material.

7.2 Unless otherwise specified, the vendor of finished or semi-finished parts shall furnish with each shipment three copies of a report showing the purchase order number, material specification number, contractor or other direct supplier of material, supplier's material designation, part number, and quantity. When material for making parts is produced or purchased by the parts vendor, that vendor shall inspect each lot of material to determine conformance to the requirements of this specification, and shall include copies of laboratory reports showing the results of tests to determine conformance.

8. IDENTIFICATION: All material shall be clearly marked to show this specification number, and manufacturer's name or trademark, or in some other manner agreeable to the purchaser.

9. PACKAGING: Packaging shall be accomplished in such a manner as to ensure that the product, during shipment and storage, will be protected against damage from exposure to weather or any normal hazard.

10. APPROVAL:

10.1 To assure adequate performance characteristics, material shall be approved by purchaser before material for production use is supplied, unless such approval be waived. Results of tests on production material shall be essentially equivalent to those on the approved sample.

18-805

WRIGHT AERONAUTICAL DIVISION • CURTISS-WRIGHT CORPORATION • WOOD-RIDGE, N J., U. S. A

10.2 Vendor shall use the same ingredients and manufacturing processes for production material as for approval sample material. If necessary to make any change in ingredients or processing which could affect any characteristics of the material, vendor shall declare such change to the purchaser.

11. <u>ACCEPTANCE</u>: Material not conforming to this specification or to authorized modifications will be subject to rejection.

Approved J. L. Marzymont   Signed QEK Joseph Doh Duley

PROGRAM SCHEDULE

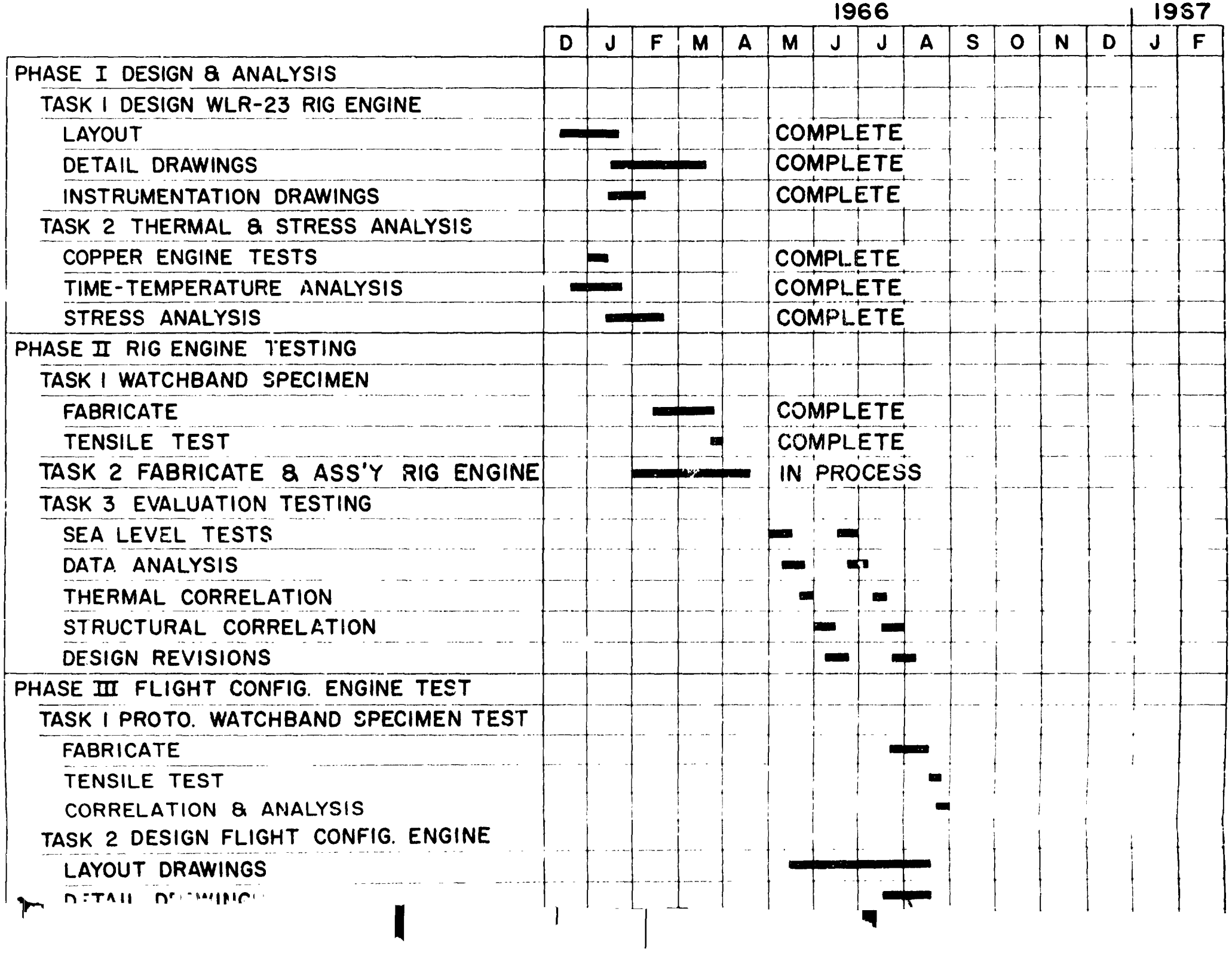

DETAIL DRAWINGS

FABRICATE

TENSILE TEST

CORRELATION & ANALYSIS

TASK 2 DESIGN FLIGHT CONFIG. ENGINE

LAYOUT DRAWINGS

DETAIL DRAWINGS

THERMAL ANALYSIS

STRUCTURAL ANALYSIS

OPERATING PARAMETERS

TASK 3 FAB. FLIGHT CONFIG. ENGINES

PROCUREMENT

FABRICATION OF COMPONENTS

ASSEMBLY & FINAL MACHINING

MODIFICATIONS

TASK 4 EVALUATION TESTING

DEVELOP INTEGRAL SPRAY INJECTOR

SEA LEVEL ENGINE TESTS

DATA ANALYSIS

THERMAL CORRELATION

STRUCTURAL CORRELATION

DESIGN REVISIONS

TASK 5 FABRICATE NASA ENGINE

PROCUREMENT

FABRICATION OF COMPONENTS

ASSEMBLY & FINAL MACHINING

ACCEPTANCE TEST

DELIVER TO NASA

TASK 6 ADVANCED PROPELLANT STUDY

THERMAL ANALYSIS

MATERIAL COMPATABILITY

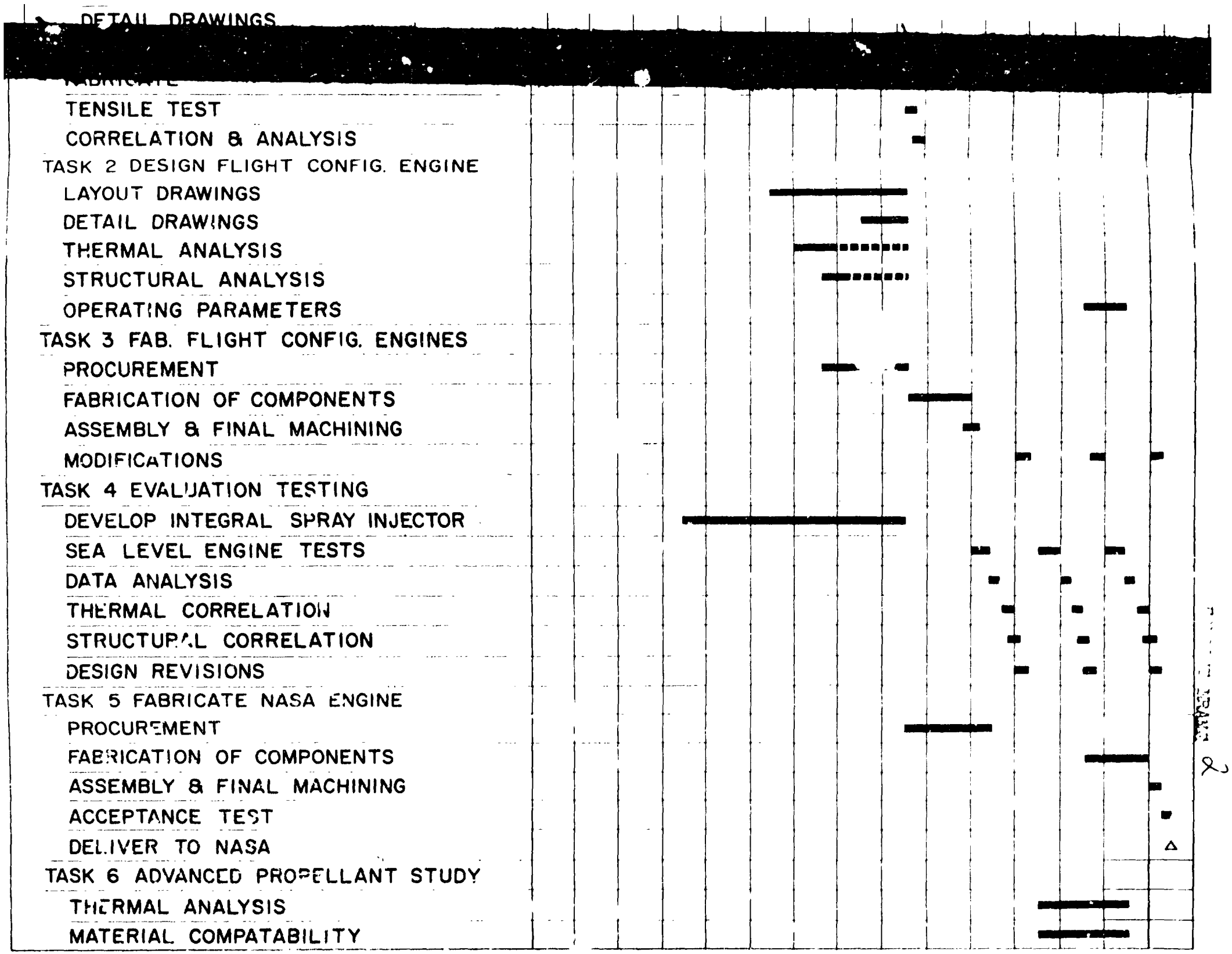

Figure 1

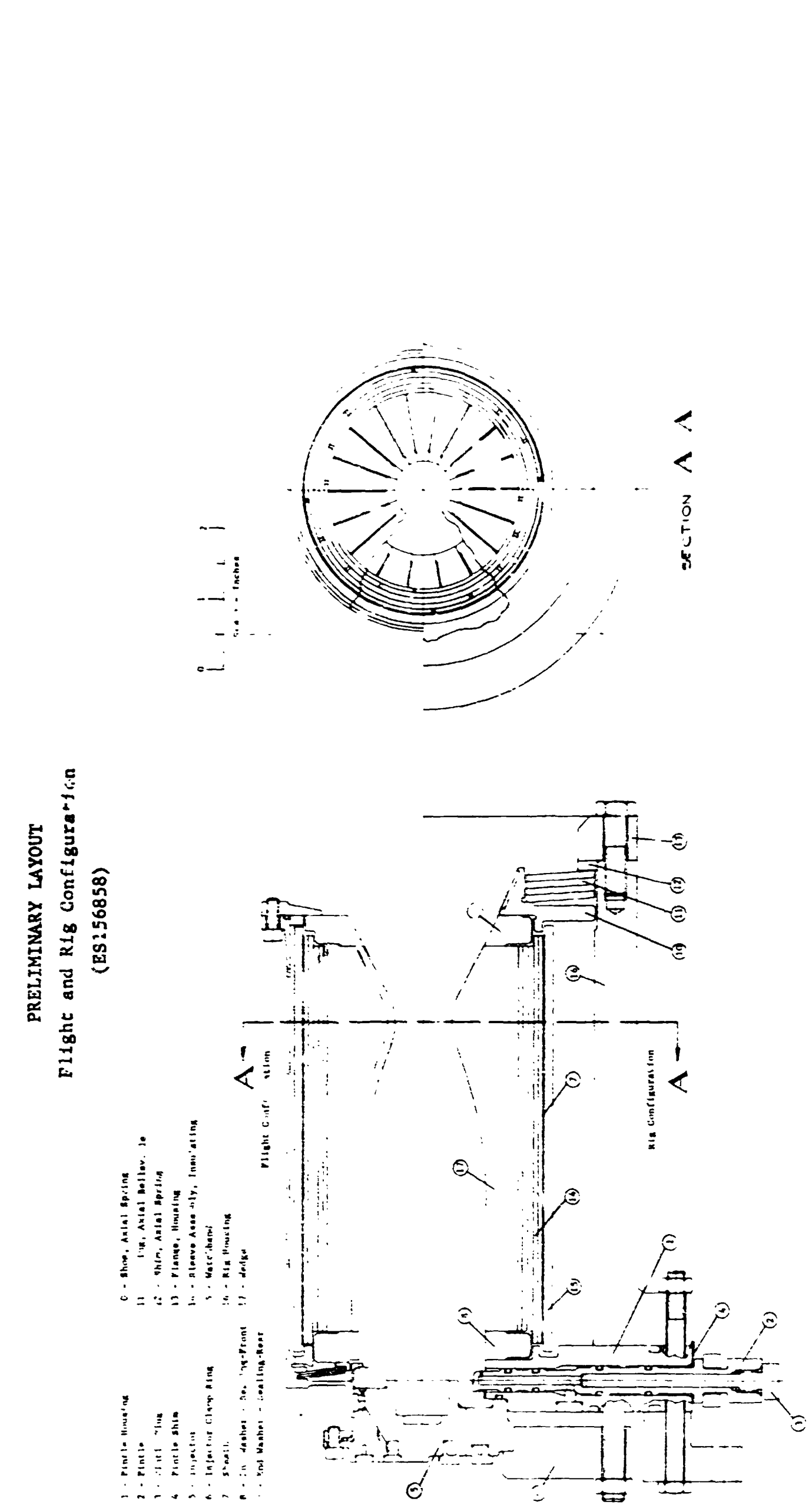
PRELIMINARY LAYOUT
Flight and Rig Configura
(ES:56858)
SECTION A A
Flight Configuration
Rig Configuration
A
A

Figure 2

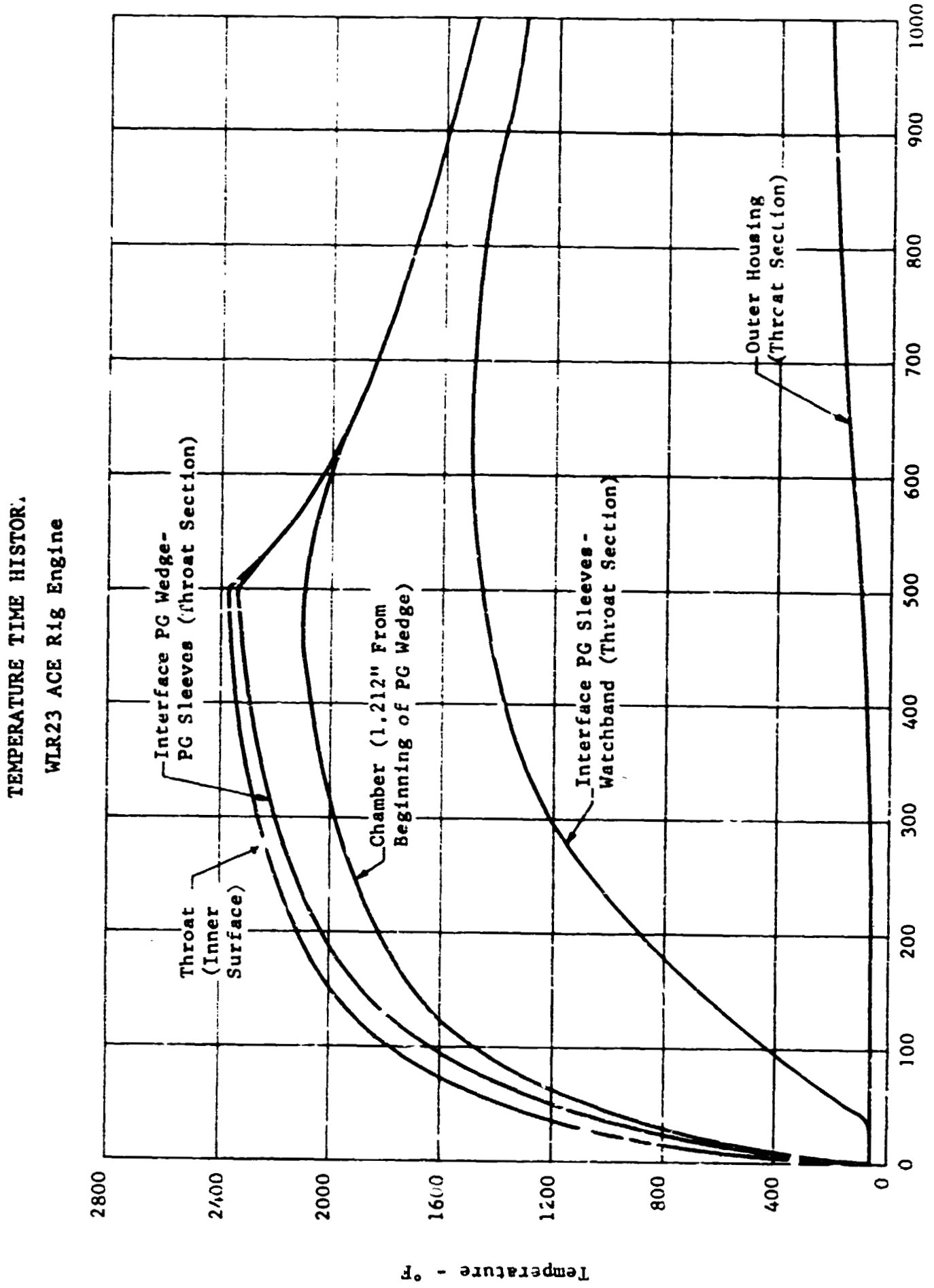

18-809

Figure 3

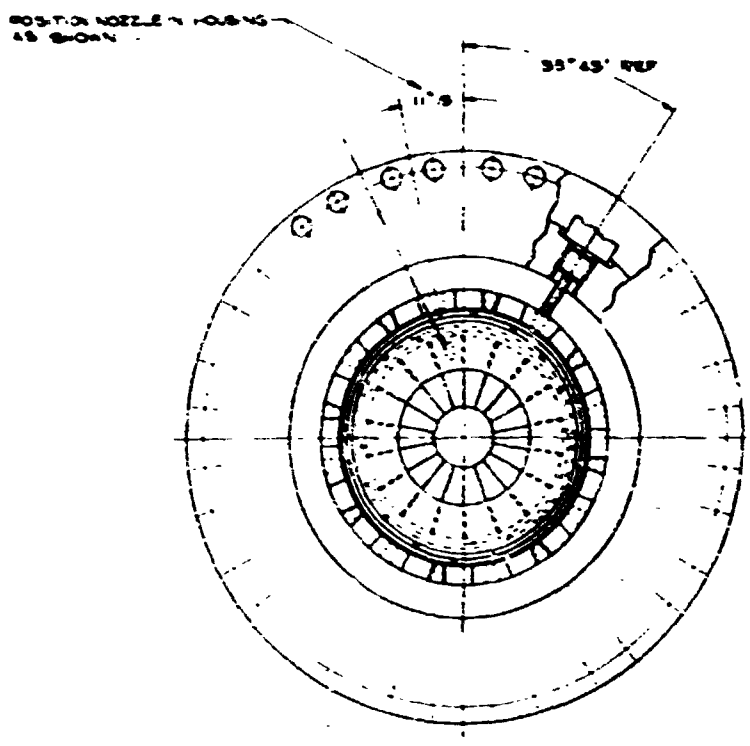

SECTION B-B

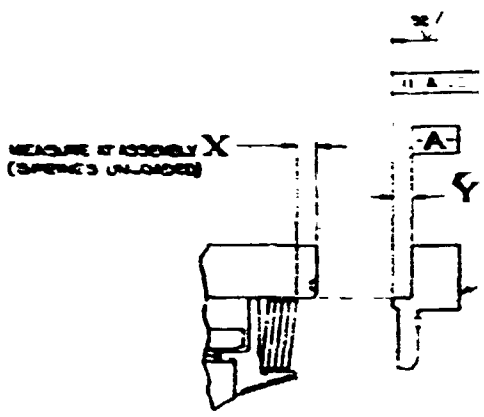

VIEW AT D
SHOWING METHOD OF OBTAINING Y DIM. OF L33E746 ITEM A3

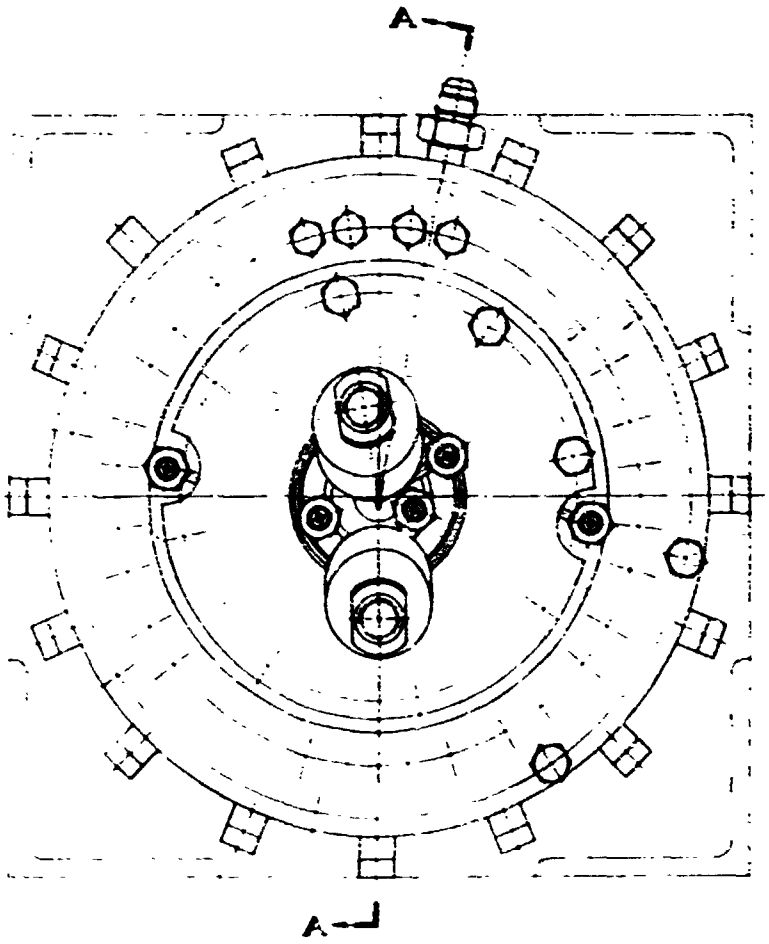

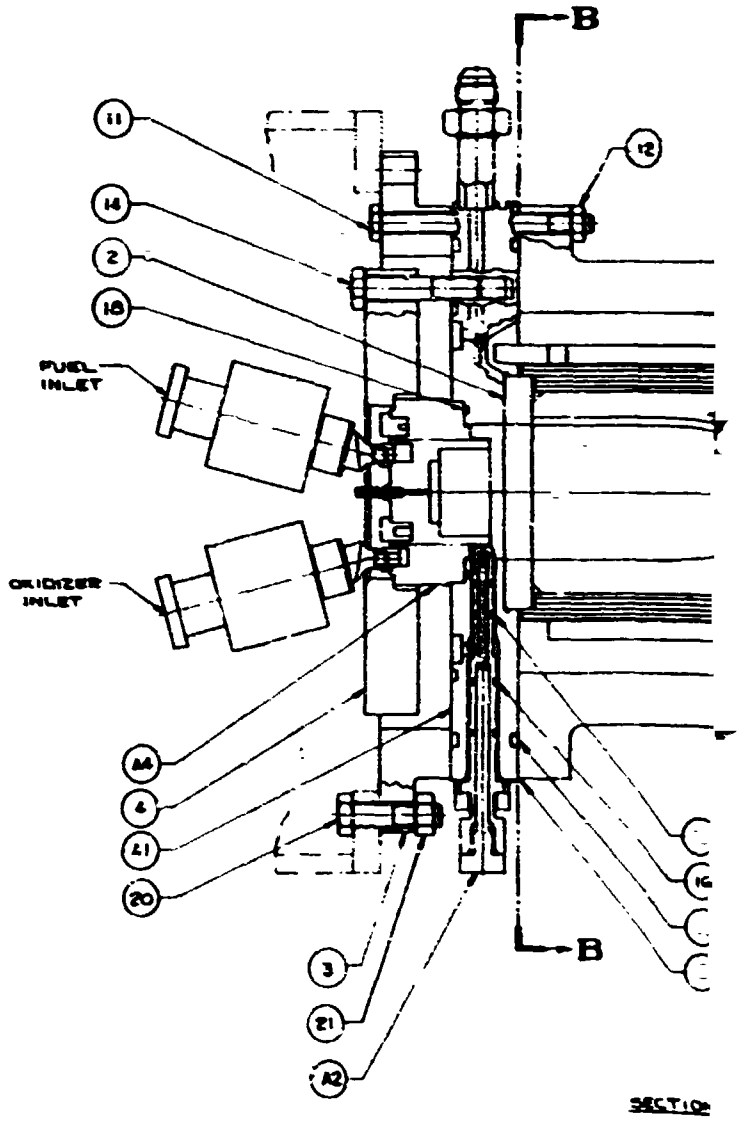

SECTION

FOLDOUT FRAME 2

WLR23 RIG ENGINE ASSEMBLY (LS32746)

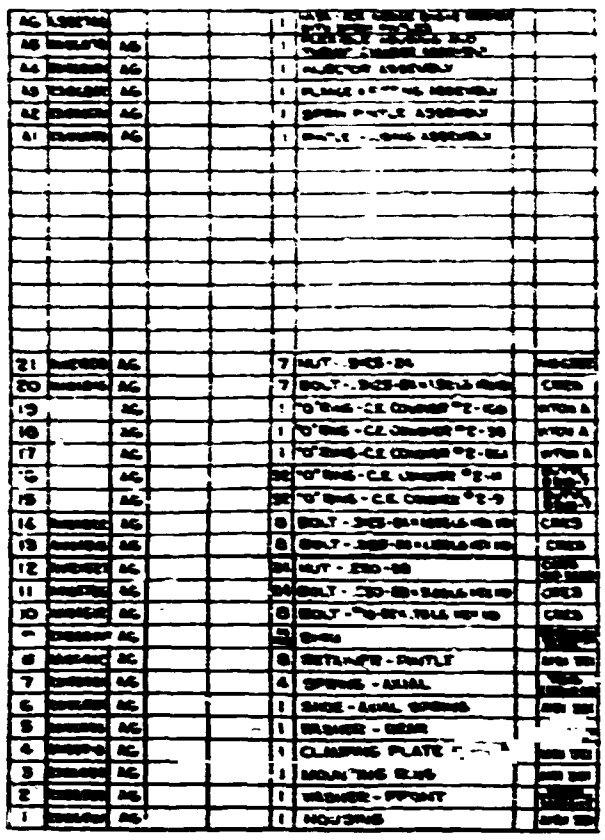

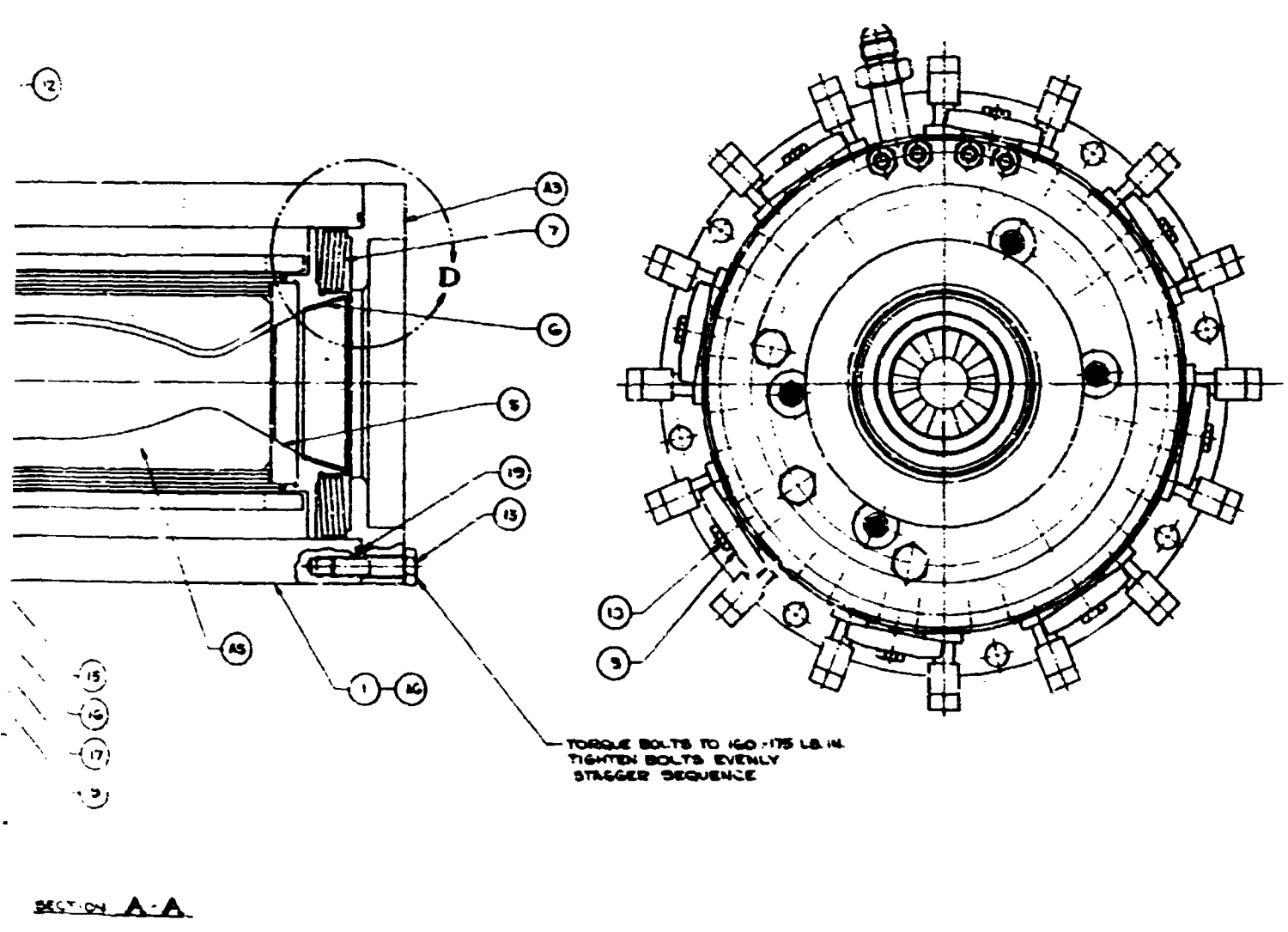

SECTION A-A

Figure 4

SKETCH OF THE WLR23 ENGINE INTERNAL DESIGN

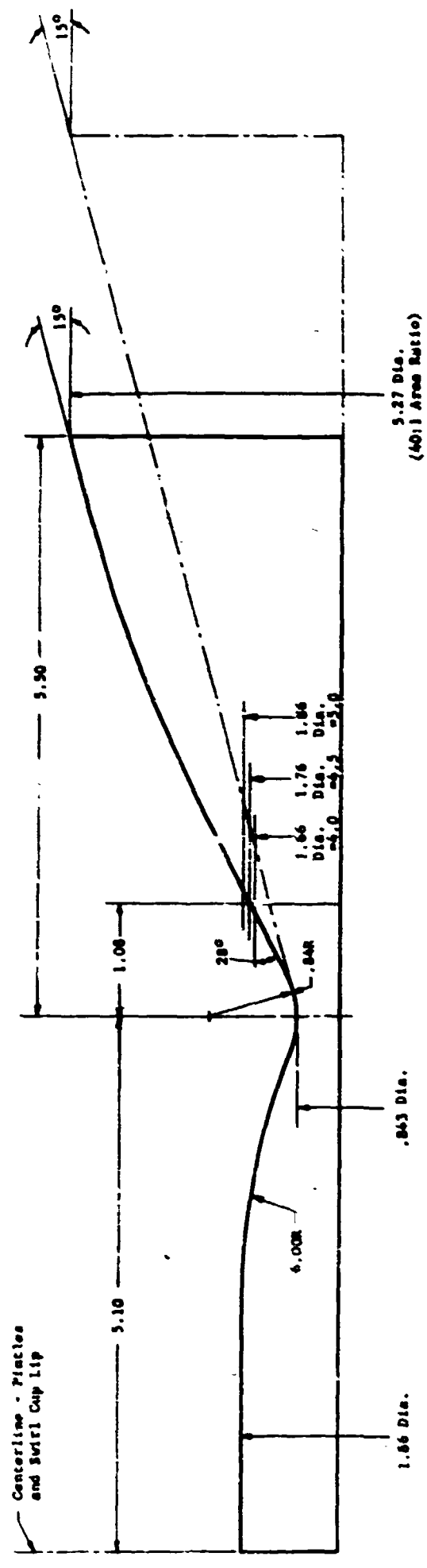

Figure 5

WLR23 AXIAL BELLEVILLE SPRING ASSEMBLY

Load and Stress vs Deflection

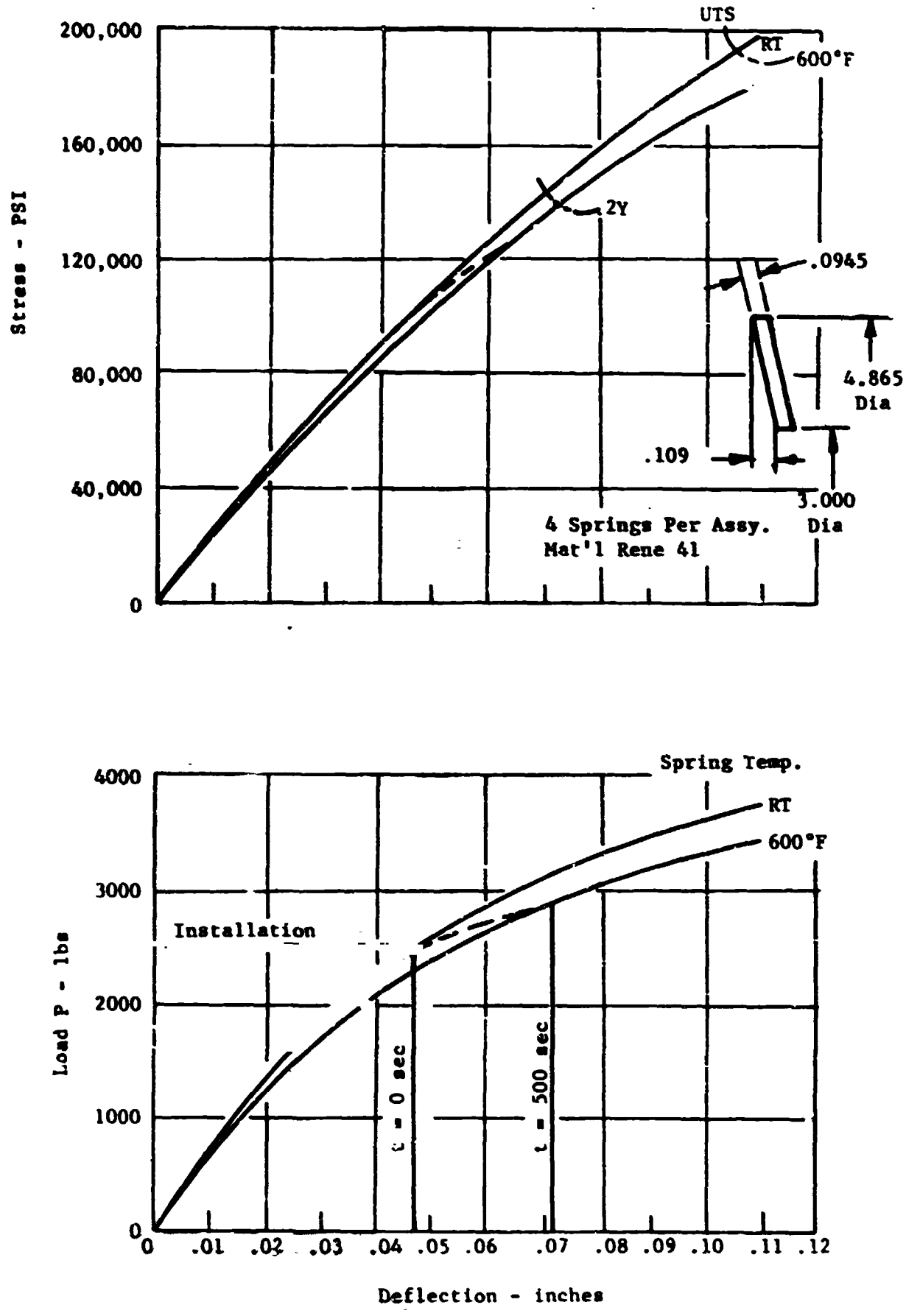

Figure 6

FOLLOW FRAME 1

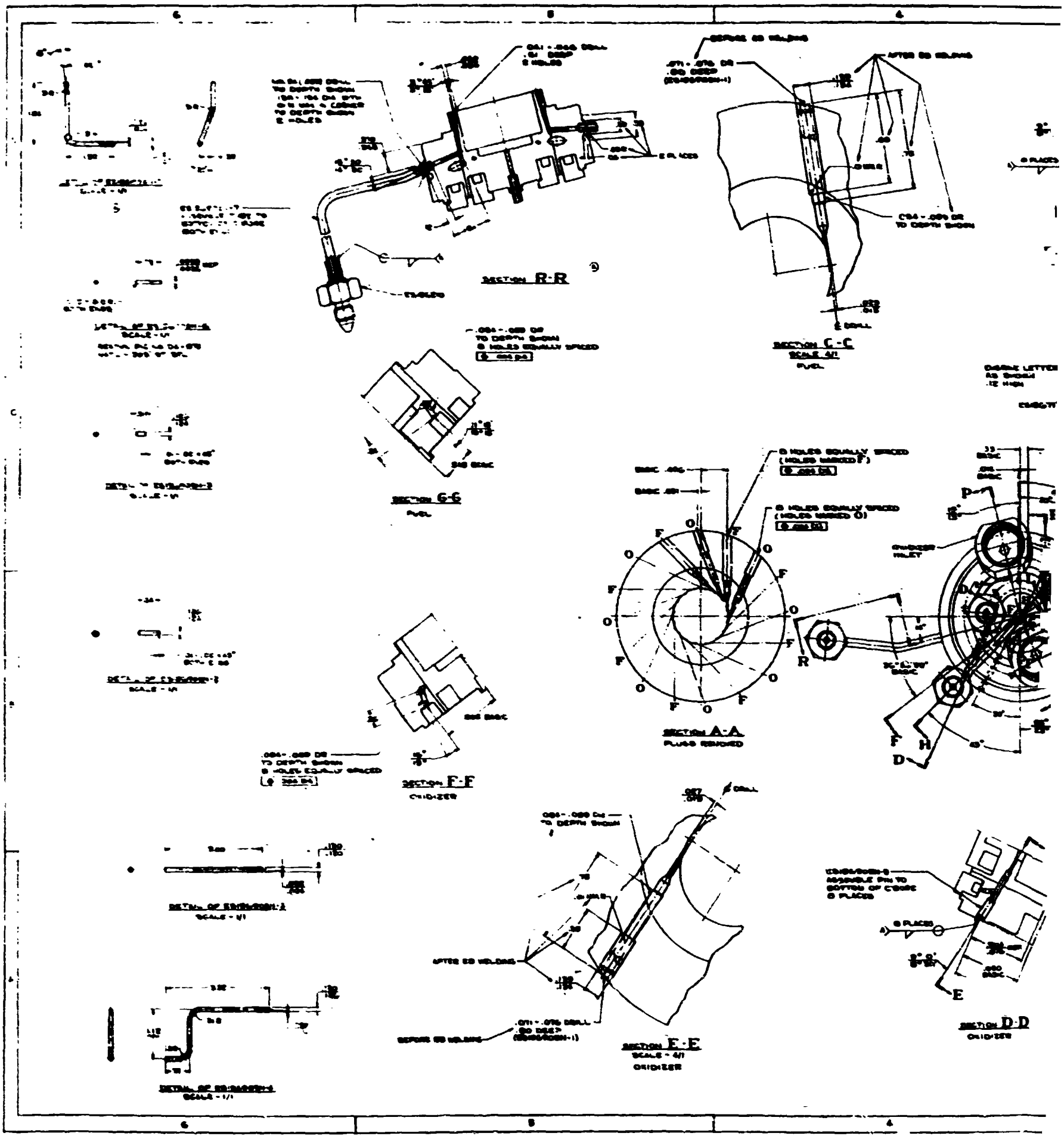

FOLDOUT FRAME 2

INJECTOR ASSEMBLY
(ES156903N)

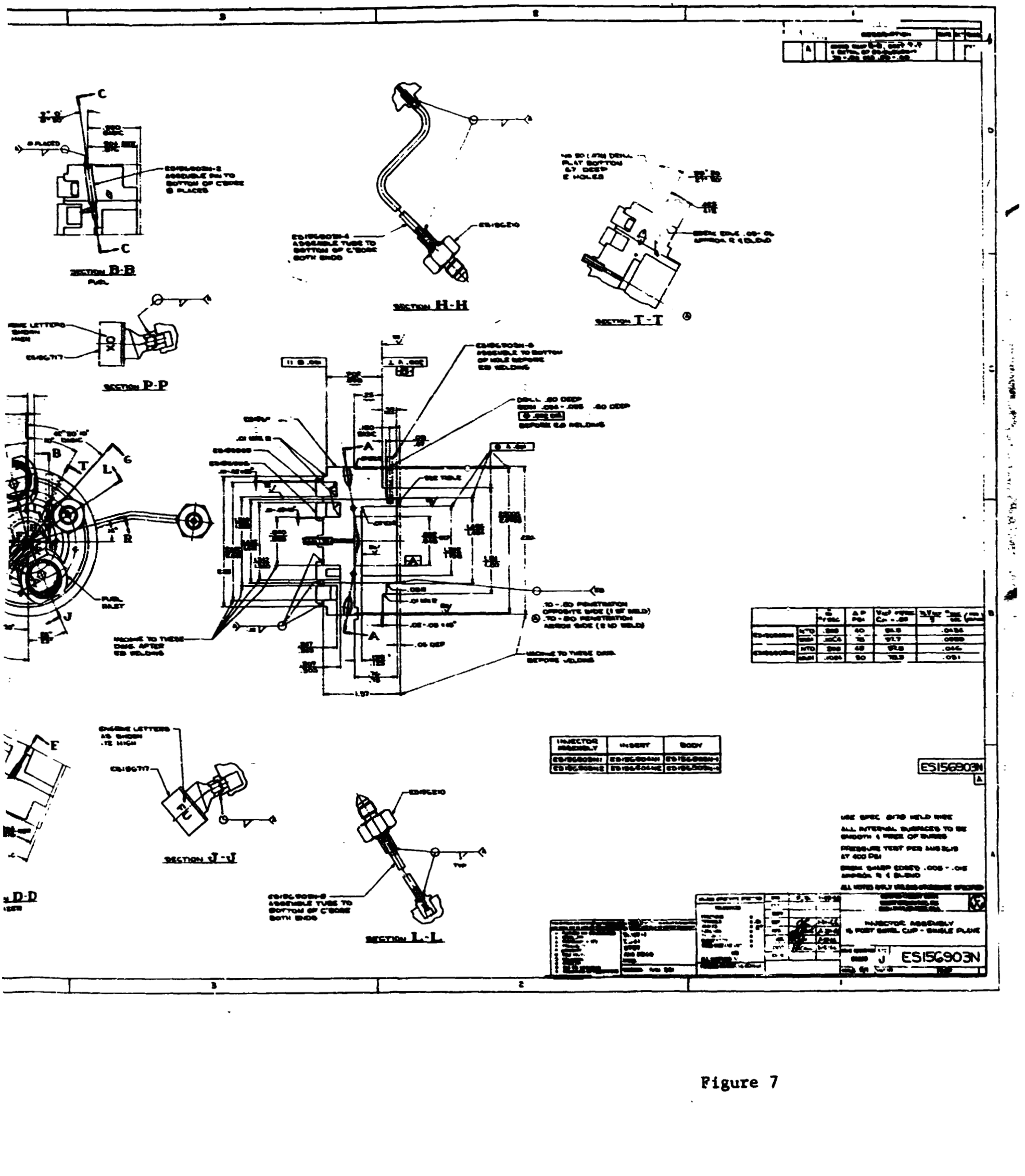

Figure 7

FOLDOUT FRAME 1

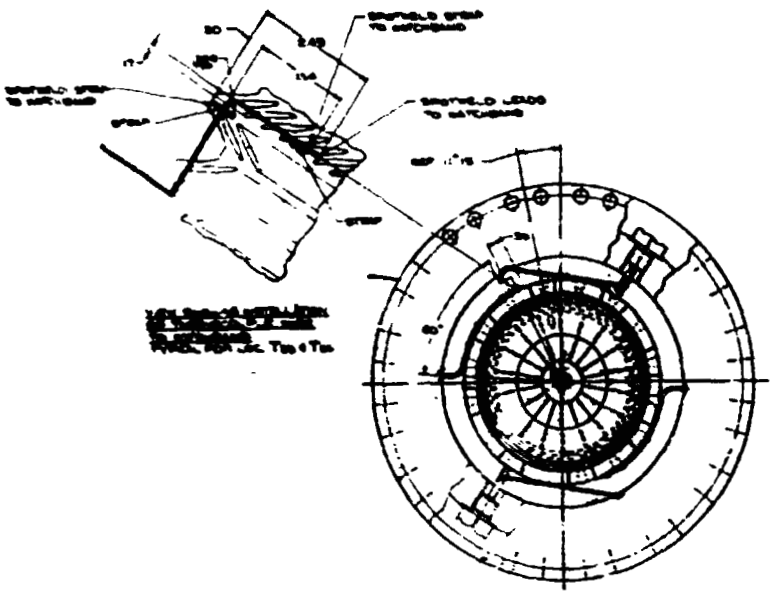

SECTION B-B

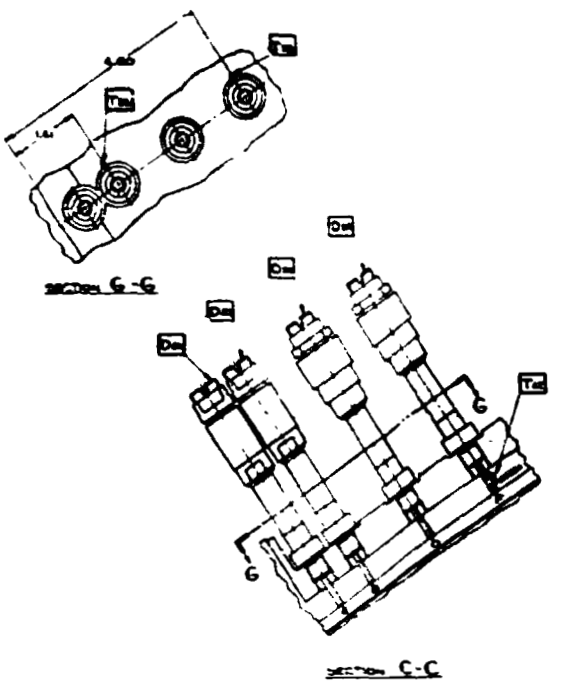

SECTION C-C

SECTION G-G

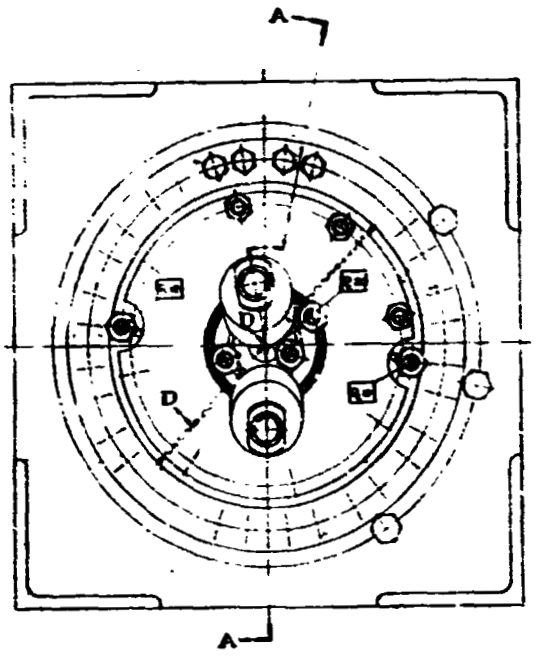

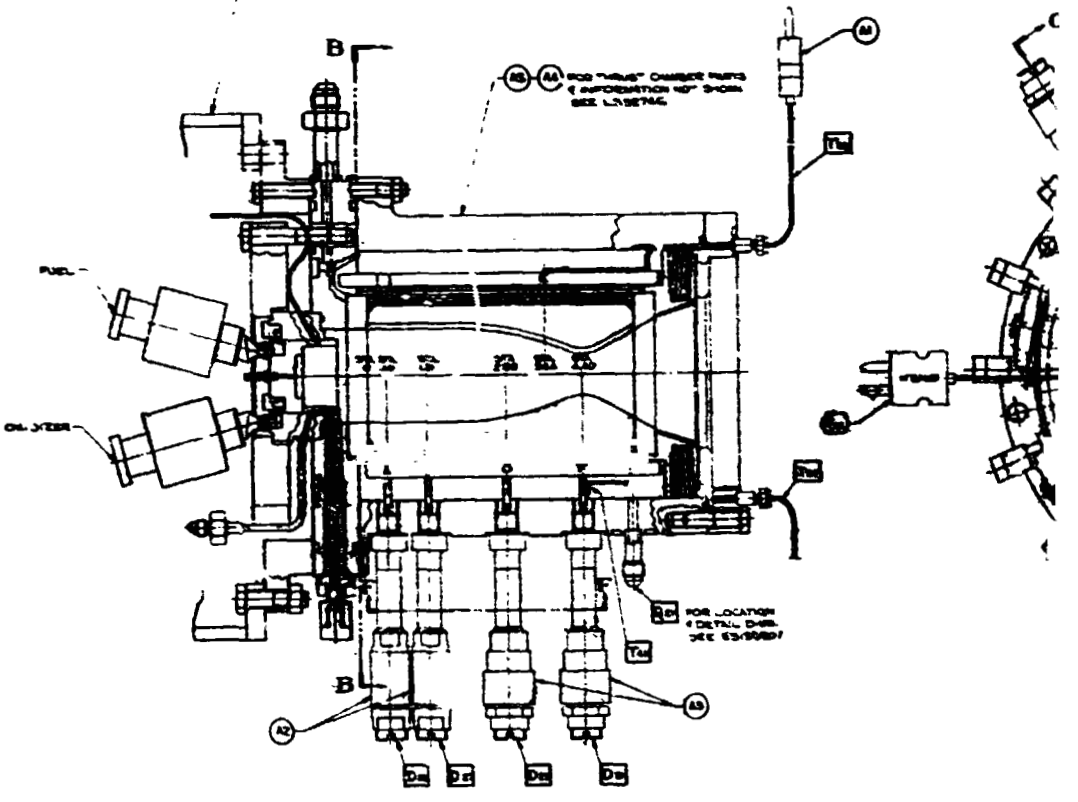

SECTION A-A

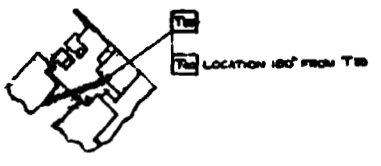

SECTION D-D

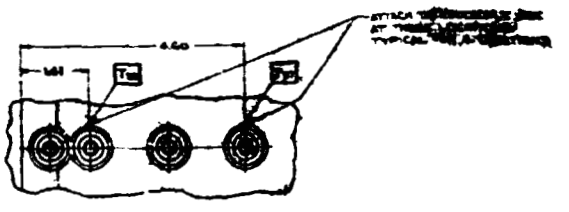

SECTION E-E

FOLDOUT FRAME 2

WLR23 RIG ENGINE INSTRUMENTATION (LS32766)

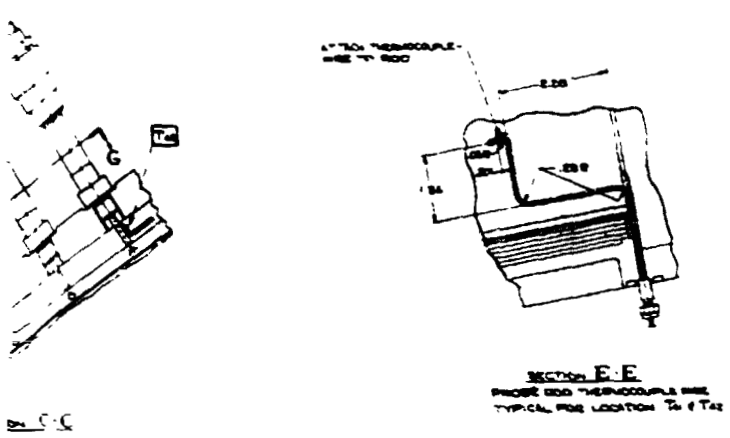

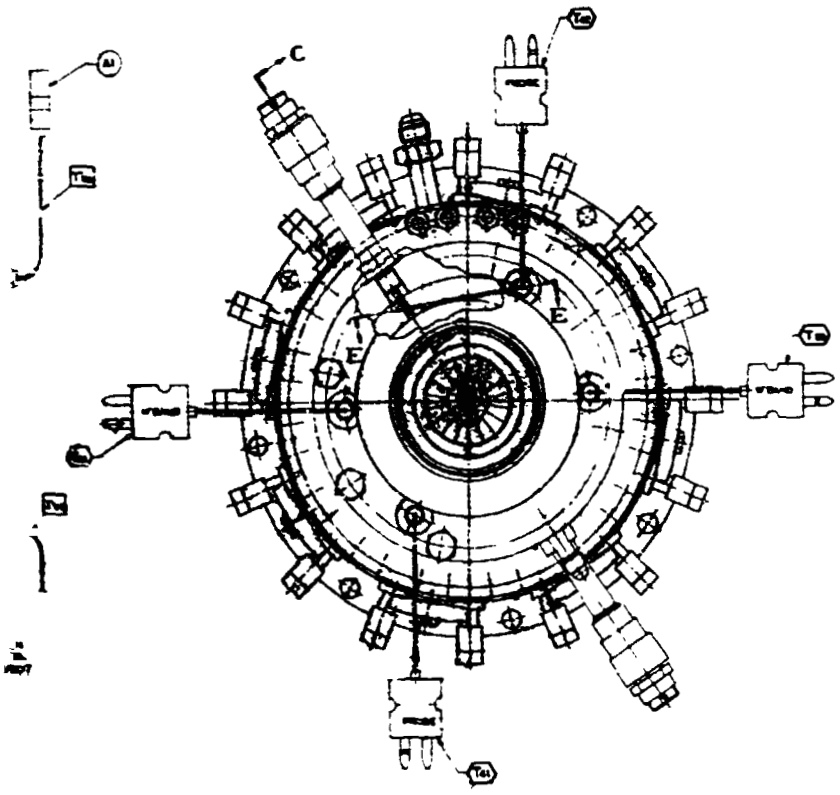

PERMANENT VAN DYKE

Figure 8

RIG ENGINE WITH COPPER CHAMBER (LS32643)

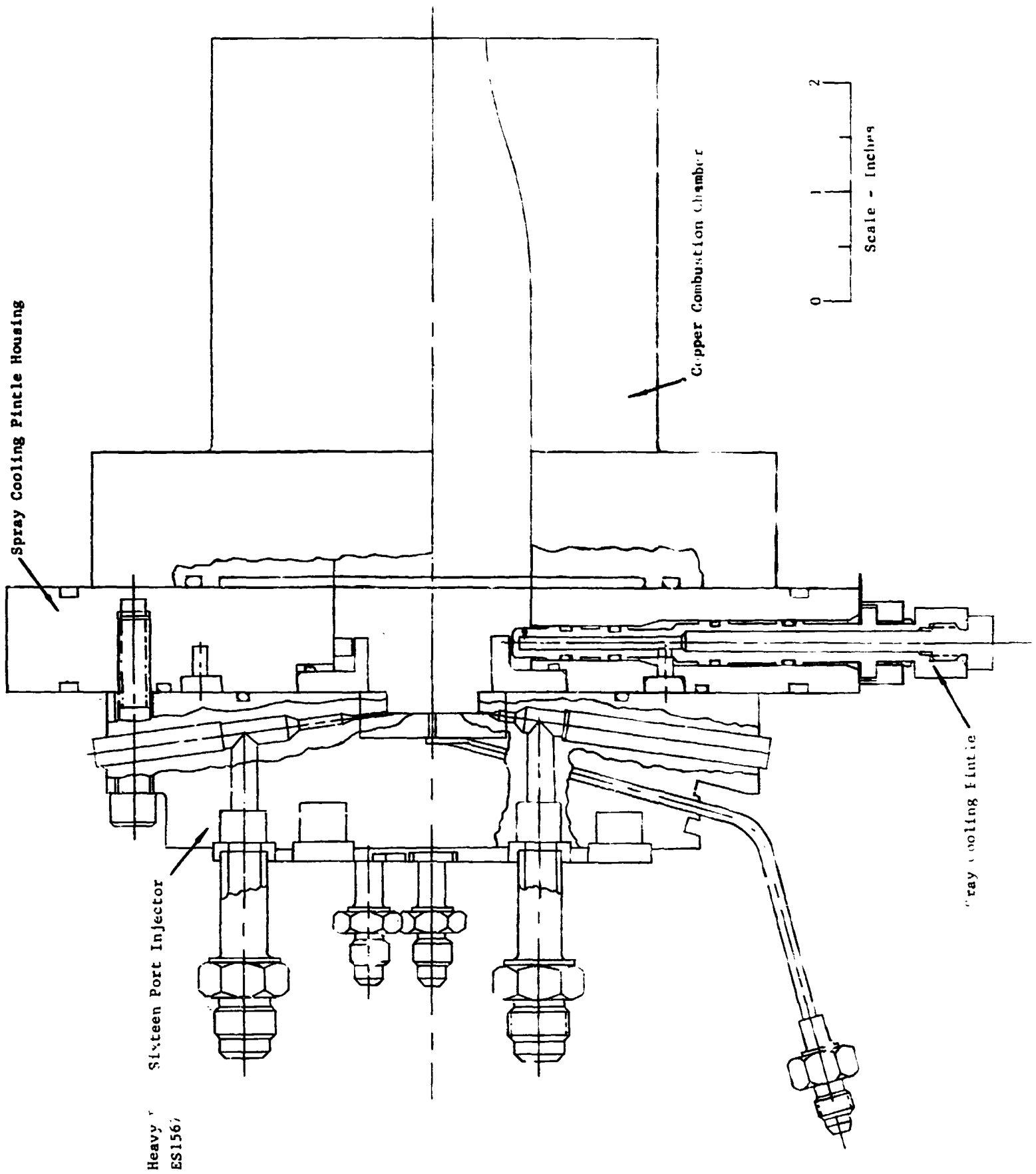

Figure 9

COPPER COMBUSTION CHAMBER THERMOCOUPLE LOCATIONS

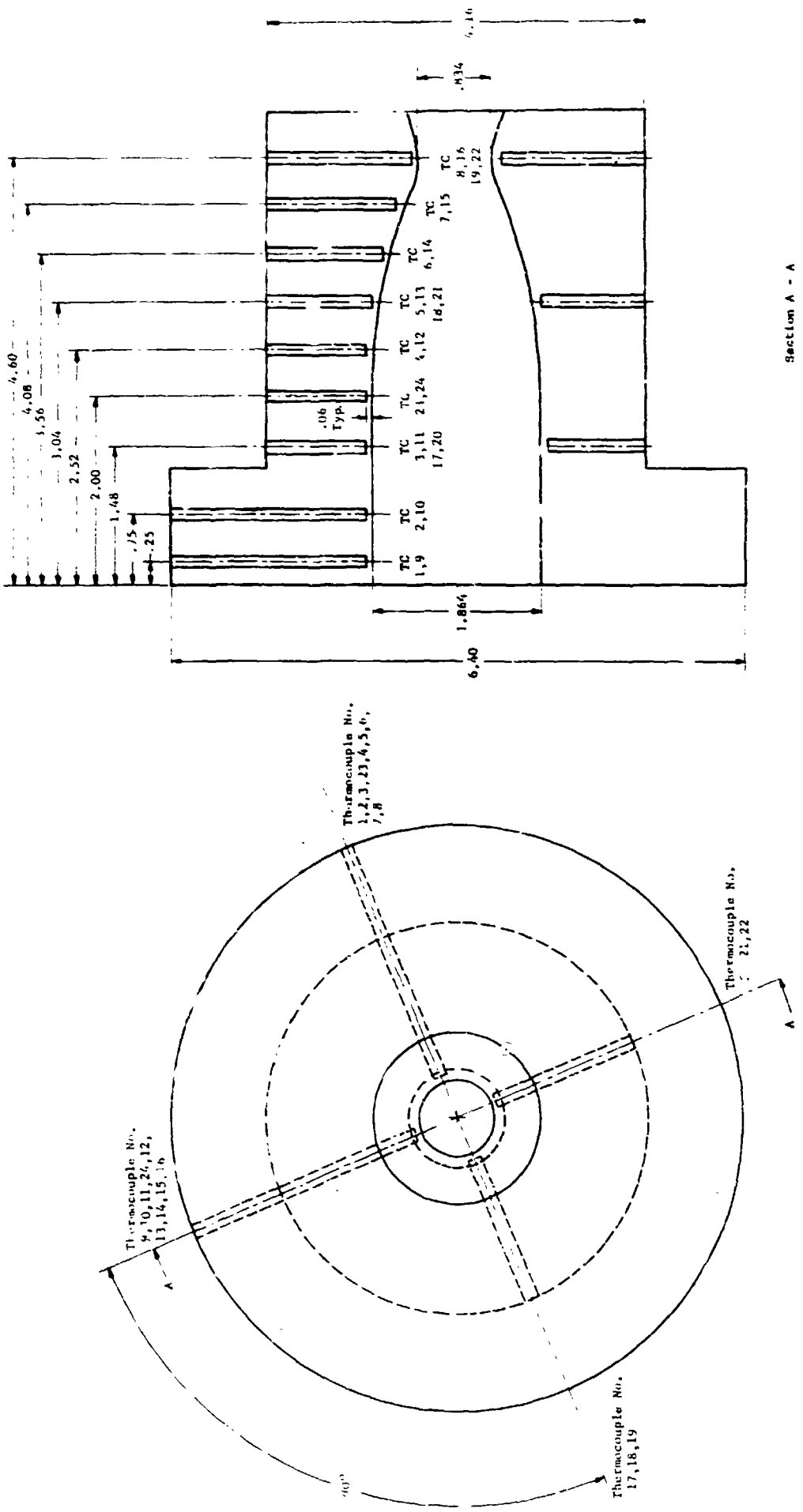

18-508

Figure 10

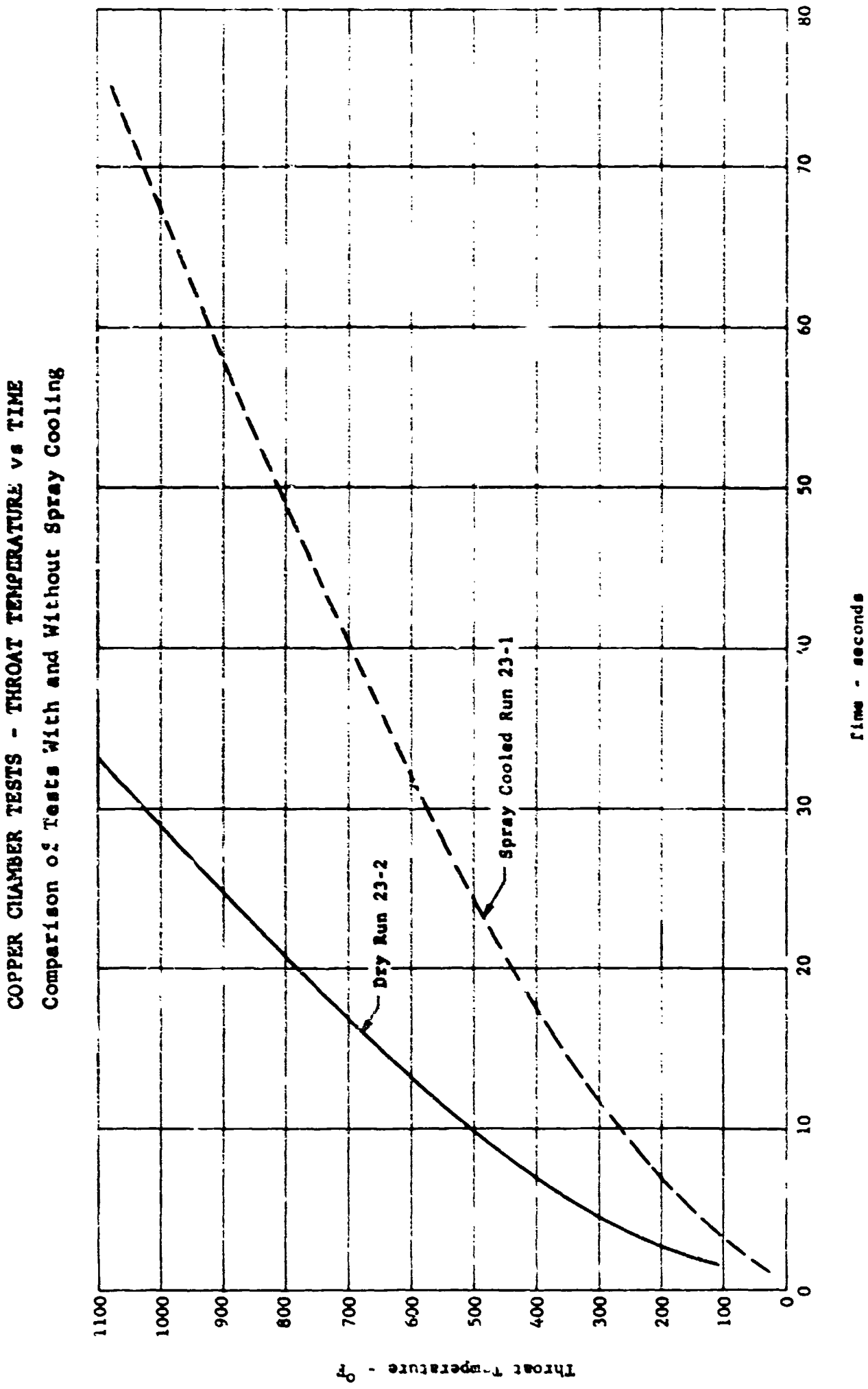
COPPER CHAMBER TESTS - THROAT TEMPERATURE vs TIME
Comparison of Tests With and Without Spray Cooling
Dry Run 23-2
Spray Cooled Run 23-1
Throat Temperature - °F
Time - seconds
1100
1000
900
800
700
600
500
400
300
200
100
0
10
20
30
40
50
60
70
80

Figure 11

TRANSIENT PRESSURE MEASUREMENTS

Engine Firing Time 28 Seconds

Test No.23-1

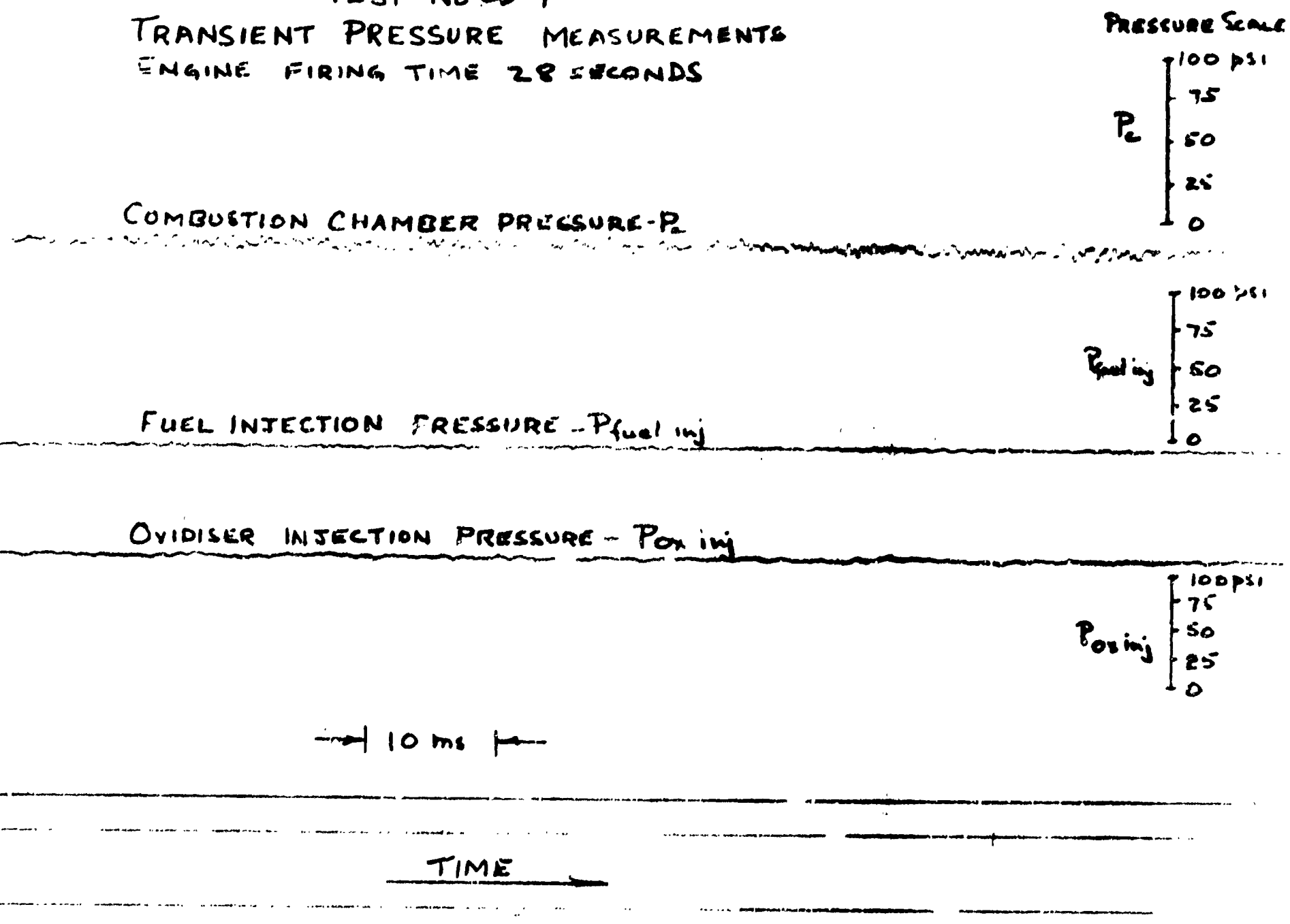

Figure 12

TRANSIENT PRESSURE MEASUREMENTS

Engine Firing Time 28 Seconds

Test No.23-2

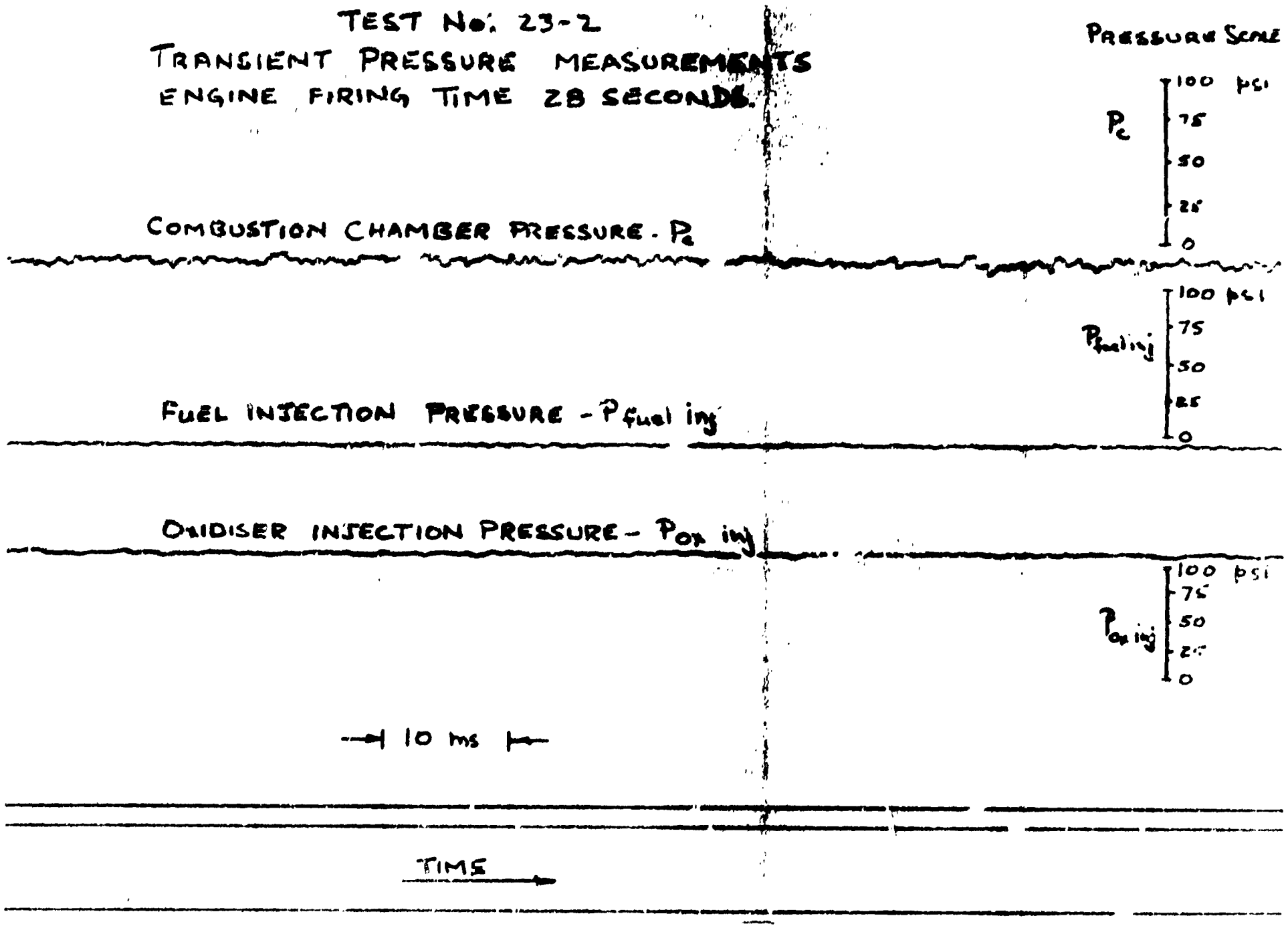

Figure 13

WRIGHT AERONAUTICAL DIVISION • CURTISS-WRIGHT CORPORATION • WOOD-RIDGE, N. J., U. S. A.

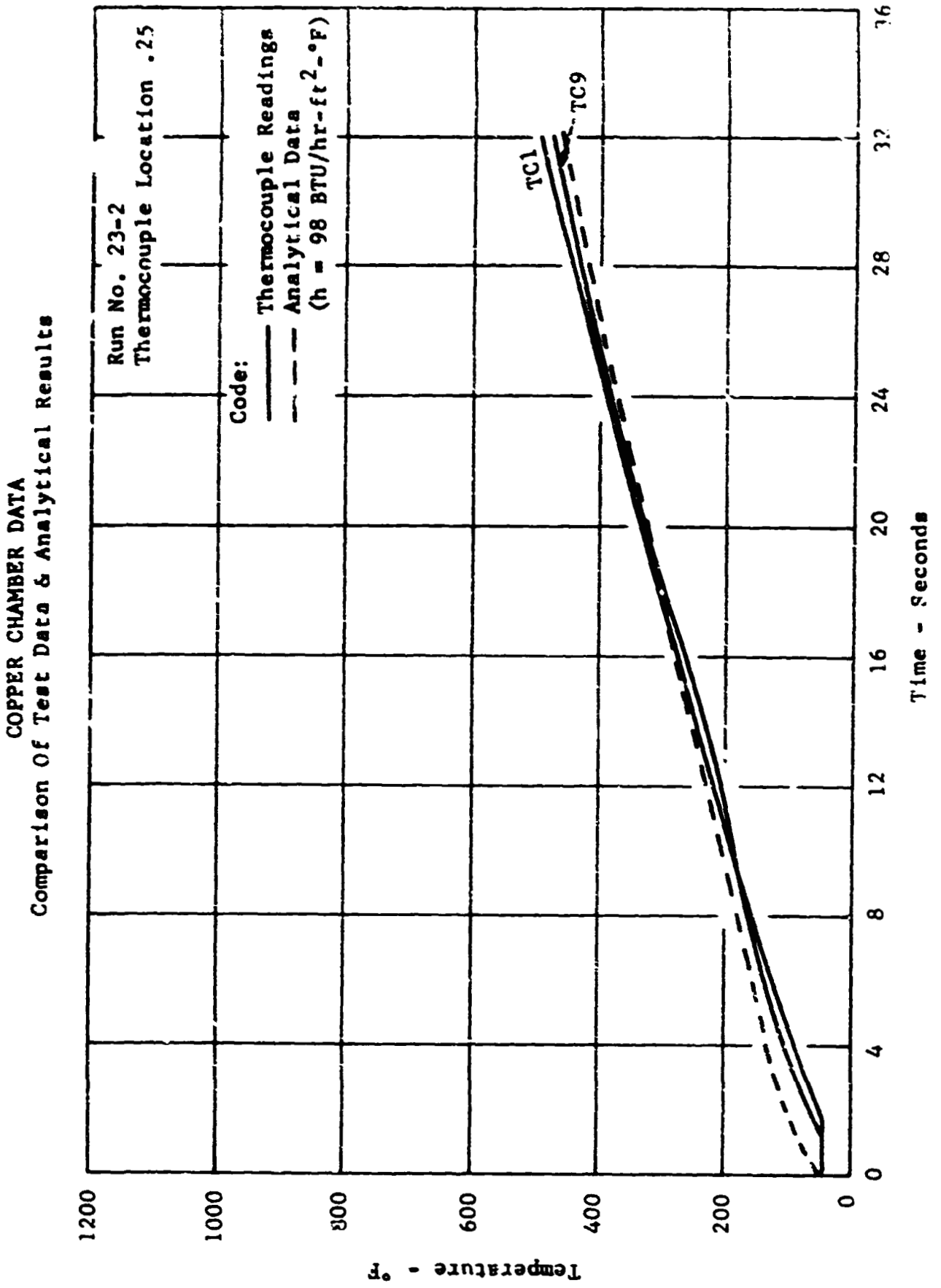
COPPER CHAMBER DATA
Comparison Of Test Data & Analytical Results
Run No. 23-2
Thermocouple Location .25
Code:
—— Thermocouple Readings
— — — Analytical Data
(h = 98 BTU/hr-ft²-°F)
TC1
TC9
Temperature - °F
1200
1000
800
600
400
200
0
Time - Seconds
0
4
8
12
16
20
24
28
32

Figure 14

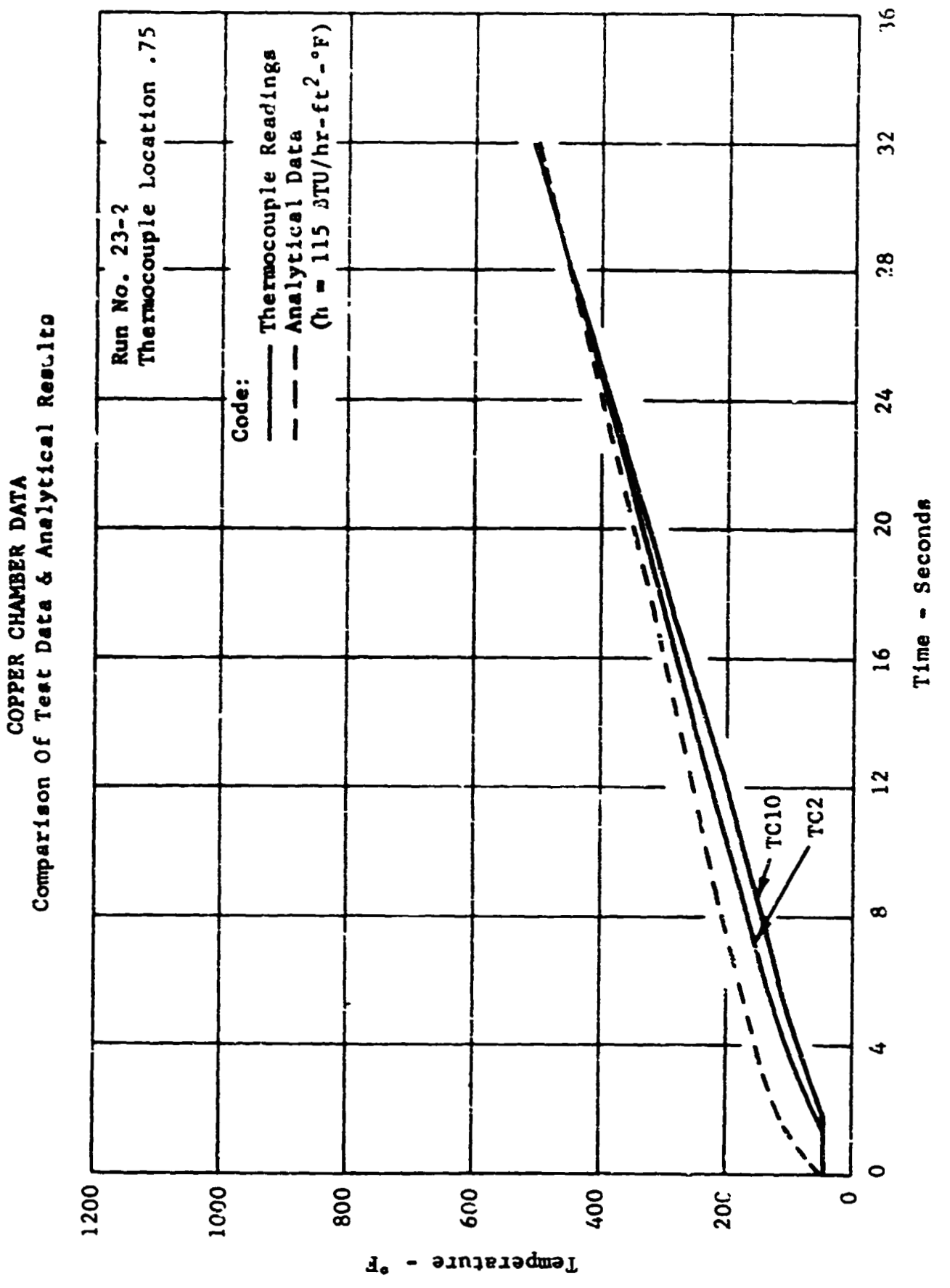
COPPER CHAMBER DATA
Comparison Of Test Data & Analytical Results
Run No. 23-2
Thermocouple Location .75
Code:
Thermocouple Readings
Analytical Data
(h = 115 BTU/hr-ft²-°F)
TC10
TC2
Temperature - °F
1200
1000
800
600
400
200
0
0
4
8
12
16
20
24
28
32
36
Time - Seconds

Figure 15

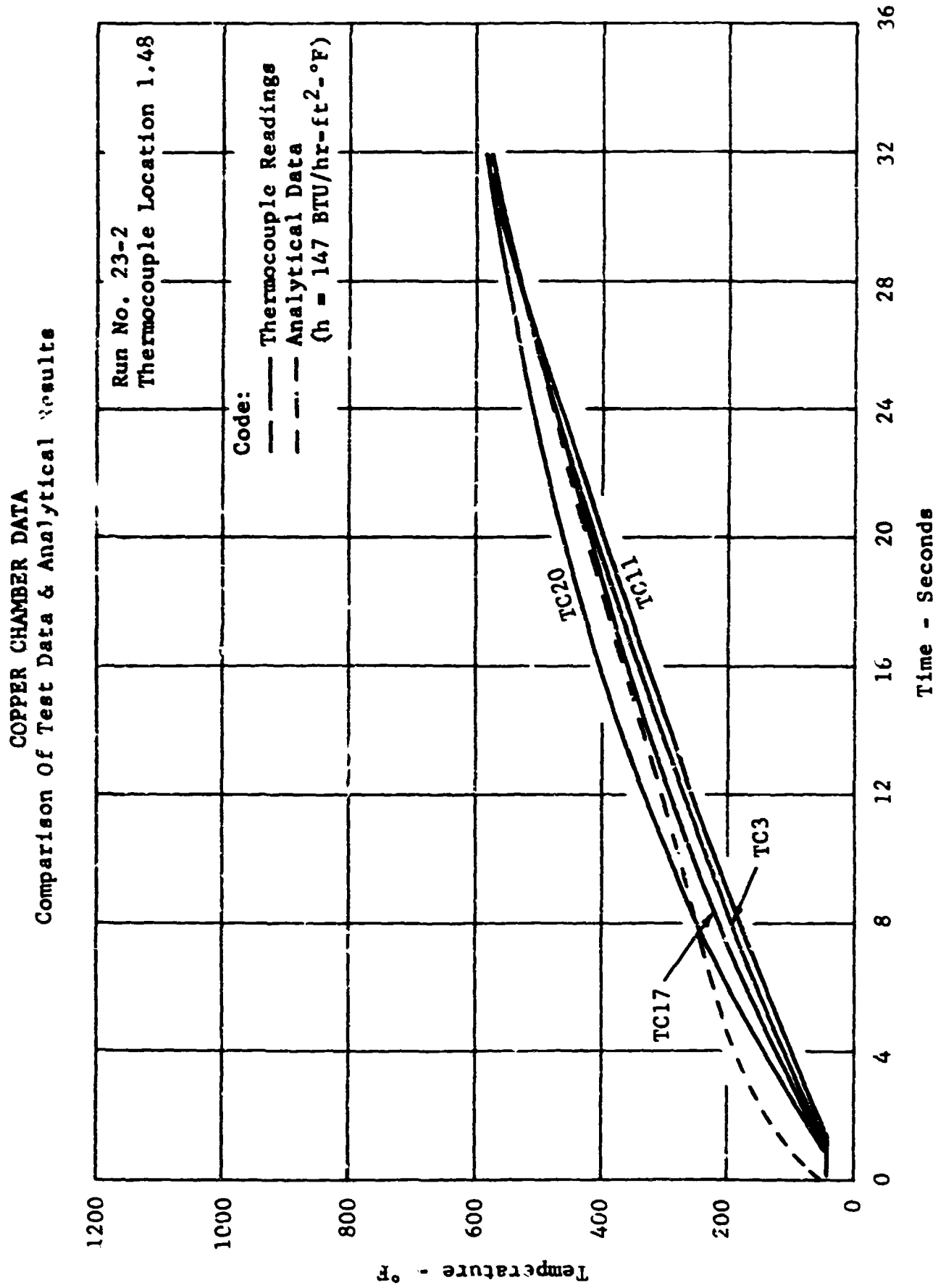
COPPER CHAMBER DATA
Comparison Of Test Data & Analytical Results
Run No. 23-2
Thermocouple Location 1.48
Code:
—— Thermocouple Readings
— —. — Analytical Data
(h = 147 BTU/hr-ft²-°F)
TC20
TC11
TC3
TC17
Temperature - °F
1200
1000
800
600
400
200
0
Time - Seconds
0
4
8
12
16
20
24
28
32
36

Figure 16

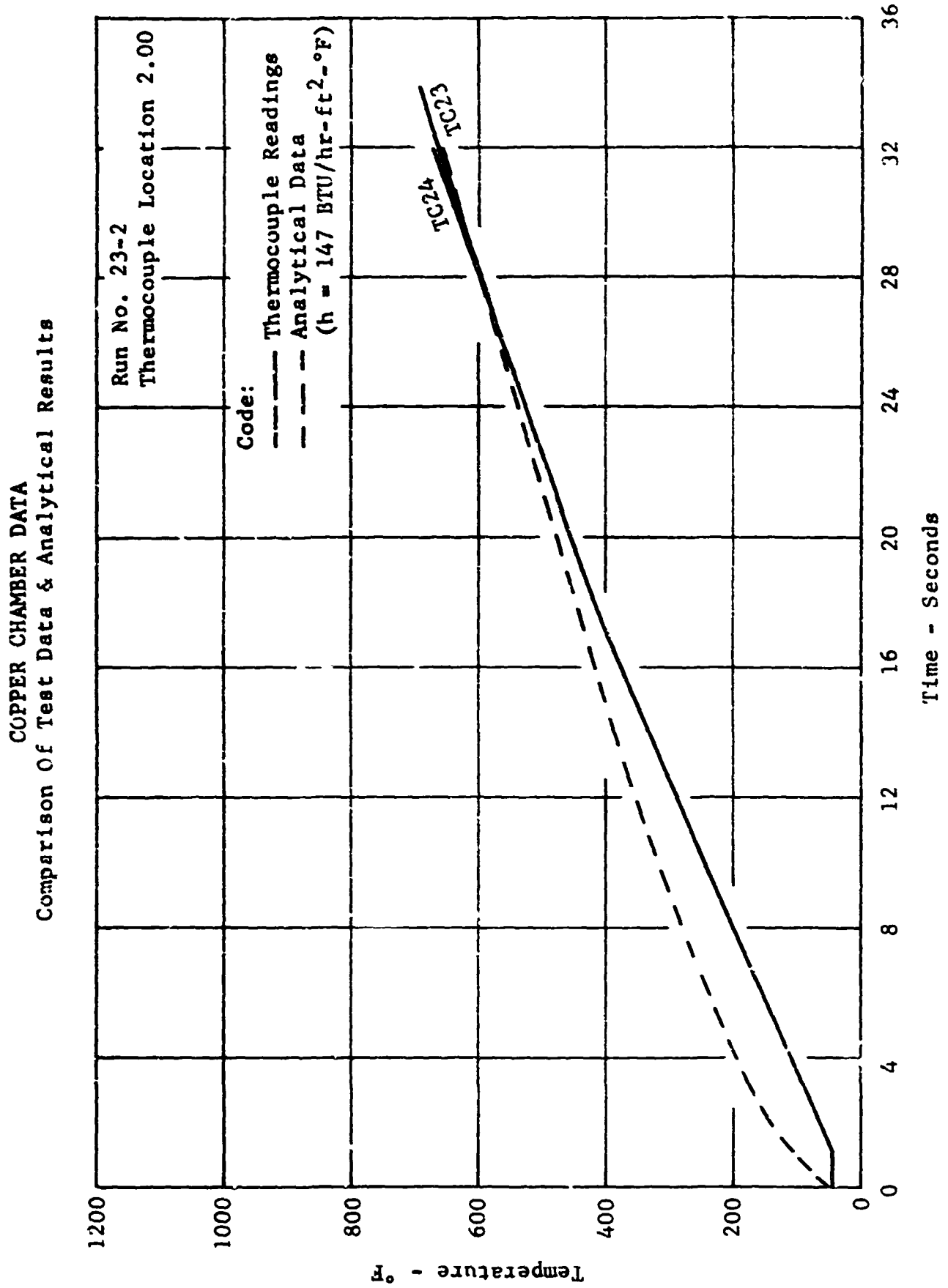
COPPER CHAMBER DATA
Comparison Of Test Data & Analytical Results
Run No. 23-2
Thermocouple Location 2.00
Code:
—— —— Thermocouple Readings
— — — Analytical Data
(h = 147 BTU/hr-ft²-°F)
TC24
TC23
Temperature - °F
1200
1000
800
600
400
200
0
Time - Seconds
0
4
8
12
16
20
24
28
32
36

Figure 17

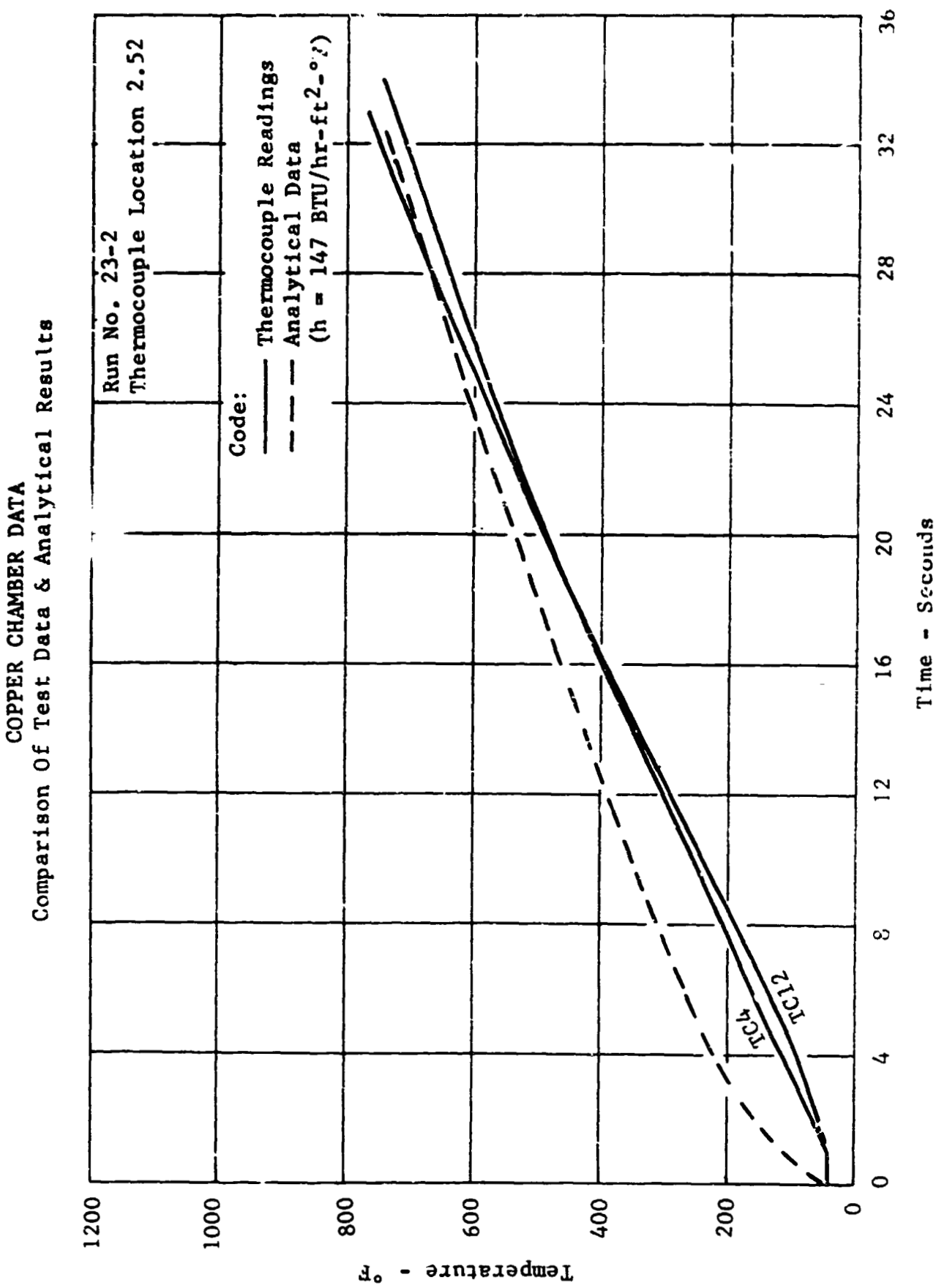
COPPER CHAMBER DATA
Comparison Of Test Data & Analytical Results
Run No. 23-2
Thermocouple Location 2.52
Code:
——— Thermocouple Readings
— — — Analytical Data
(h = 147 BTU/hr-ft²-°F)
TC12
TC4
Temperature - °F
1200
1000
800
600
400
200
0
0
4
8
12
16
20
24
28
32
36
Time - Seconds

Figure 18

COPPER CHAMBER DATA
Comparison Of Test Data & Analytical Results

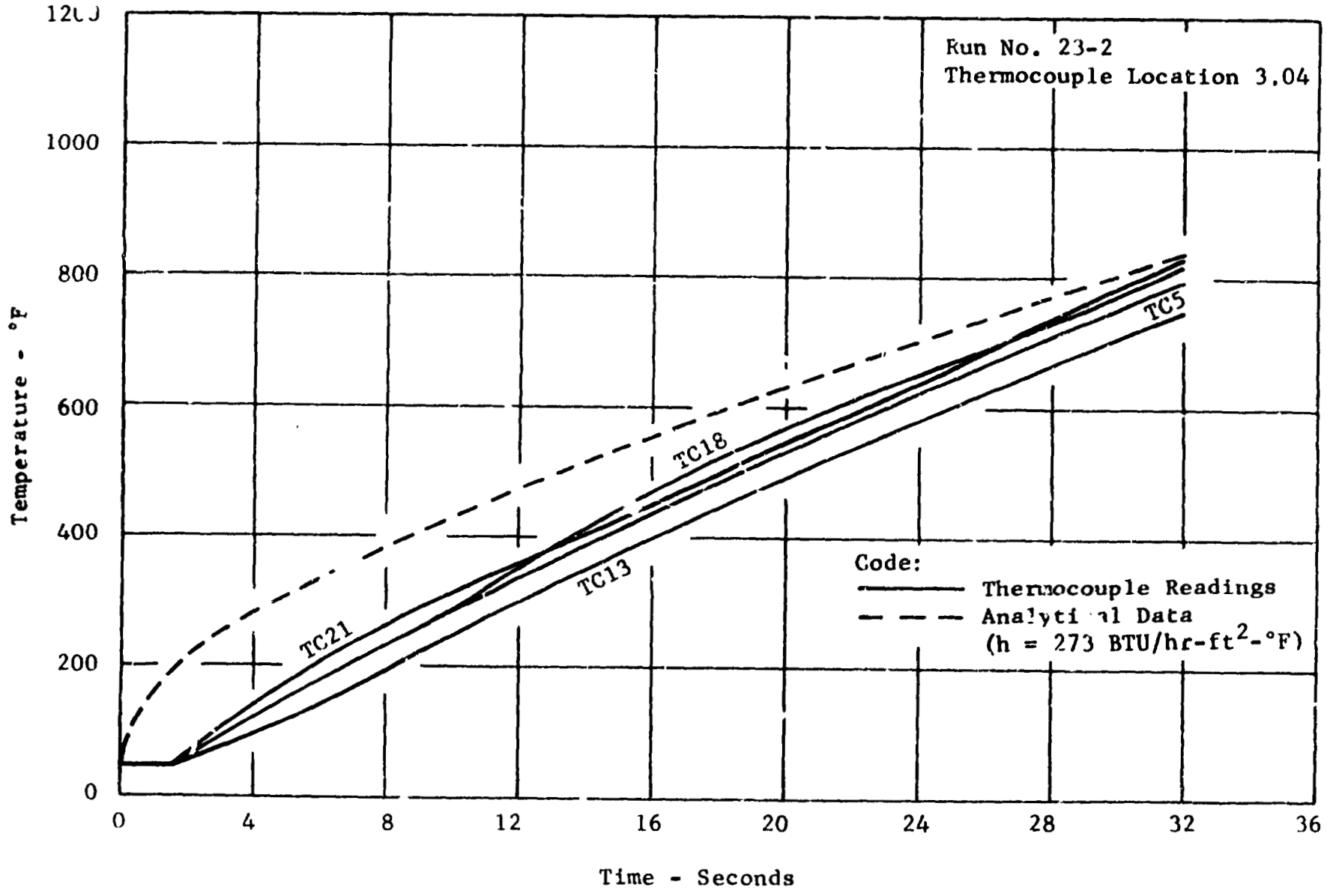

Figure 19

COPPER CHAMBER DATA
Comparison Of Test Data & Analytical Results

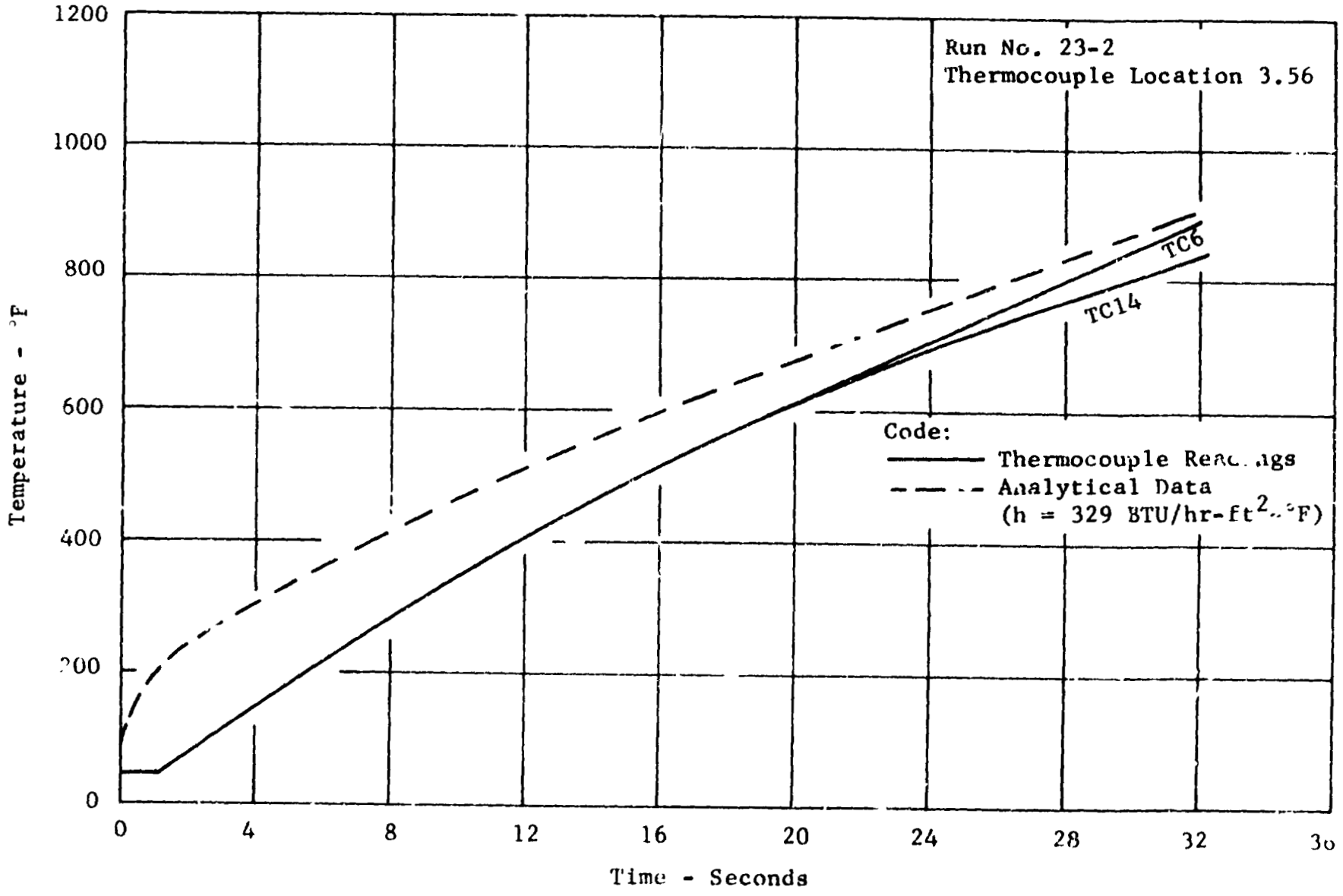

Figure 20

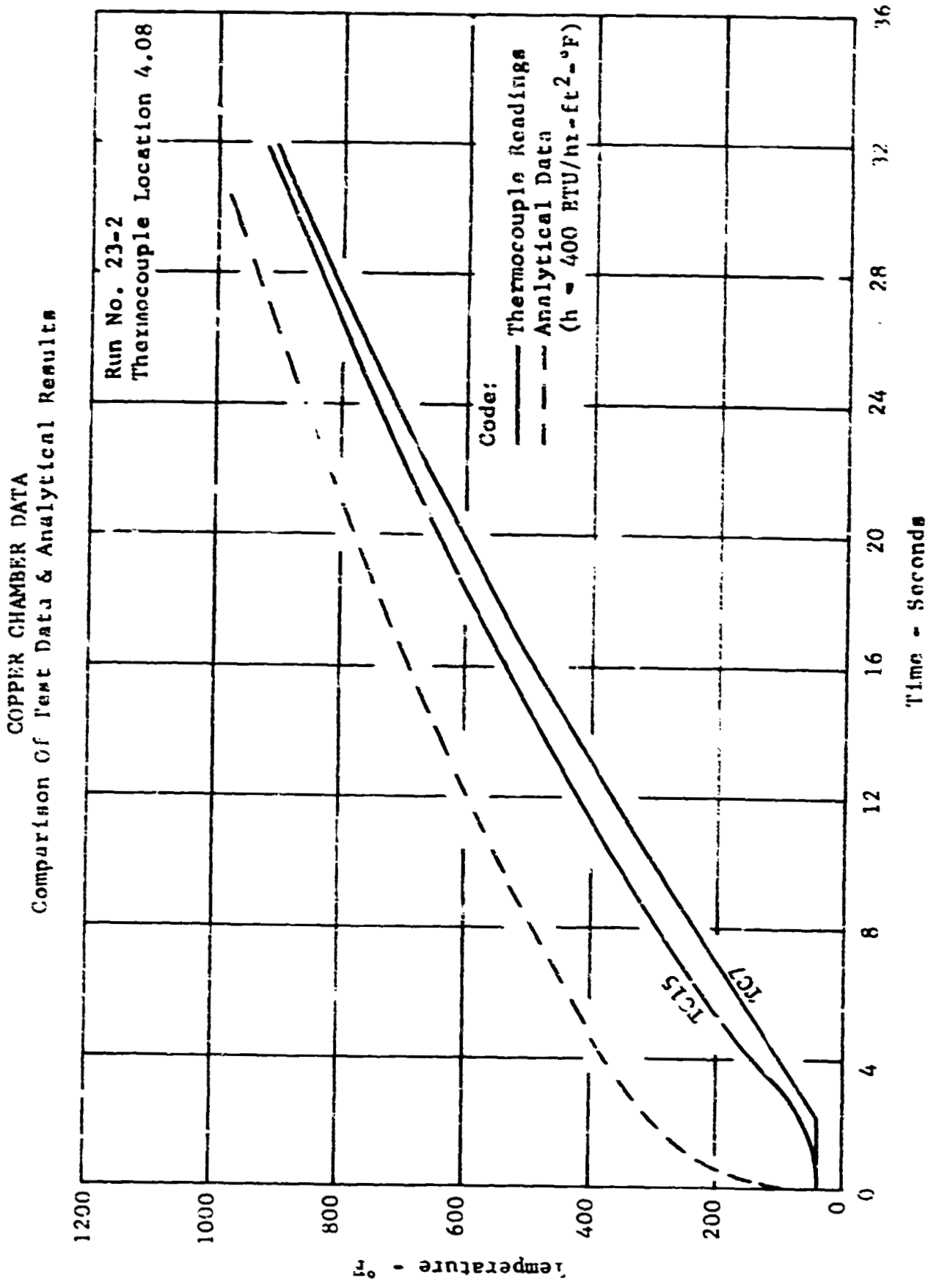
COPPER CHAMBER DATA
Comparison Of Test Data & Analytical Results
Run No. 23-2
Thermocouple Location 4.08
Code:
—— Thermocouple Readings
– – – Analytical Data
(h = 400 BTU/hr-ft²-°F)
TC7
TC15
Temperature - °F
1200
1000
800
600
400
200
0
Time - Seconds
0
4
8
12
16
20
24
28
32
36

Figure 21

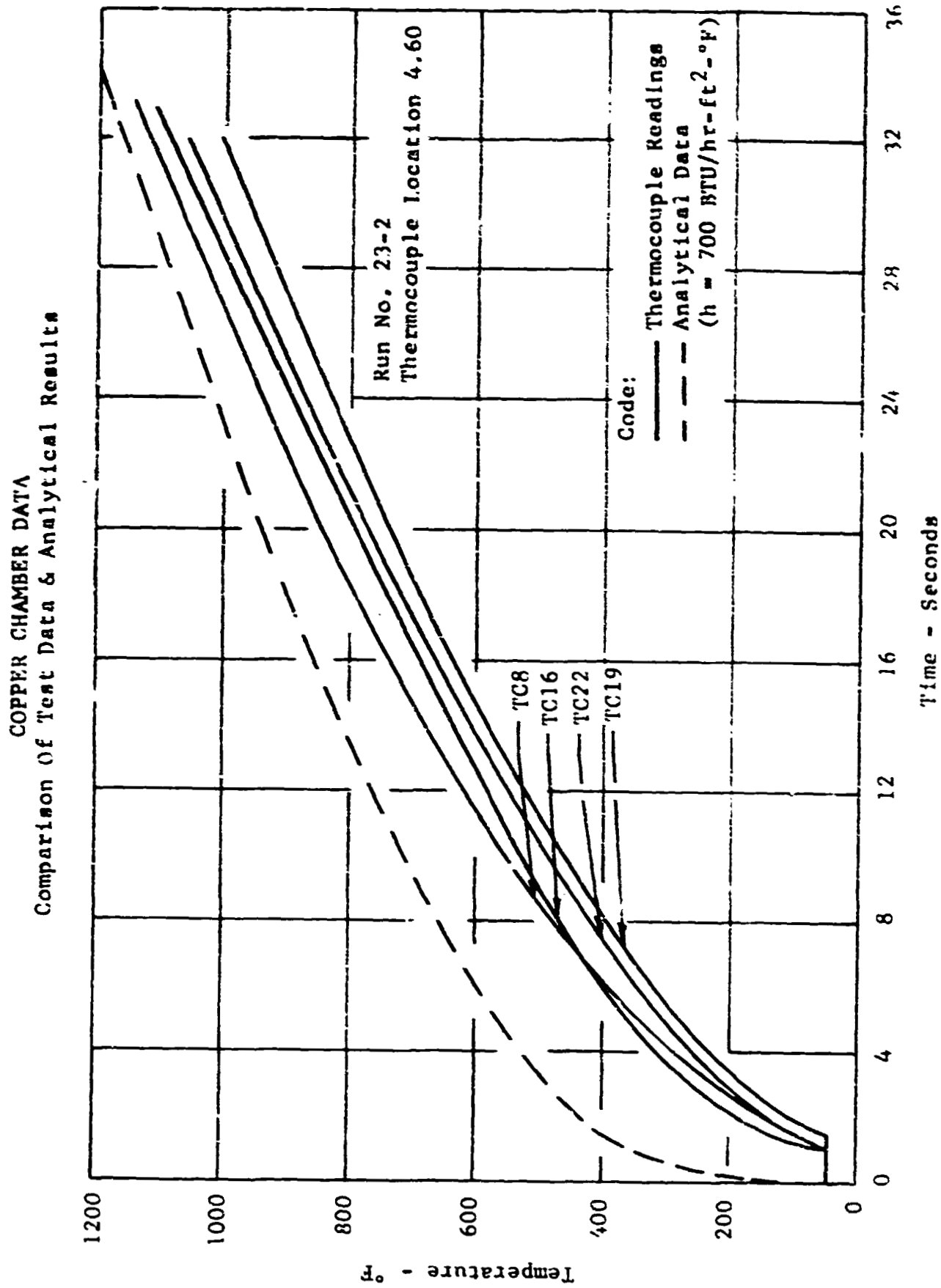
COPPER CHAMBER DATA
Comparison Of Test Data & Analytical Results
Run No. 23-2
Thermocouple Location 4,60
Code:
——— Thermocouple Readings
— — — Analytical Data
(h = 700 BTU/hr-ft²-°F)
TC8
TC16
TC22
TC19
Temperature - °F
Time - Seconds
1200
1000
800
600
400
200
0
0
4
8
12
16
20
24
28
32
36

Figure 22

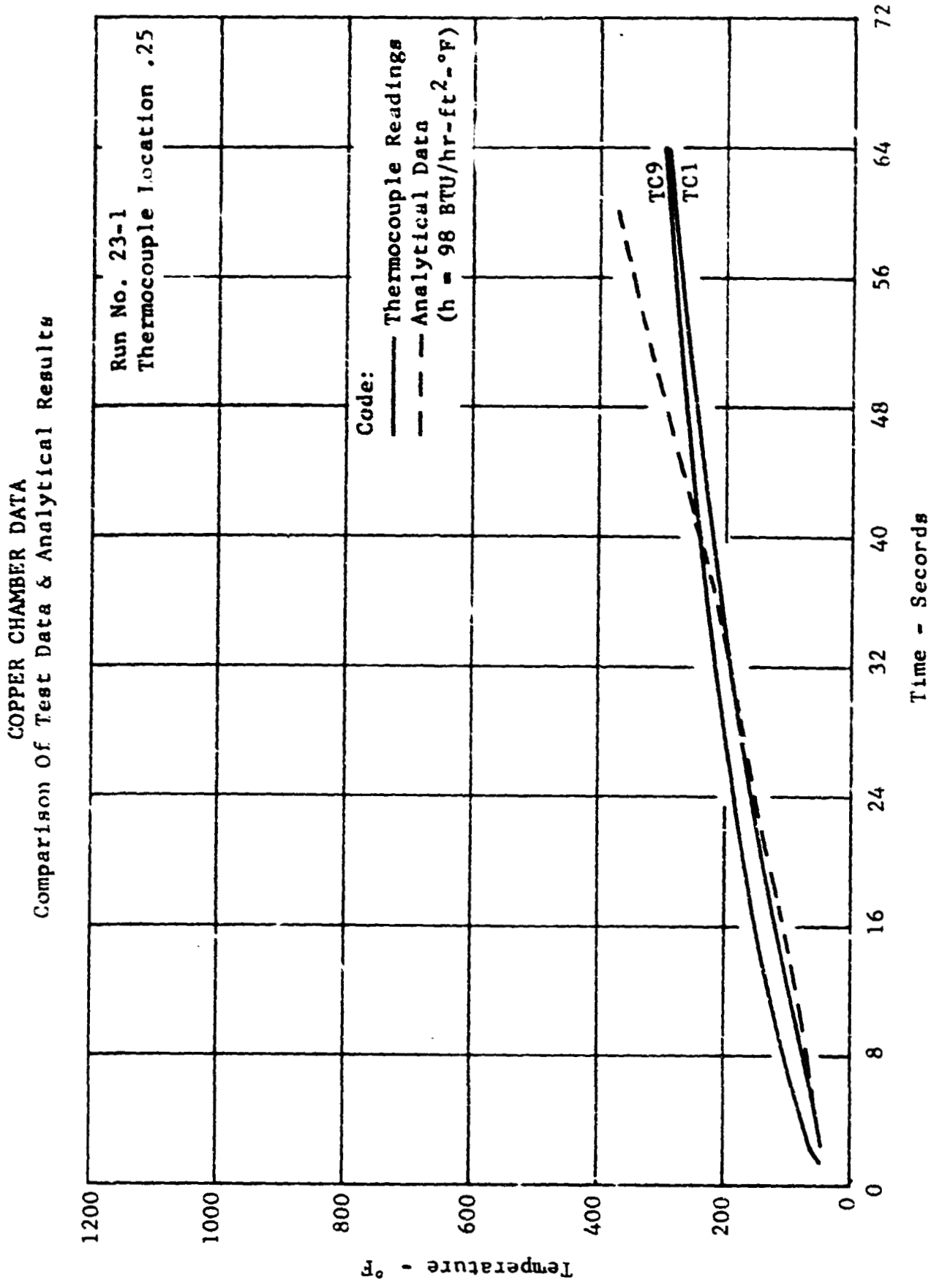

13-258

Figure 23

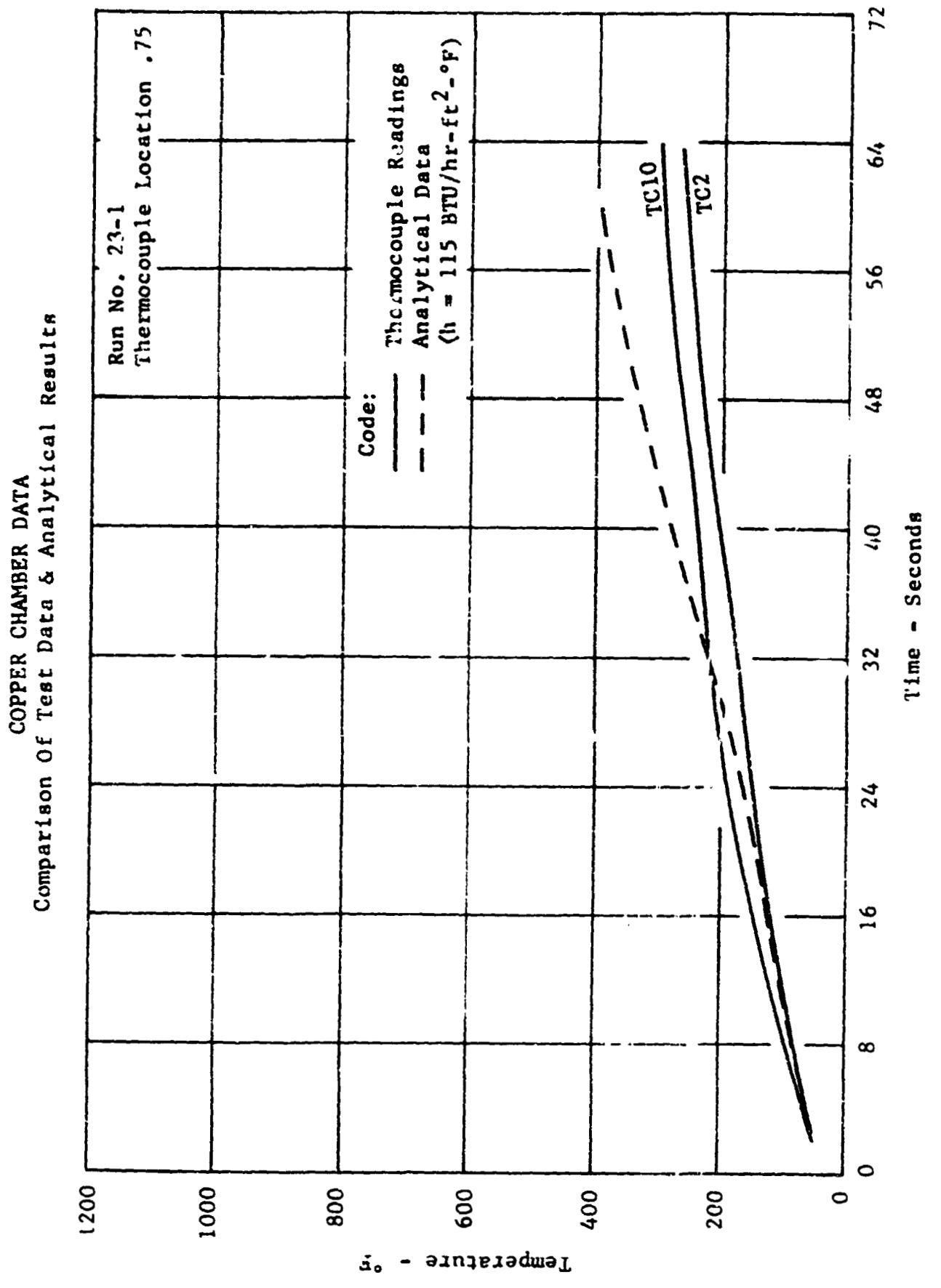

13-255

Figure 24

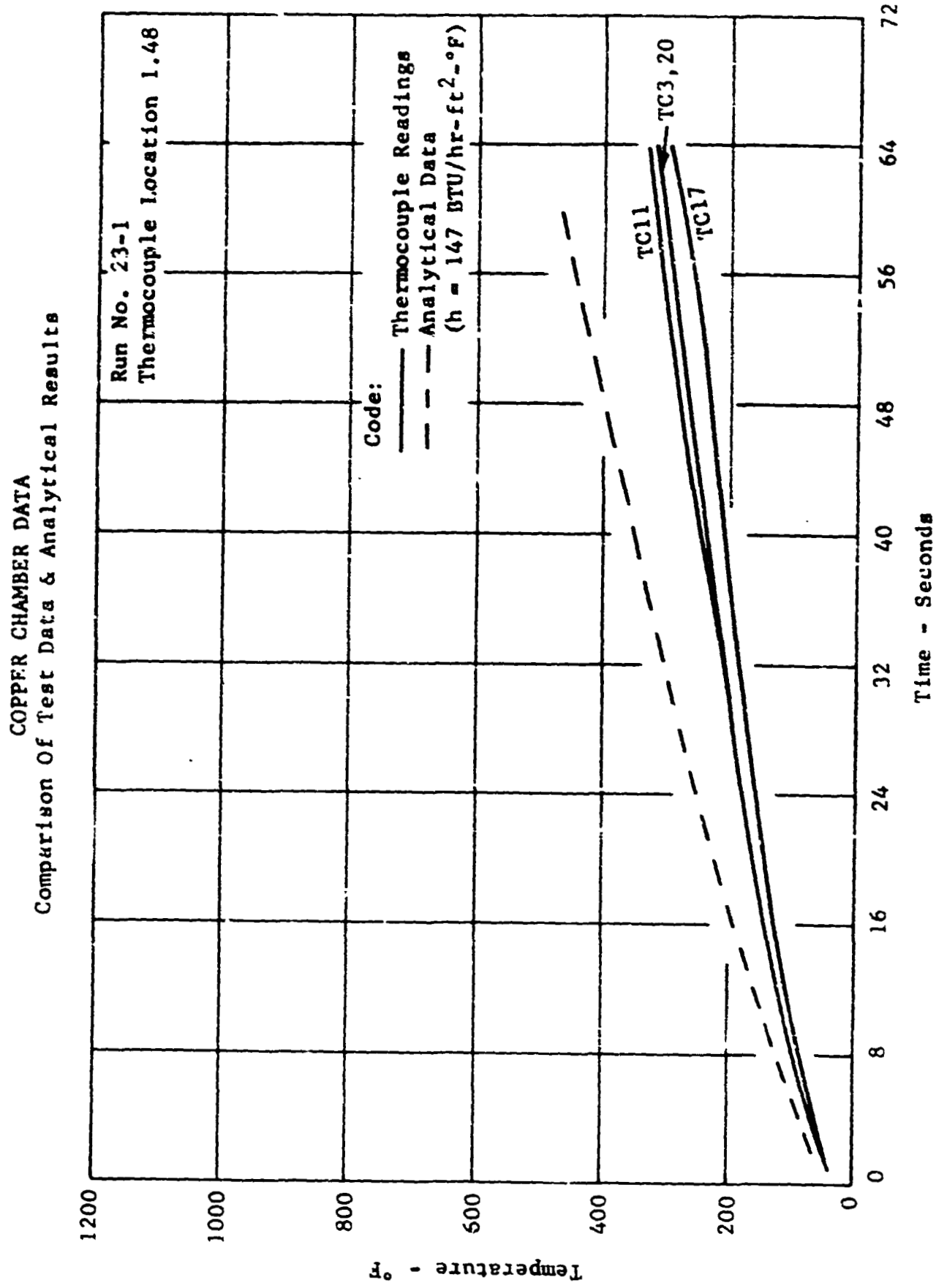
COPPER CHAMBER DATA
Comparison Of Test Data & Analytical Results
Run No. 23-1
Thermocouple Location 1.48
Code:
Thermocouple Readings
Analytical Data
(h = 147 BTU/hr-ft²-°F)
TC11
TC3,20
TC17
Temperature - °F
1200
1000
800
600
400
200
0
Time - Seconds
0
8
16
24
32
40
48
56
64
72

Figure 25

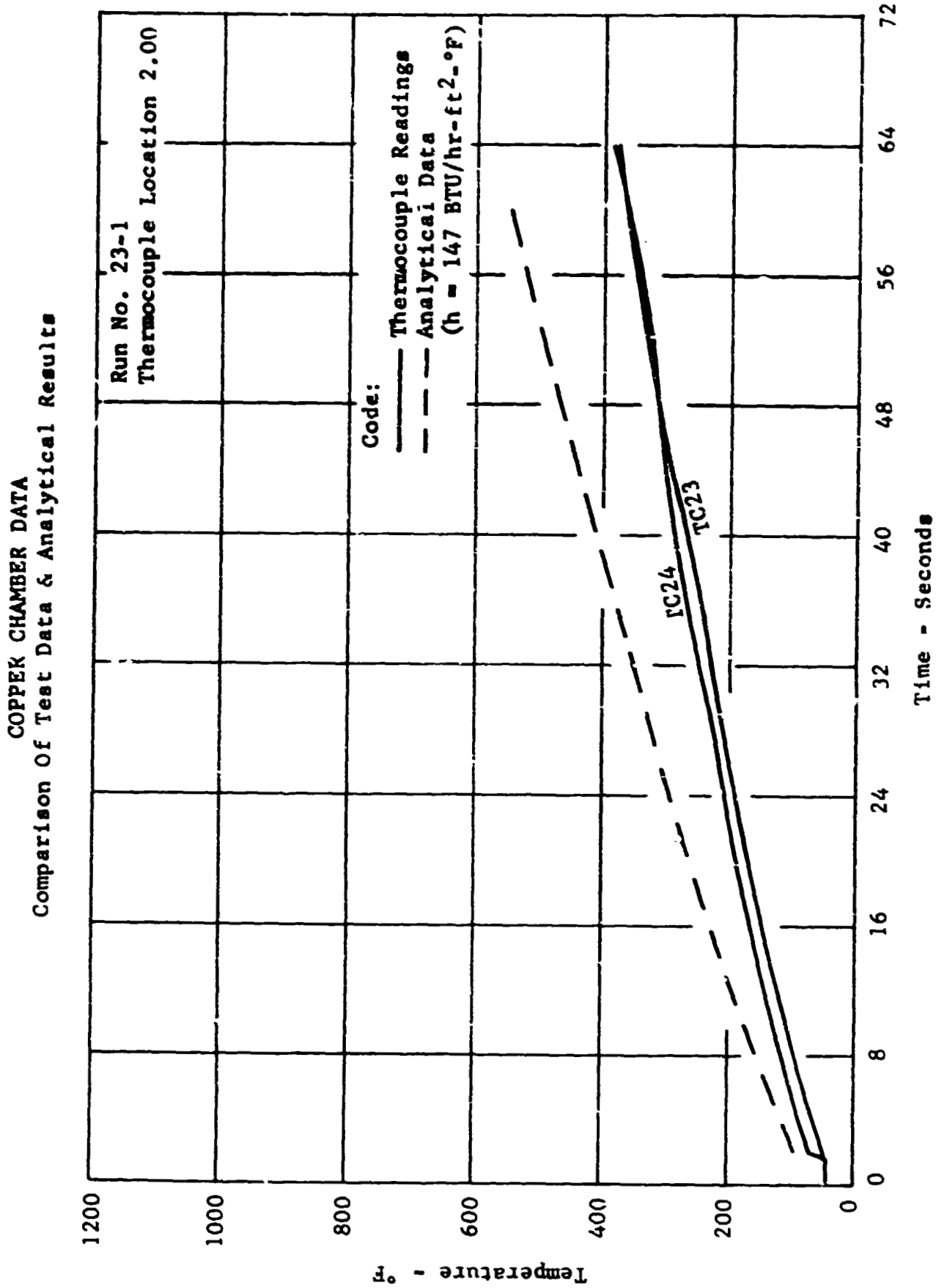
COPPER CHAMBER DATA
Comparison Of Test Data & Analytical Results
Run No. 23-1
Thermocouple Location 2.00
Code:
Thermocouple Readings
Analytical Data
(h = 147 BTU/hr-ft²-°F)
TC24
TC23
Temperature - °F
1200
1000
800
600
400
200
0
Time - Seconds
0
8
16
24
32
40
48
56
64
72

Figure 26

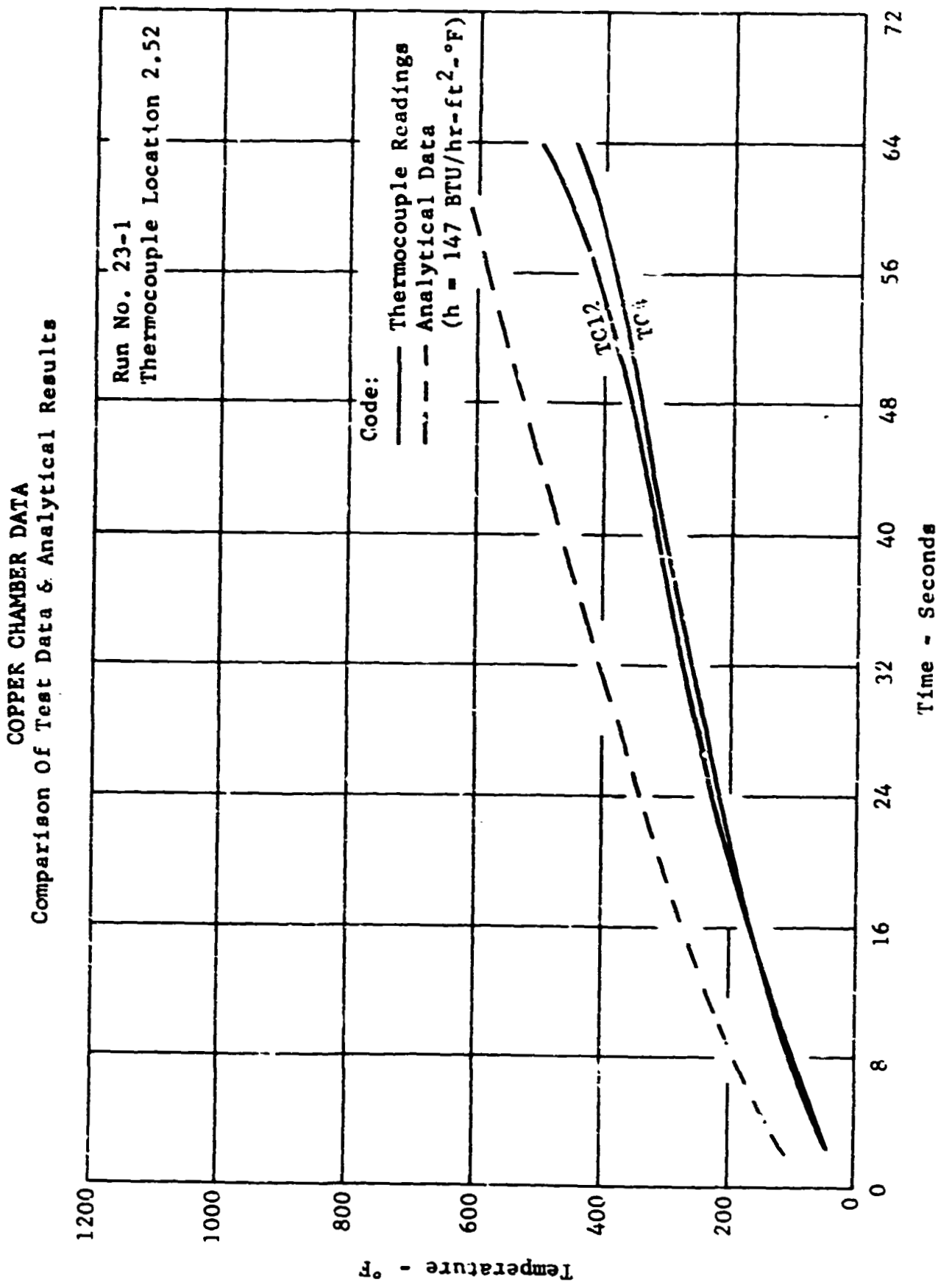
COPPER CHAMBER DATA
Comparison Of Test Data & Analytical Results
Run No. 23-1
Thermocouple Location 2.52
Code:
Thermocouple Readings
Analytical Data
(h = 147 BTU/hr-ft²-°F)
TC12
TC14
Temperature - °F
1200
1000
800
600
400
200
0
Time - Seconds
0
8
16
24
32
40
48
56
64
72

Figure 27

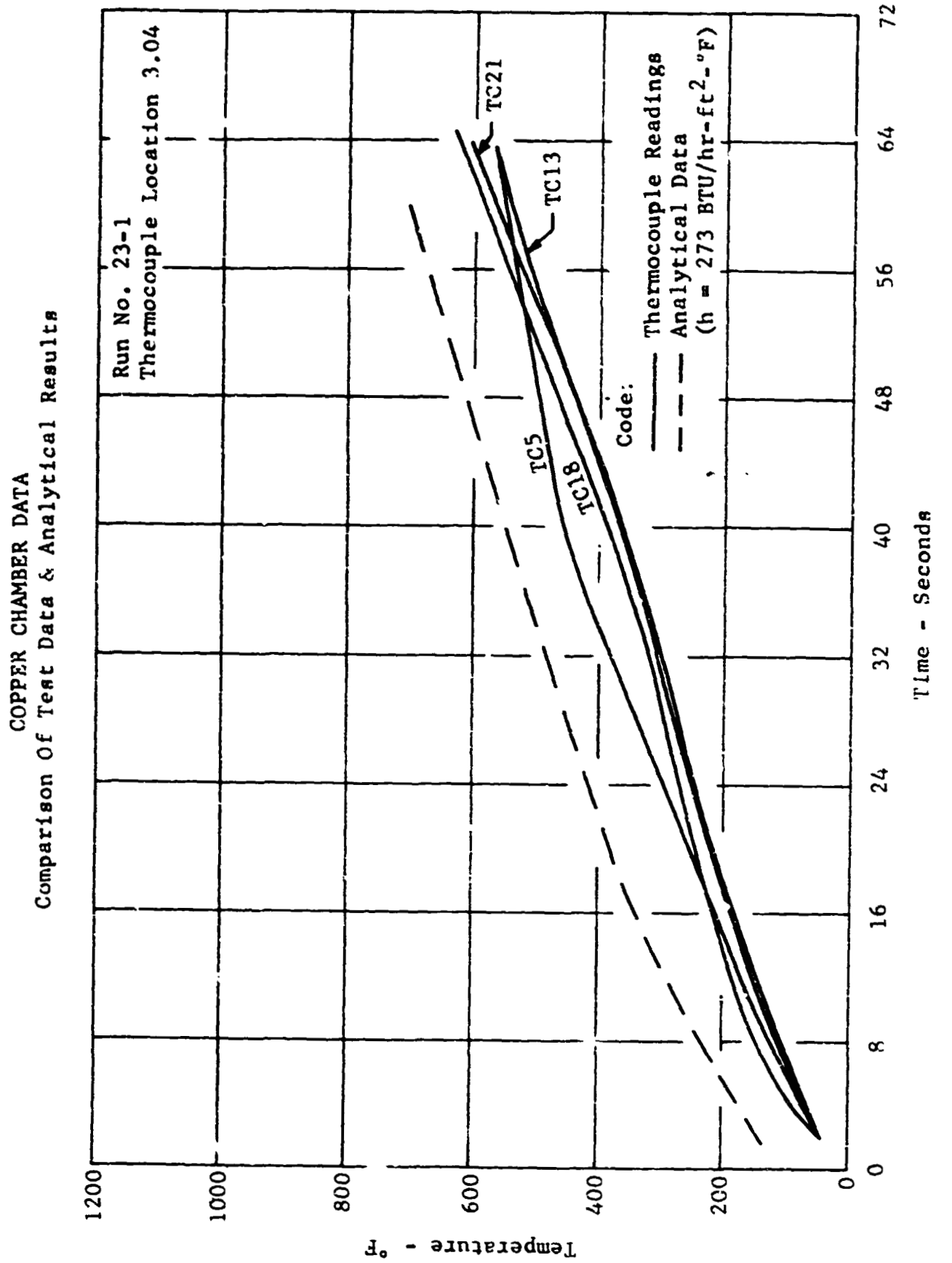

18-270

Figure 28

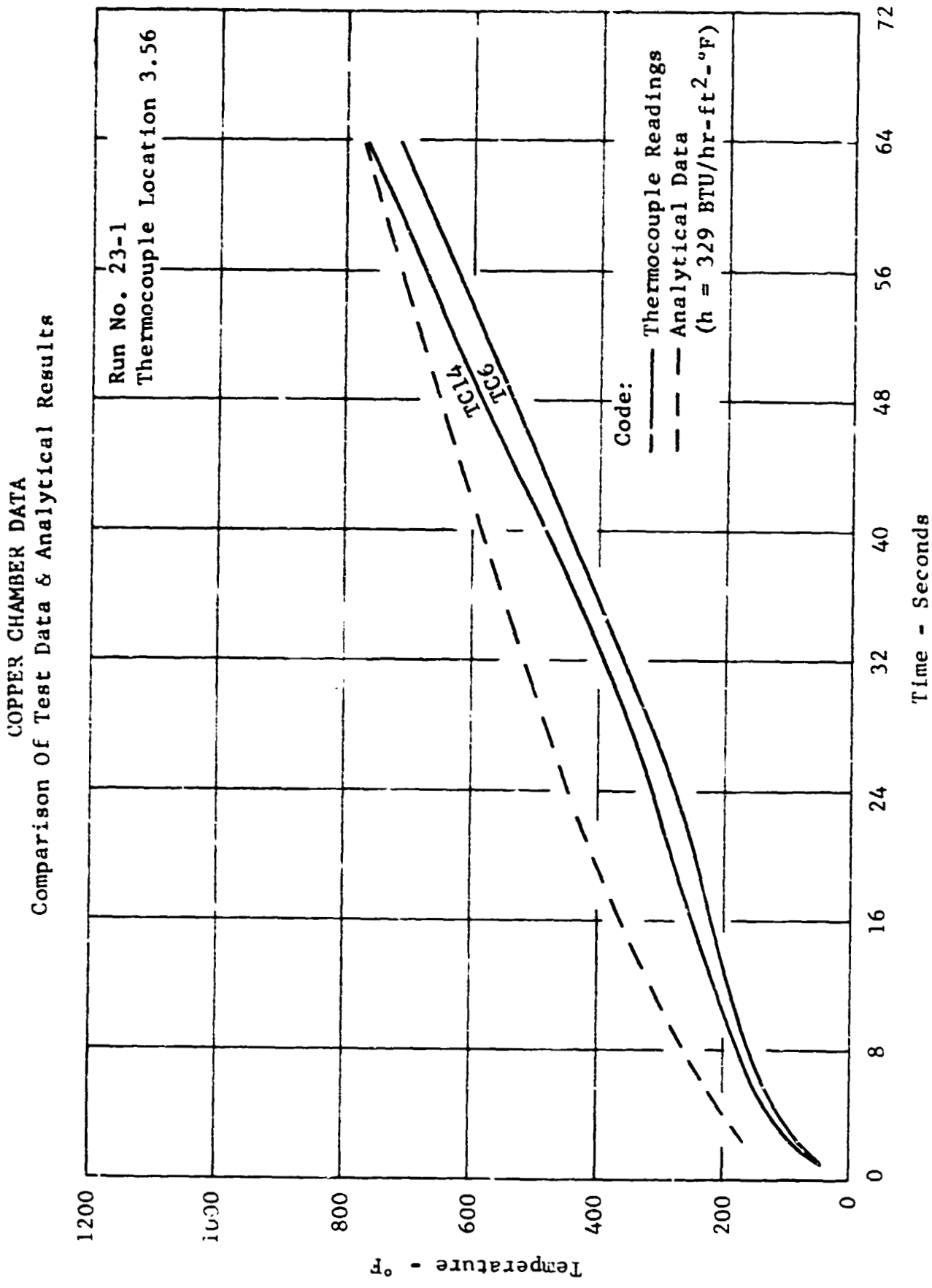
COPPER CHAMBER DATA
Comparison Of Test Data & Analytical Results
Run No. 23-1
Thermocouple Location 3.56
Code:
Thermocouple Readings
Analytical Data
(h = 329 BTU/hr-ft²-°F)
TC14
TC6
Temperature - °F
1200
1000
800
600
400
200
0
Time - Seconds
0
8
16
24
32
40
48
56
64
72

Figure 29

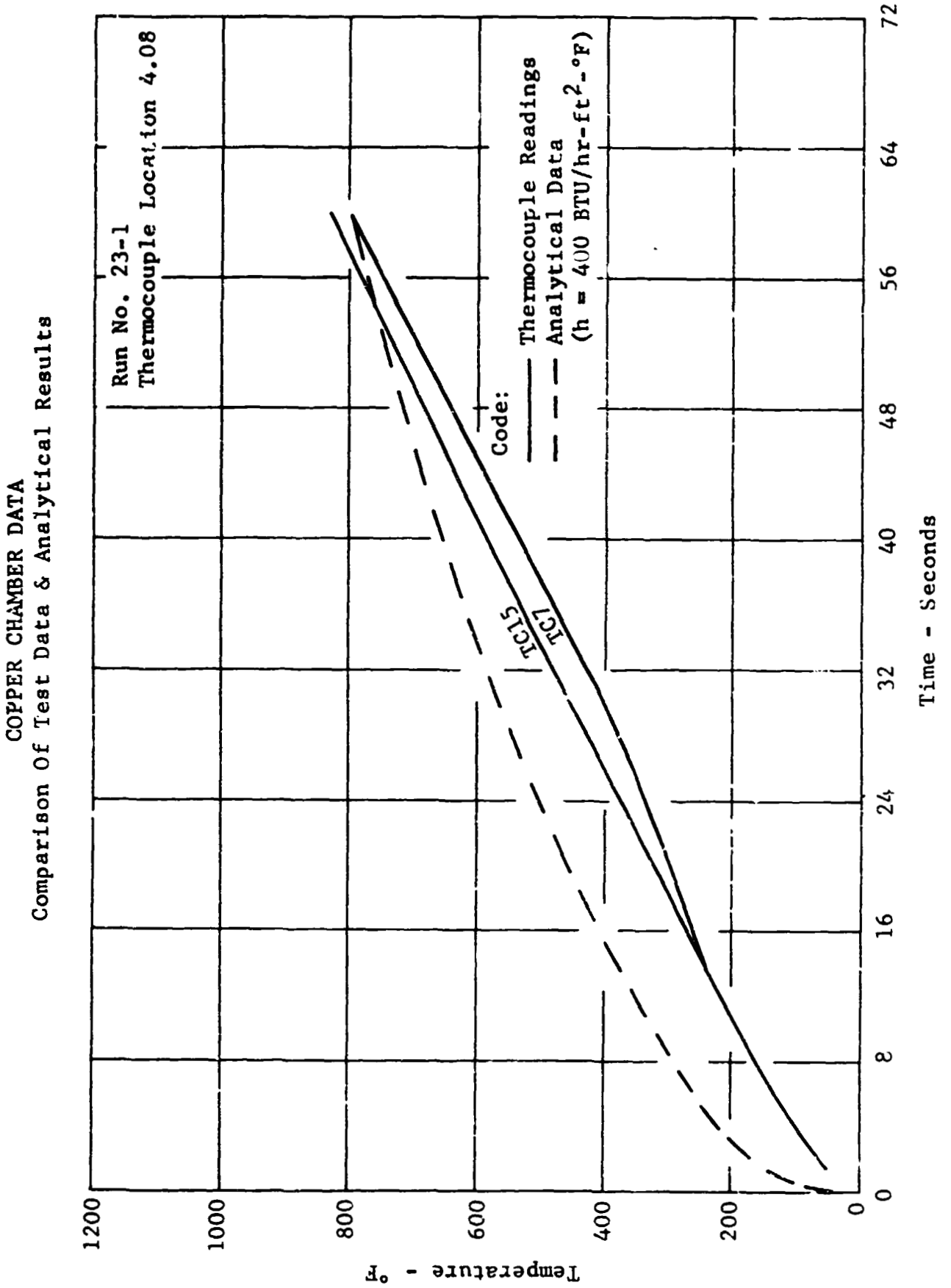
COPPER CHAMBER DATA
Comparison Of Test Data & Analytical Results
Run No. 23-1
Thermocouple Location 4.08
Code:
Thermocouple Readings
Analytical Data
(h = 400 BTU/hr-ft²-°F)
TC15
TC7
Temperature - °F
1200
1000
800
600
400
200
0
0
8
16
24
32
40
48
56
64
72
Time - Seconds

Figure 30

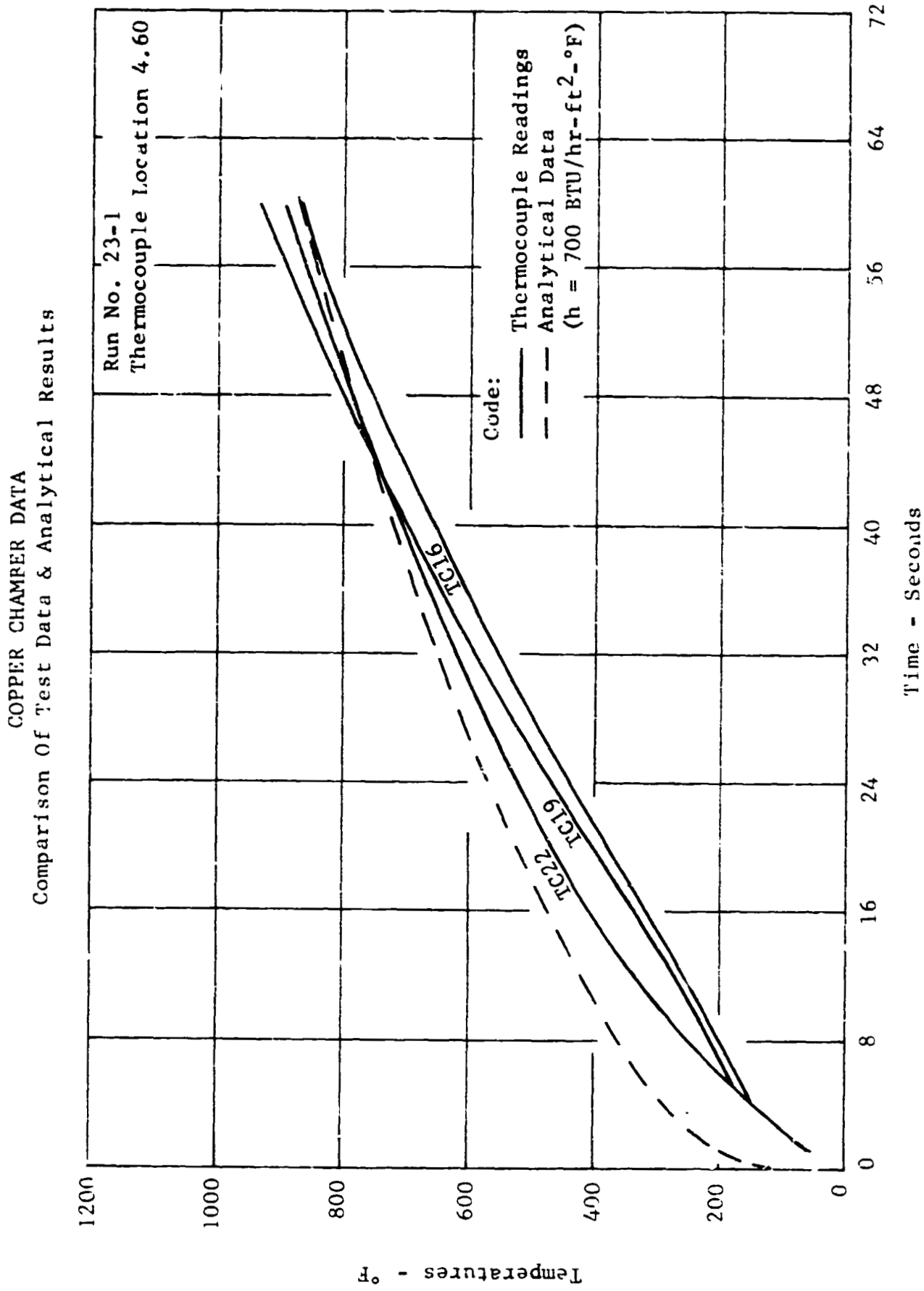
COPPER CHAMBER DATA
Comparison Of Test Data & Analytical Results
Run No. 23-1
Thermocouple Location 4.60
Code:
Thermocouple Readings
Analytical Data
(h = 700 BTU/hr-ft²-°F)
TC16
TC19
TC22
Temperatures - °F
1200
1000
800
600
400
200
0
0
8
16
24
32
40
48
56
64
72
Time - Seconds

Figure 31

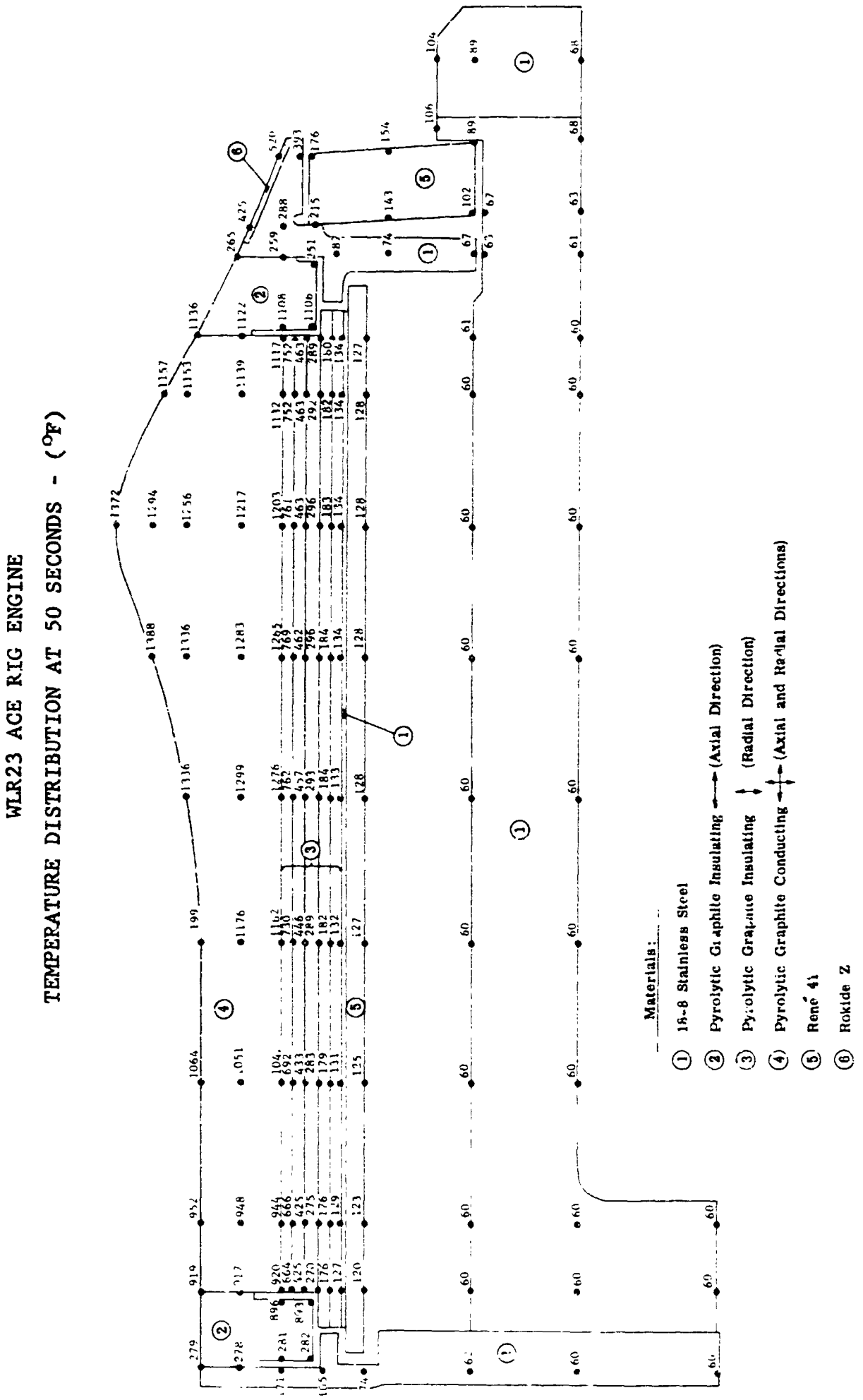
WLR23 ACE RIG ENGINE
TEMPERATURE DISTRIBUTION AT 50 SECONDS - (°F)
Materials:
① 16-8 Stainless Steel
② Pyrolytic Graphite Insulating (Axial Direction)
③ Pyrolytic Graphite Insulating (Radial Direction)
④ Pyrolytic Graphite Conducting (Axial and Radial Directions)
⑤ René 41
⑥ Rokide Z

Figure 32

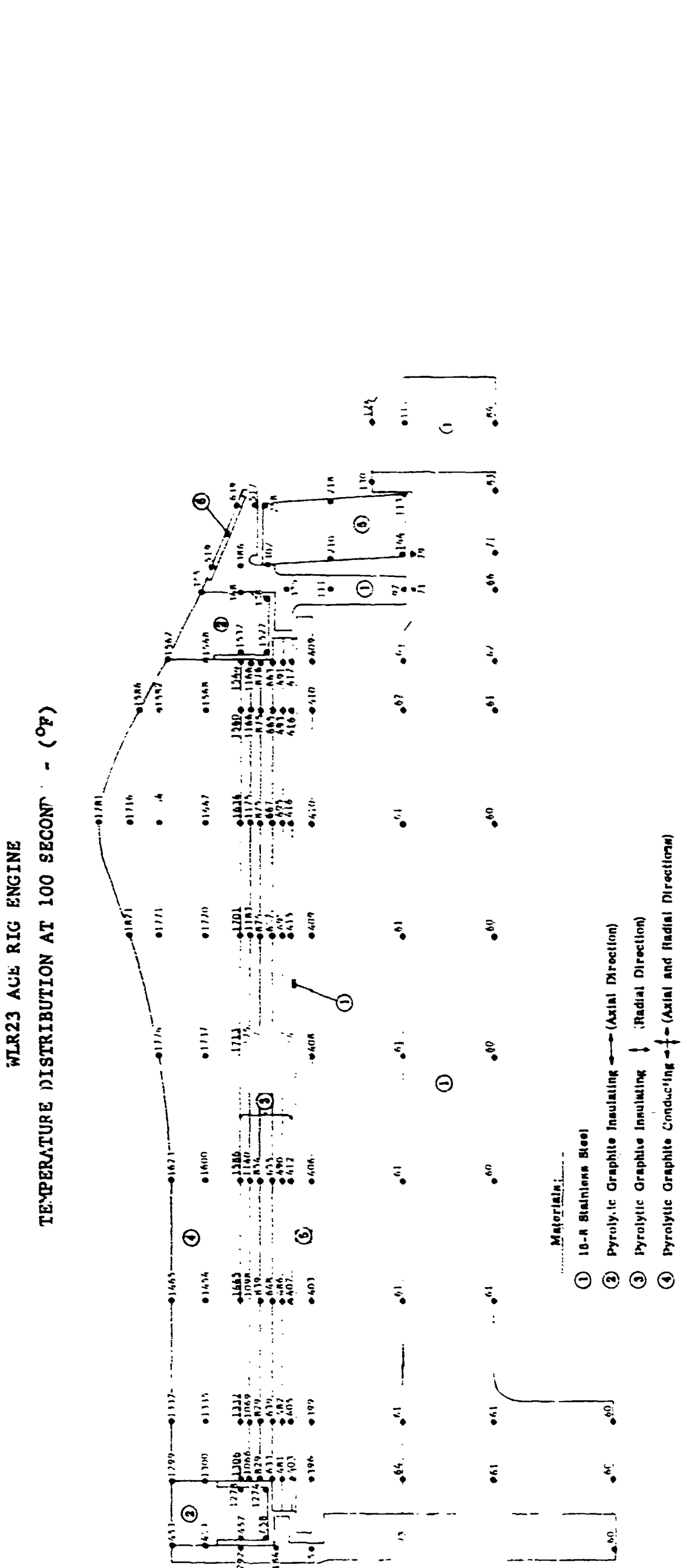
WLR23 ACE RIG ENGINE
TEMPERATURE DISTRIBUTION AT 100 SECONDS - (°F)
Materials:
① 18-8 Stainless Steel
② Pyrolytic Graphite Insulating —— (Axial Direction)
③ Pyrolytic Graphite Insulating | (Radial Direction)
④ Pyrolytic Graphite Conducting —+— (Axial and Radial Direction)
⑤ Rene' 41
⑥ Rokide Z

Figure 33

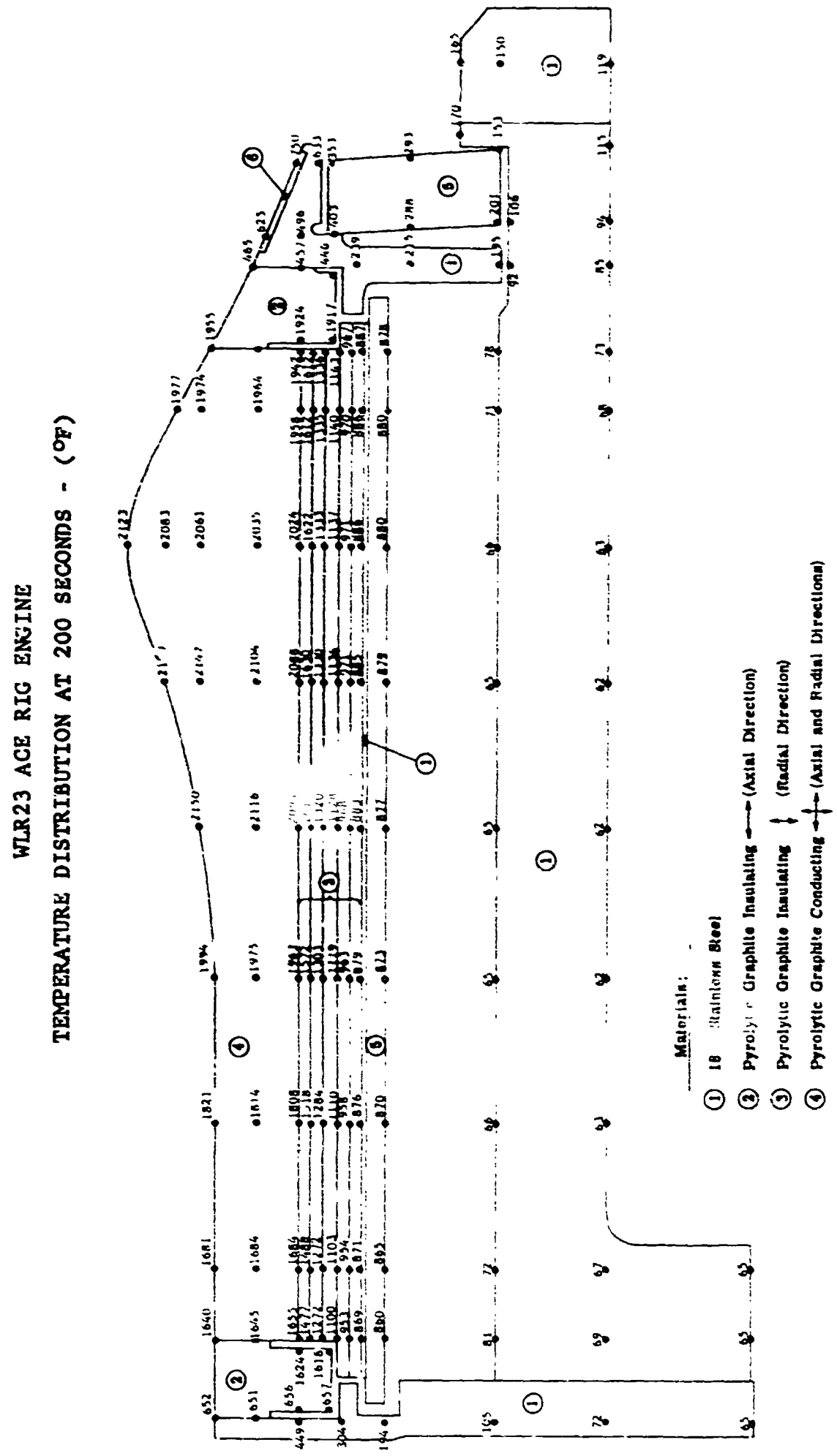

18-306

Figure 34

WLR23 ACE RIG ENGINE

TEMPERATURE DISTRIBUTION AT 300 SECONDS - (°F)

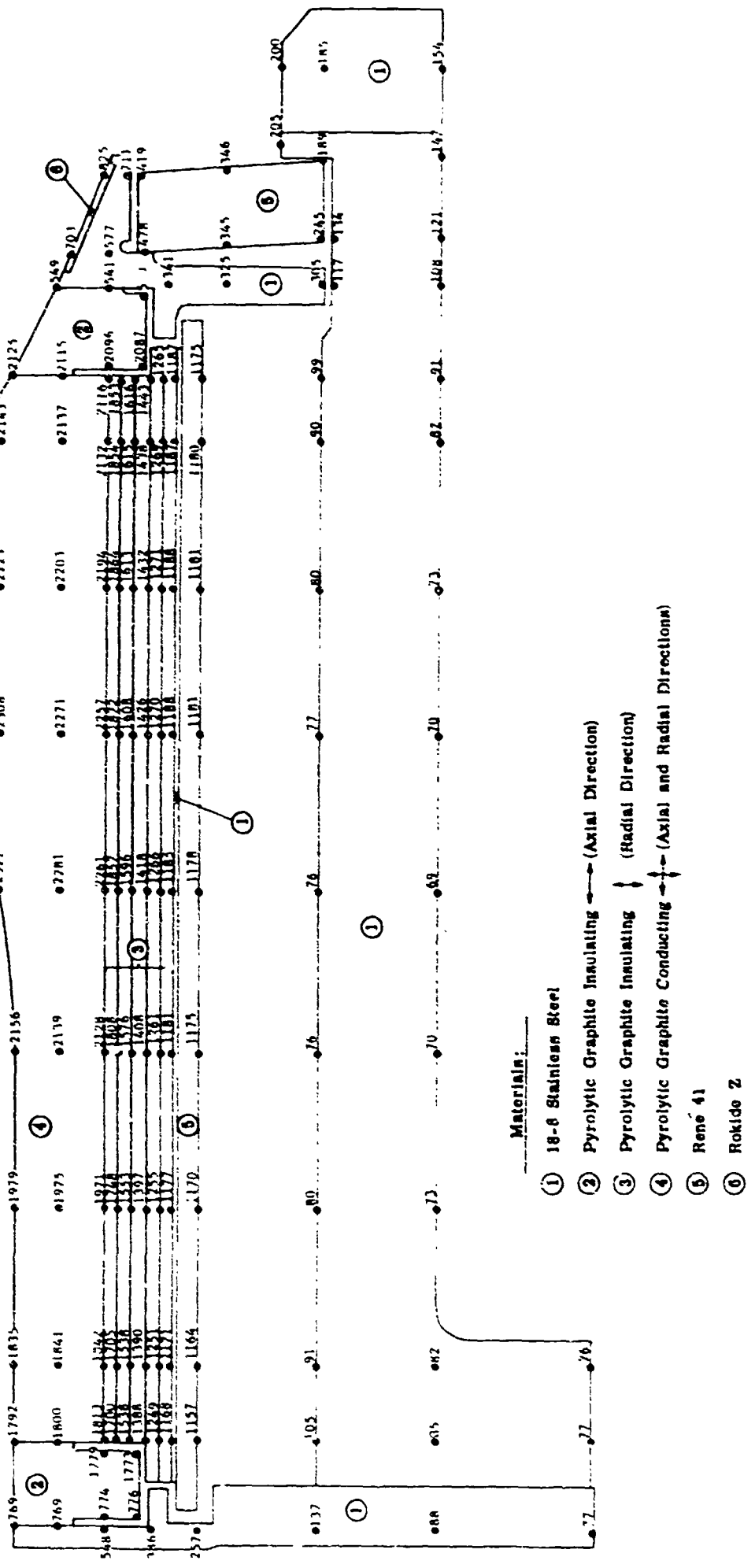

18-307

Figure 35

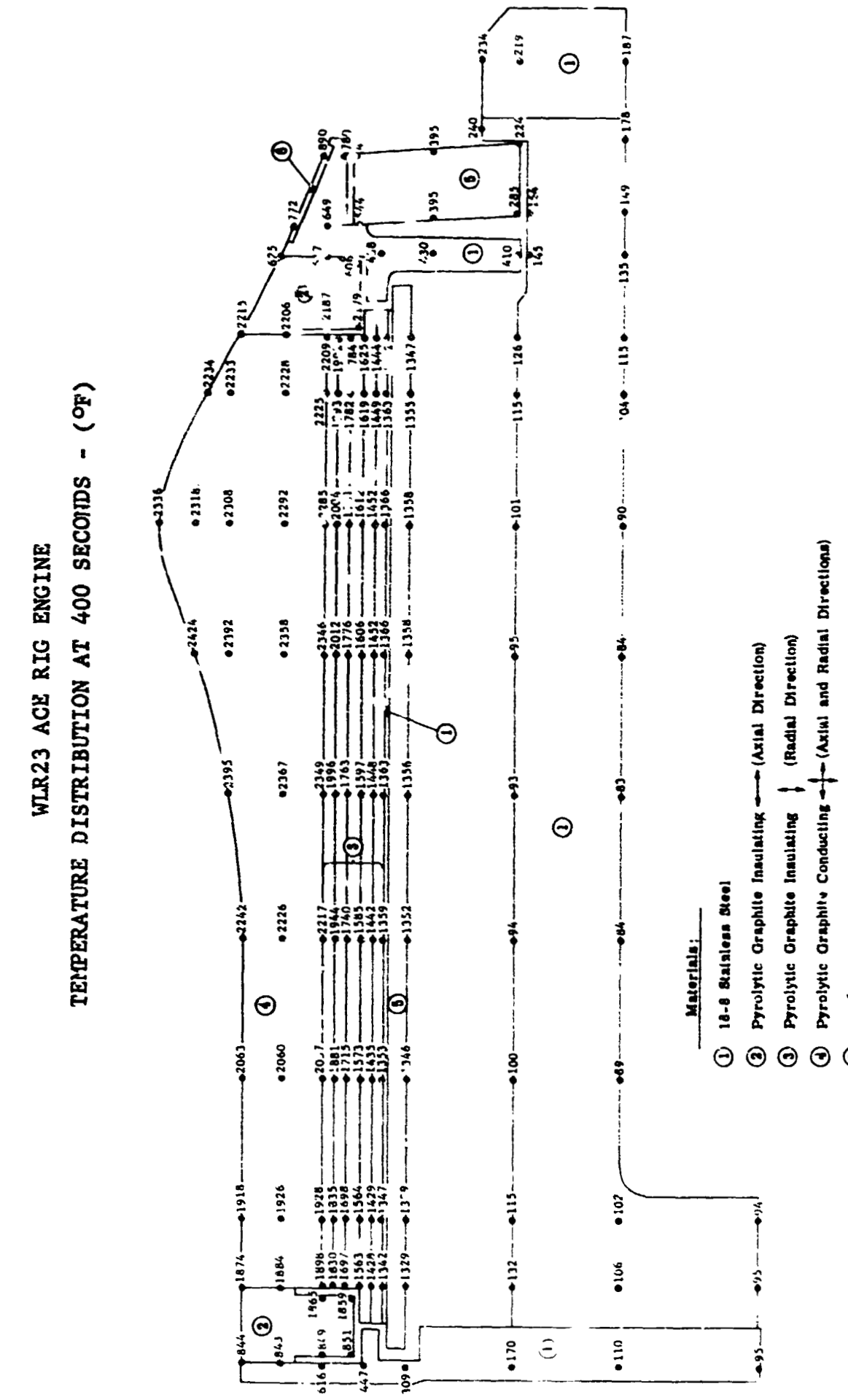
WLR23 ACE RIG ENGINE
TEMPERATURE DISTRIBUTION AT 400 SECONDS - (°F)
Materials:
① 18-8 Stainless Steel
② Pyrolytic Graphite Insulating —— (Axial Direction)
③ Pyrolytic Graphite Insulating ↕ (Radial Direction)
④ Pyrolytic Graphite Conducting —|— (Axial and Radial Directions)
⑤ Rex 41
⑥ Rokide Z

Figure 36

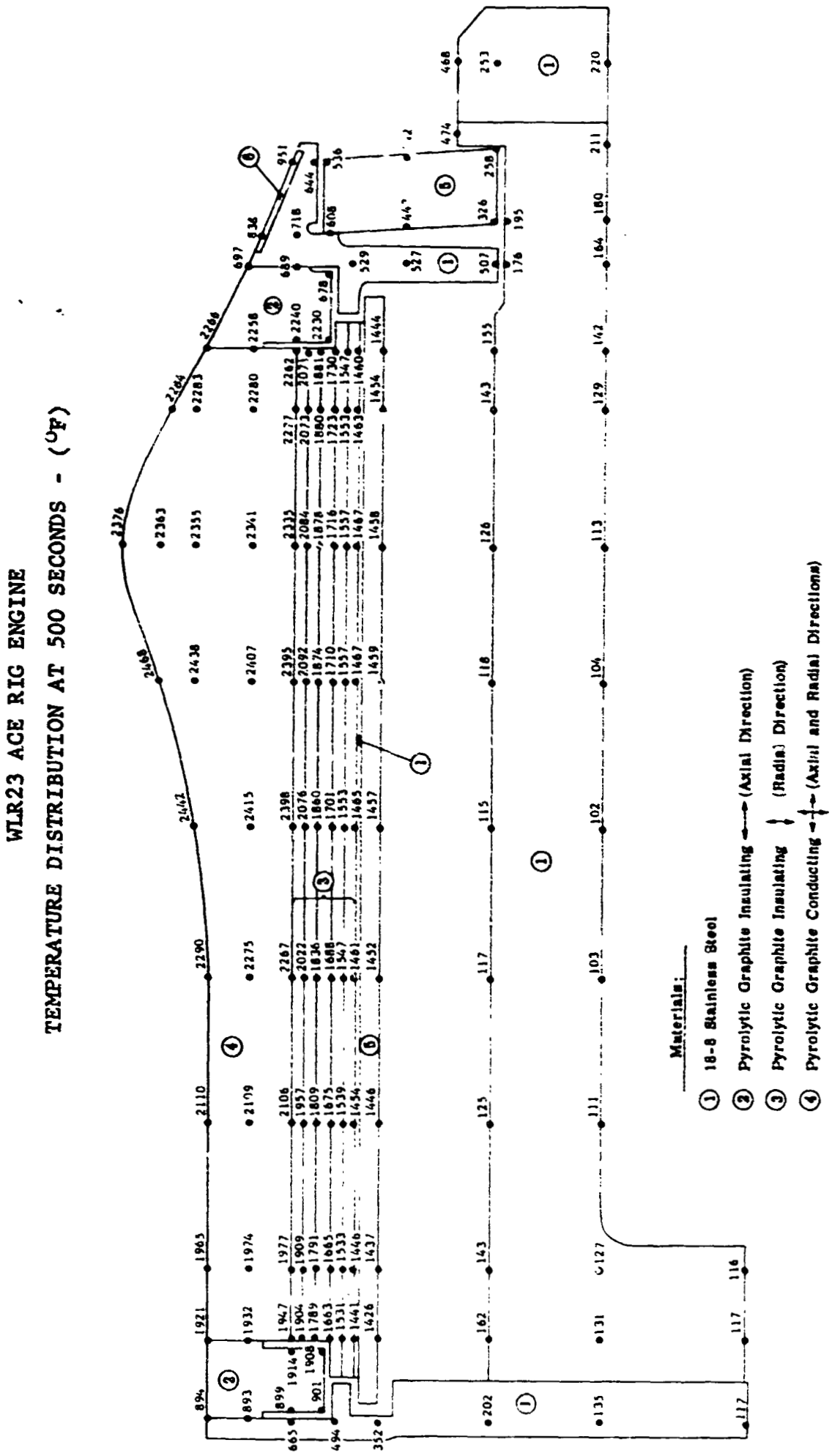
WLR23 ACE RIG ENGINE
TEMPERATURE DISTRIBUTION AT 500 SECONDS - (°F)
Materials:
① 18-8 Stainless Steel
② Pyrolytic Graphite Insulating ←→ (Axial Direction)
③ Pyrolytic Graphite Insulating ↕ (Radial Direction)
④ Pyrolytic Graphite Conducting ←↕→ (Axial and Radial Directions)
⑤ René 41
⑥ Rokide Z

Figure 37

WLR23 ACE RIG ENGINE

TEMPERATURE DISTRIBUTION AT 600 SECONDS - (°F)

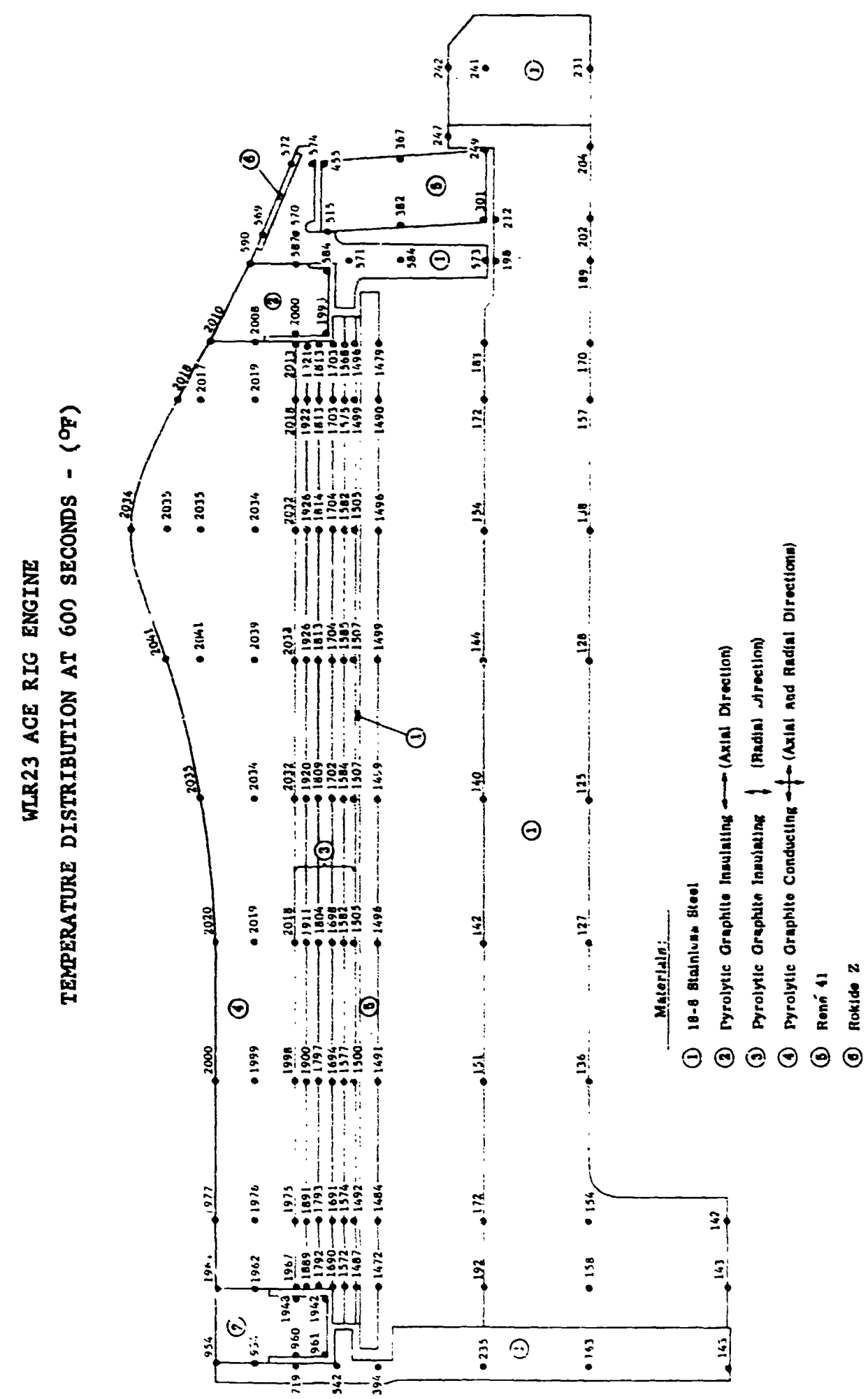

Figure 38

WEDGE STATION LOCATIONS

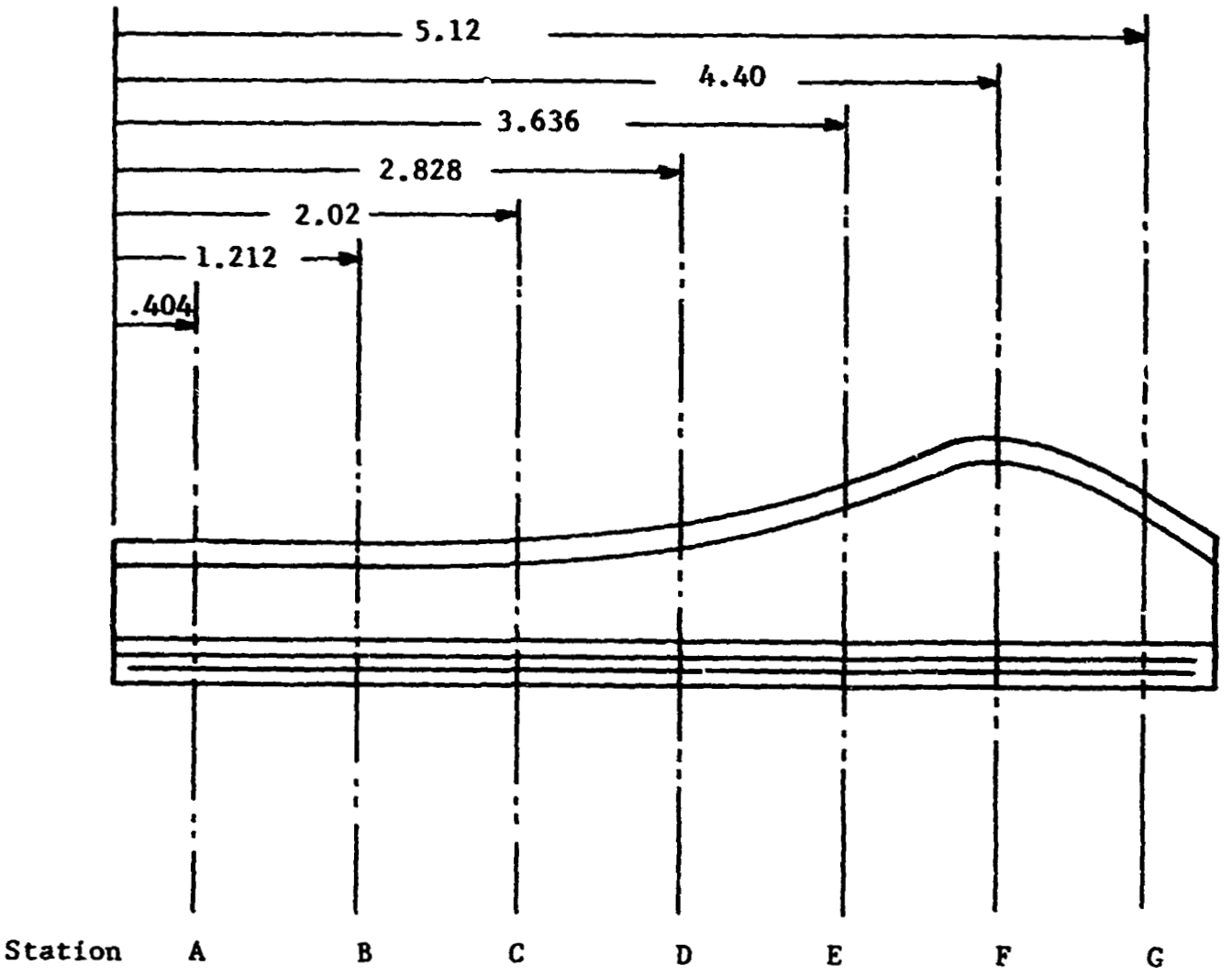

18-273

Figure 39

WLR23 WATCHBAND STRESS - TIME HISTORY

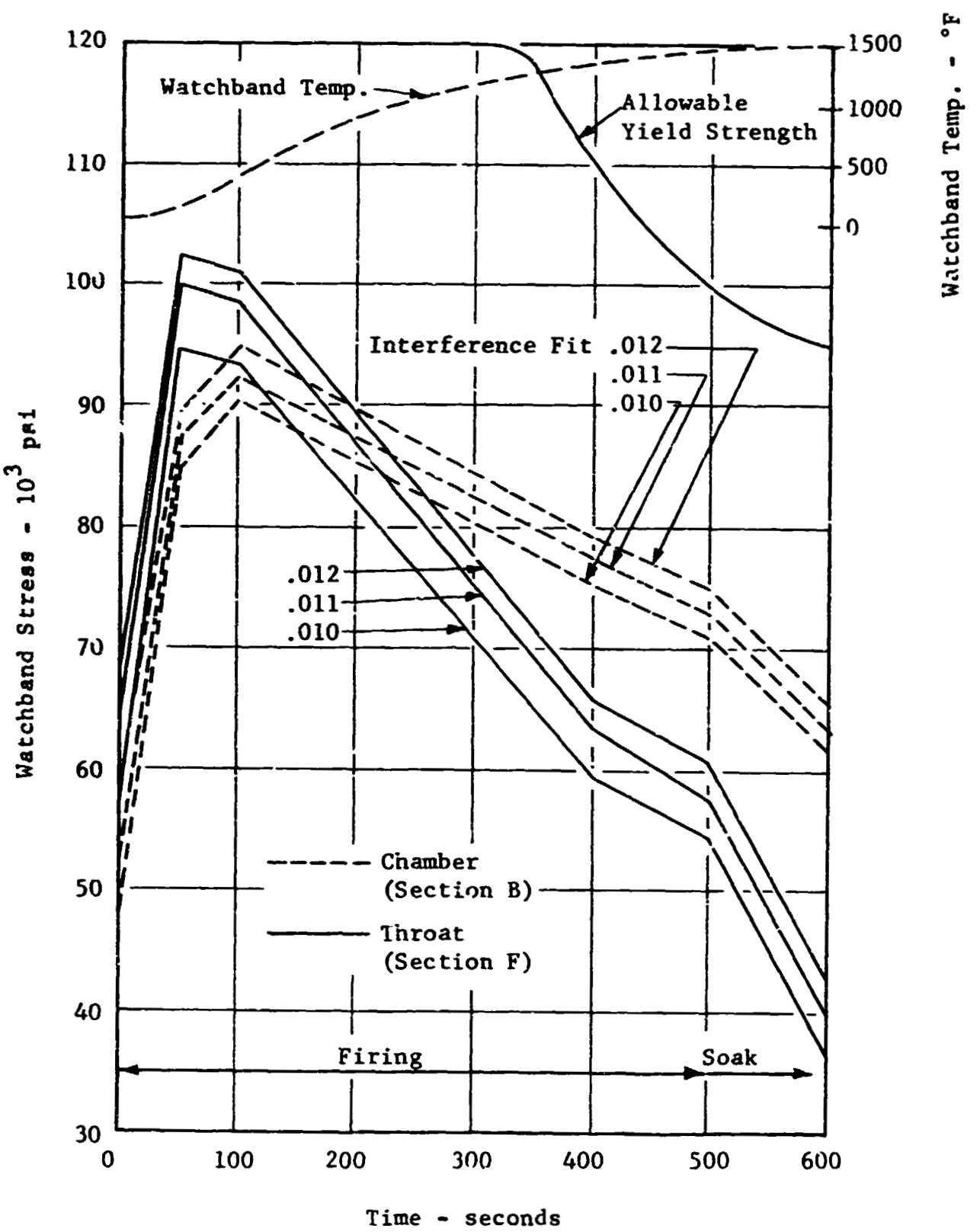

18-253

Figure 40

WLR23 THEORETICAL THROAT AREA HISTORY

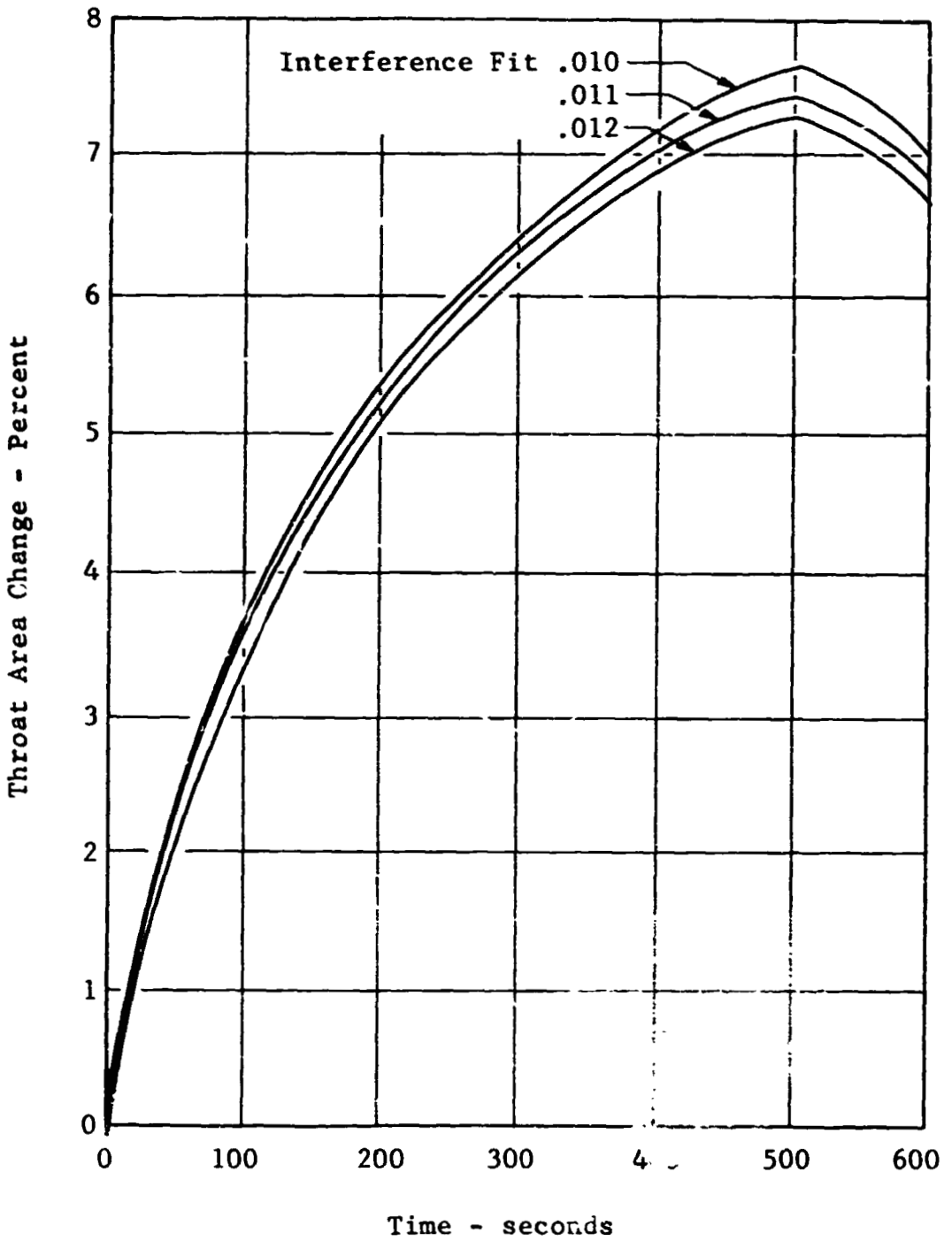

18-256

Figure 41

WLR23 RIG ENGINE

Weight of Constant Thickness Watchband

14 Beams Per Row
Material - Rene 41

16 Rows of Beams
Density = .298 lbs/in^3

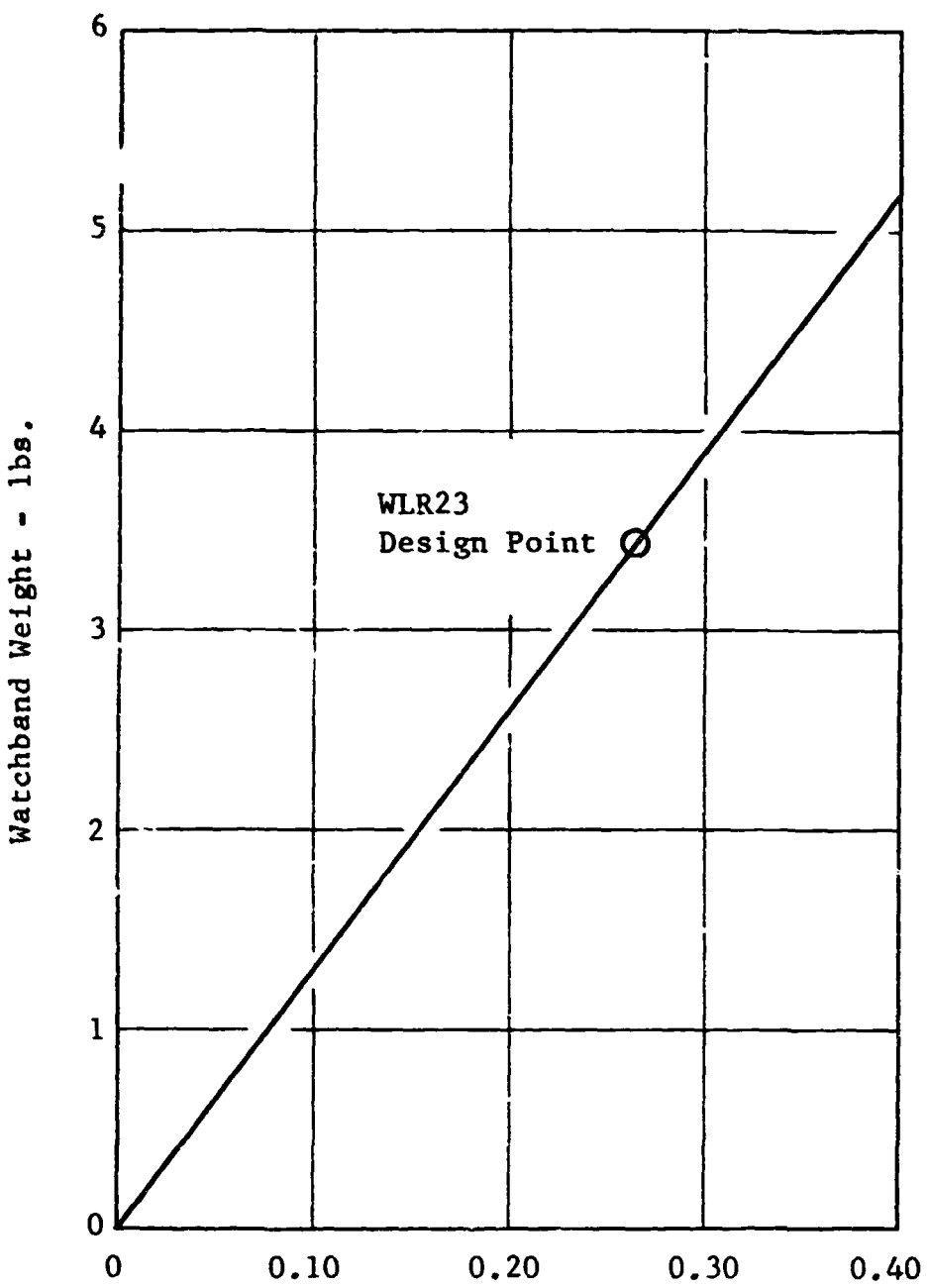

18-807

Figure 42

WLR23 FLIGHT ENGINE O.D. ENVELOPE vs WATCHBAND THICKNESS

Outer Shell Thickness = 0.060 in
Outer Shell Clearance = 0.030 in

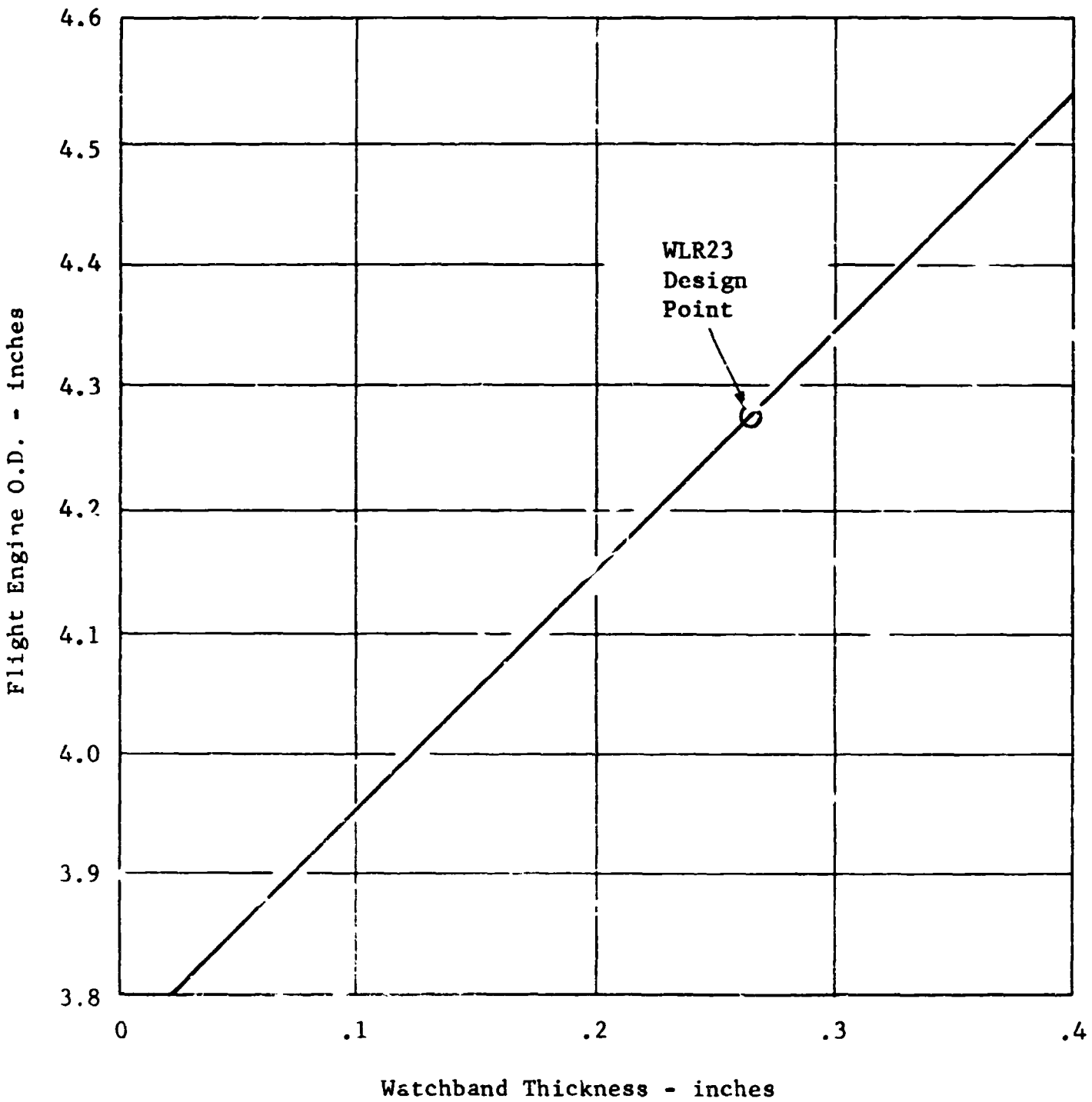

18-257

Figure 43

WLR23 WATCHBAND OVERHANG

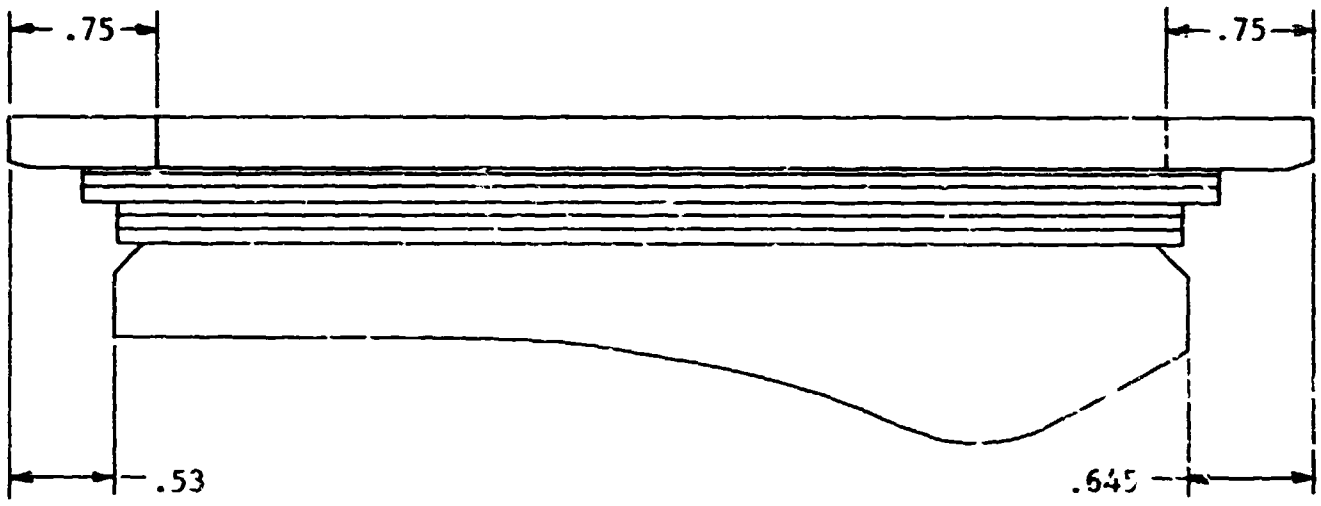

18-354

Figure 44

WATCHBAND TEST SPECIMEN - TENSILE TEST

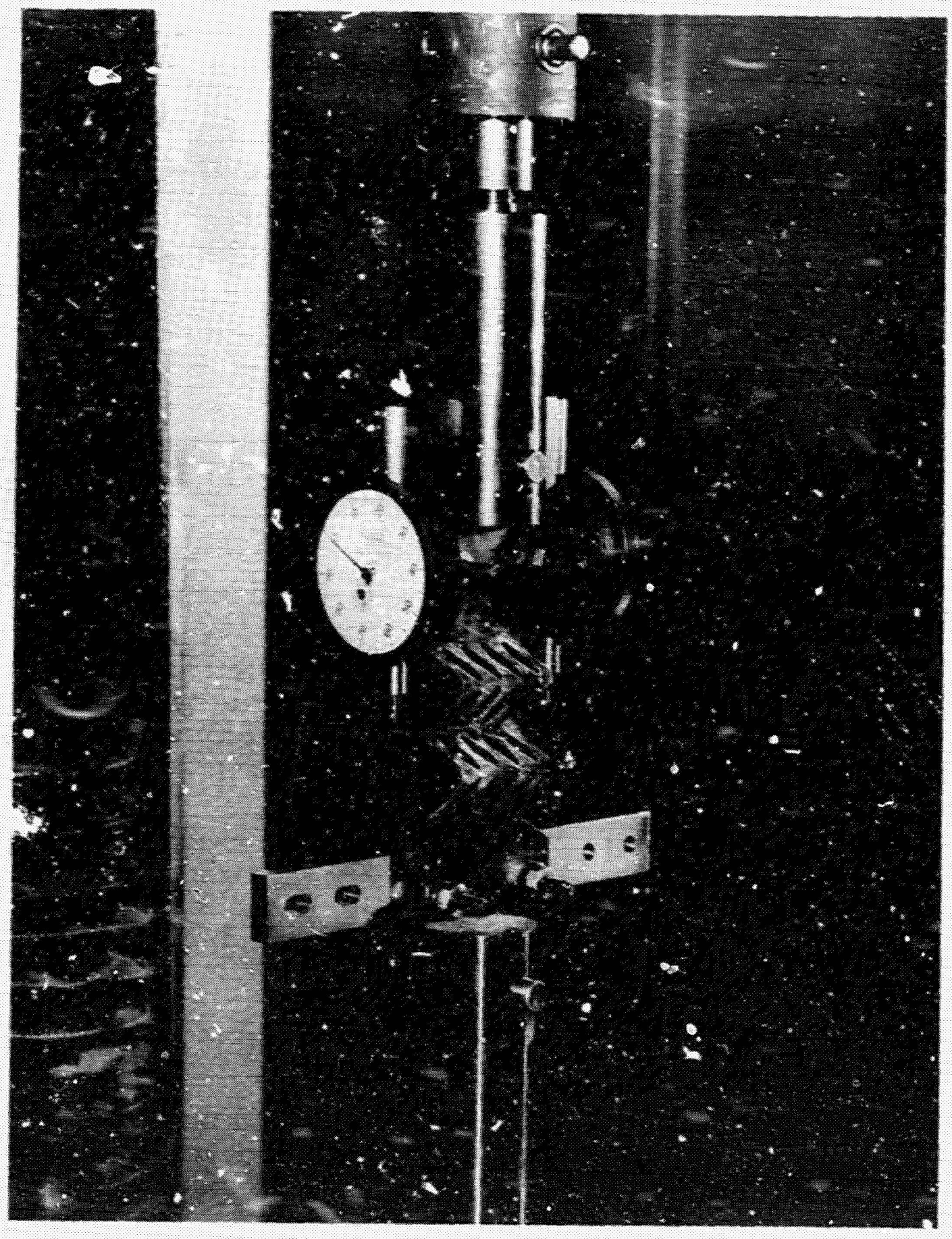

Figure 45

WATCHBAND TEST SPECIMEN - TENSILE TEST

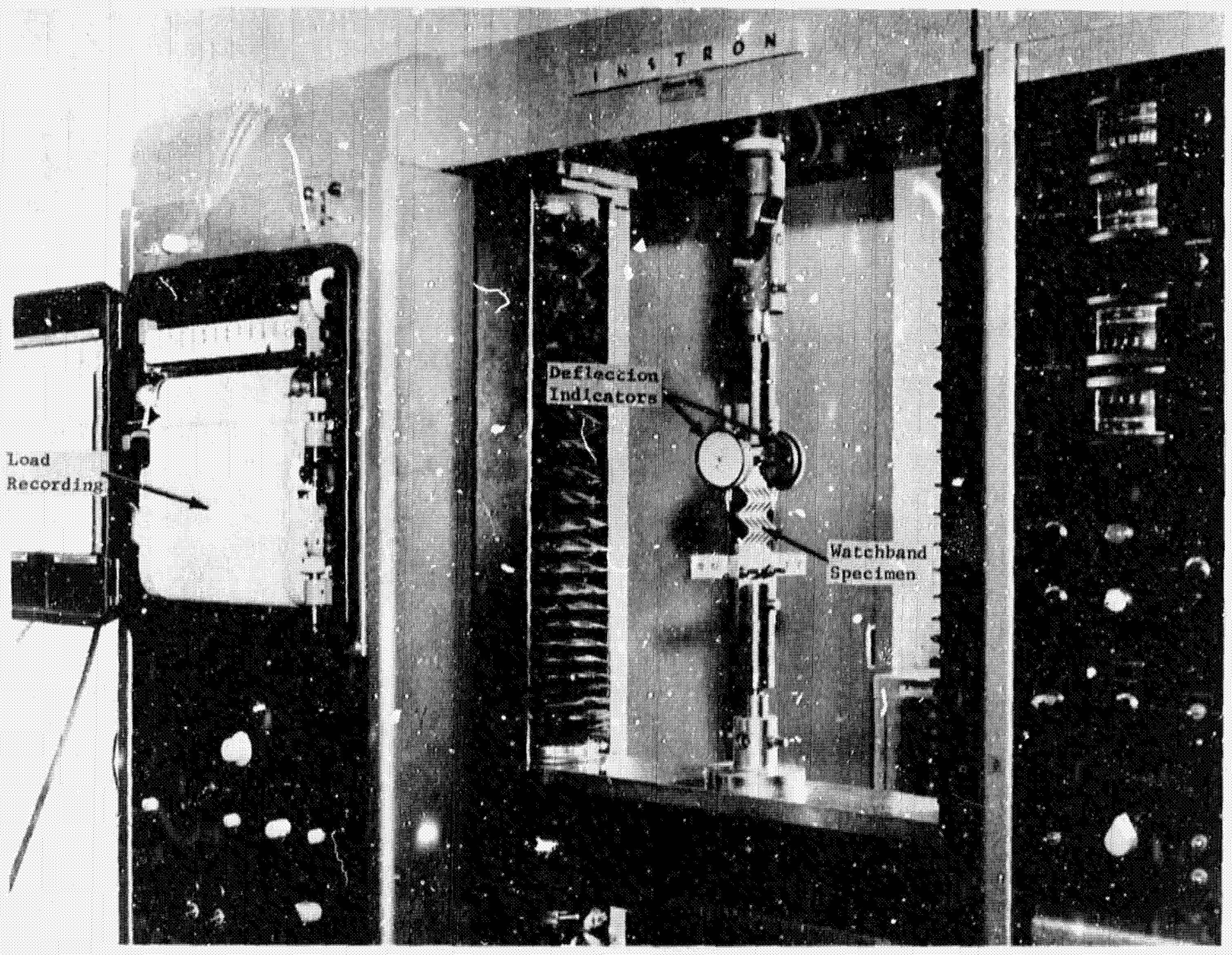

Figure 46

16-308

WLR23 WATCHBAND TENSILE SPECIMEN

Load-Deflection Curve

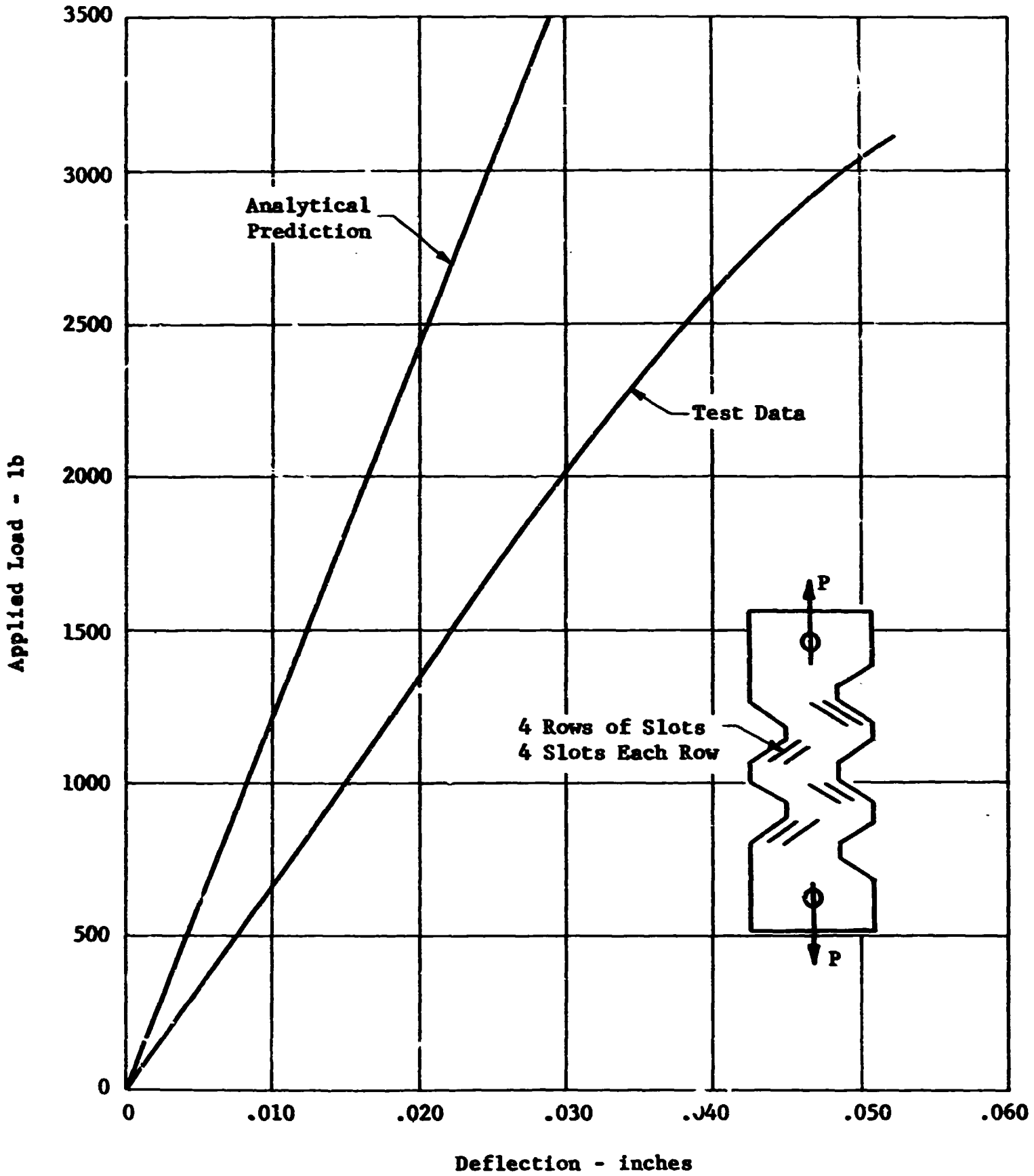

18-400

Figure 47

WLR23 WATCHBAND STRESS - TIME HISTORY

Revised Watchband - Thickness = .290 in.

.025" Interface Fit

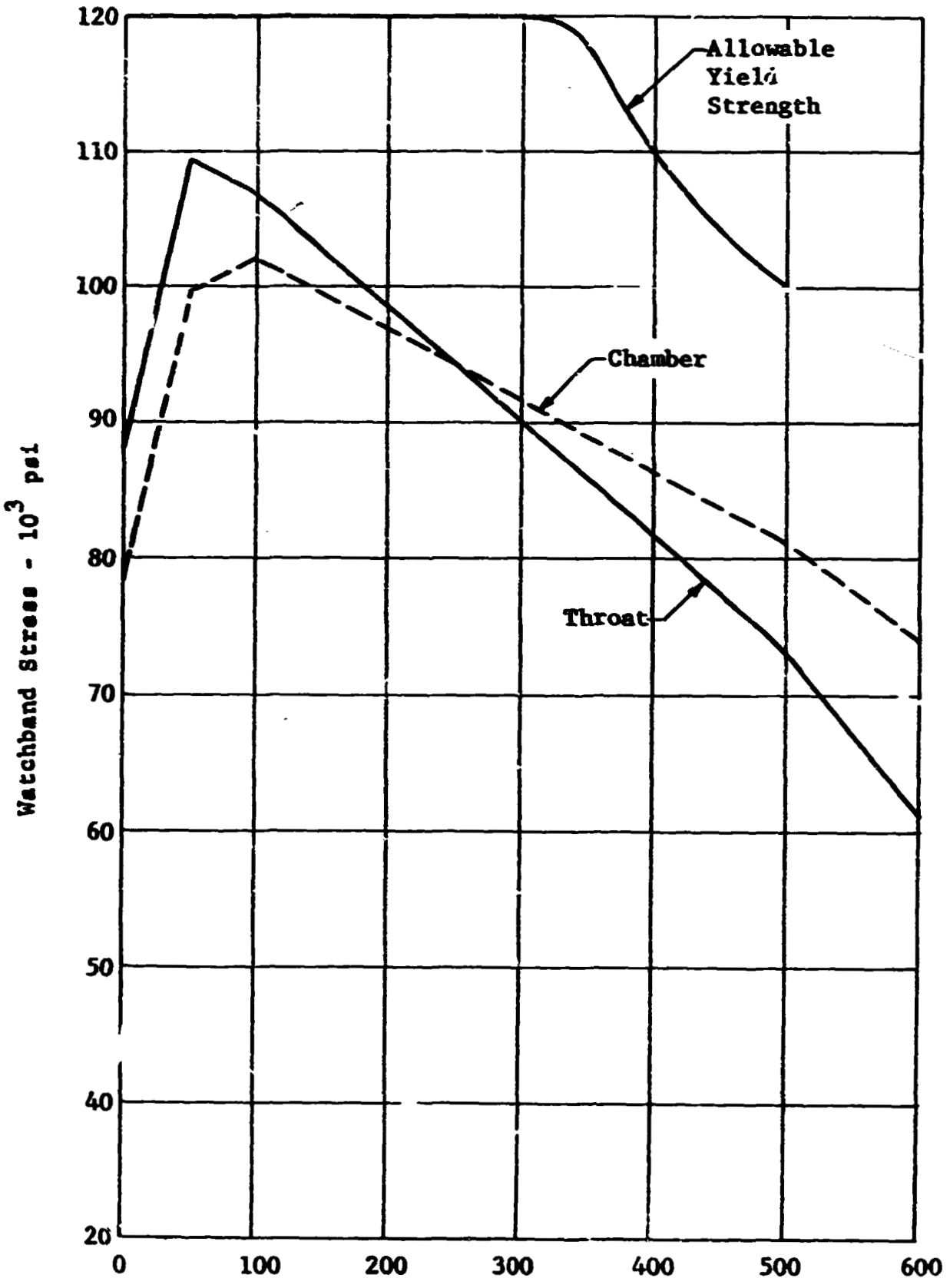

18-401

Figure 48

WEDGE ASSEMBLY MANUFACTURING FLOW CHART

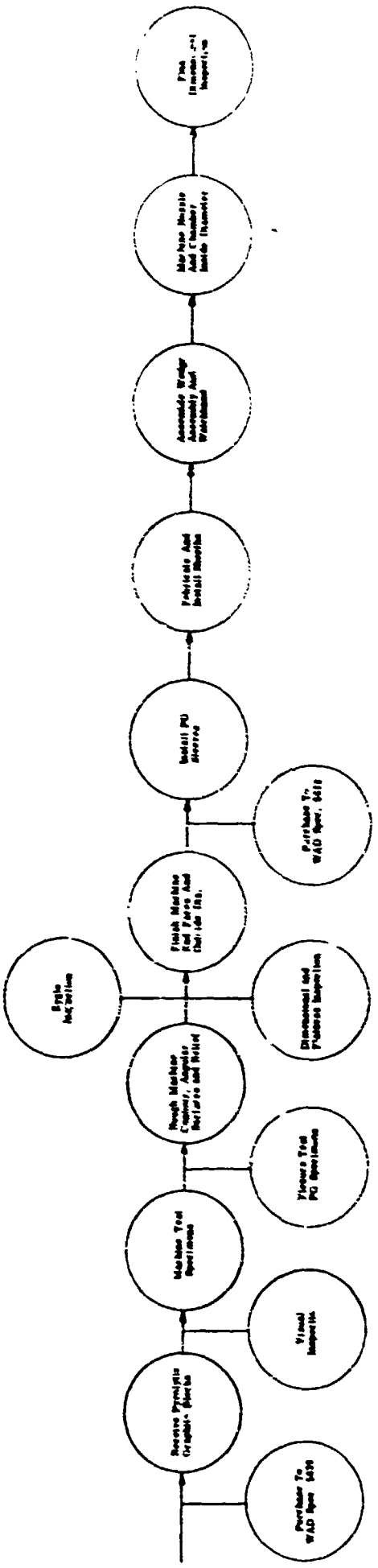

Figure 49

FLEXTURE TEST SPECIMEN LOCATION

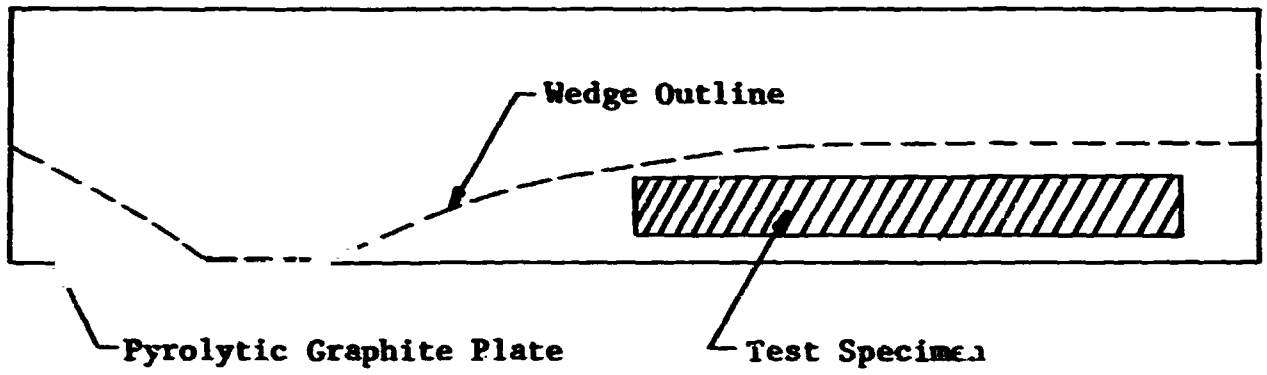

18-806

Figure 50

FLEXURE TEST CONFIGURATION

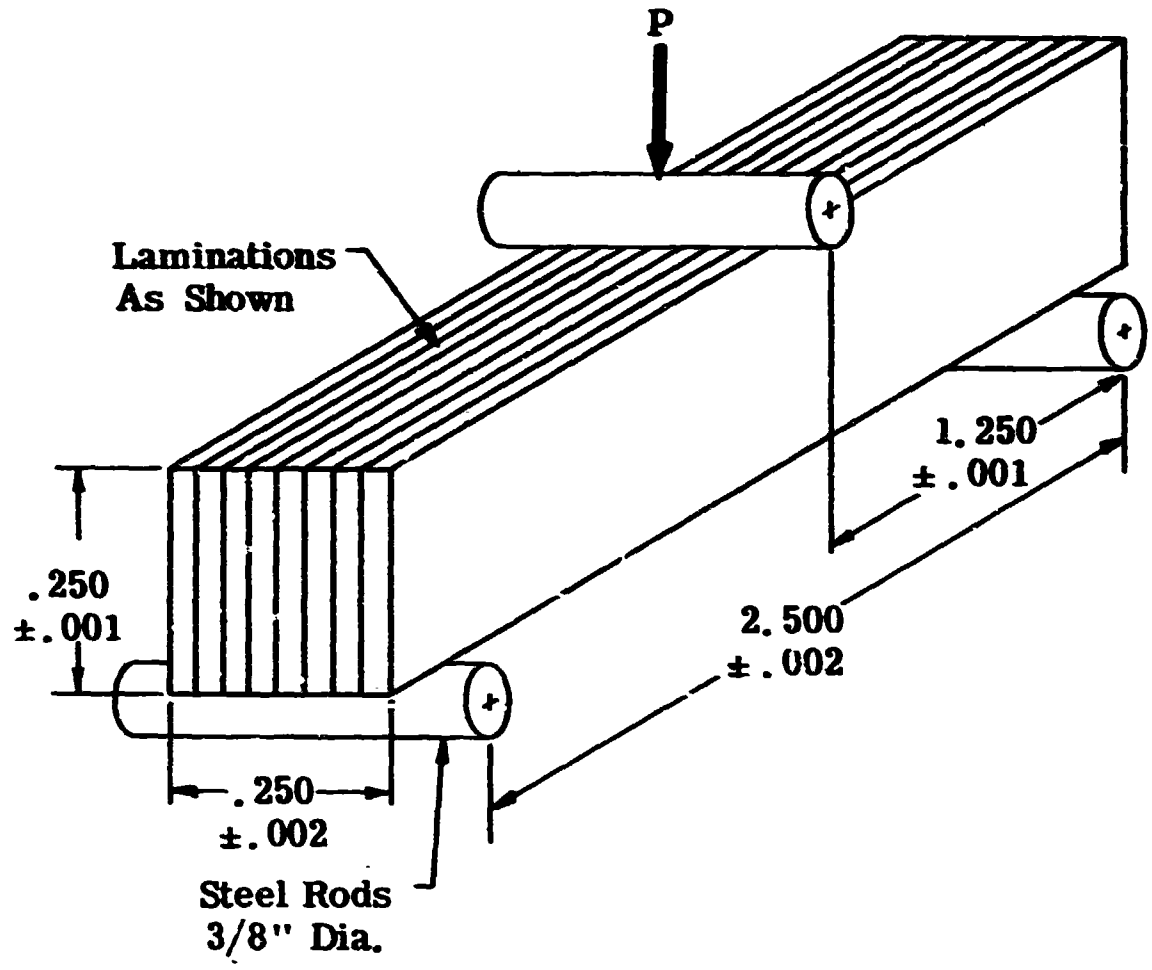

14-098

Figure 51

INSTRON TENSILE MACHINE AND BEND TEST

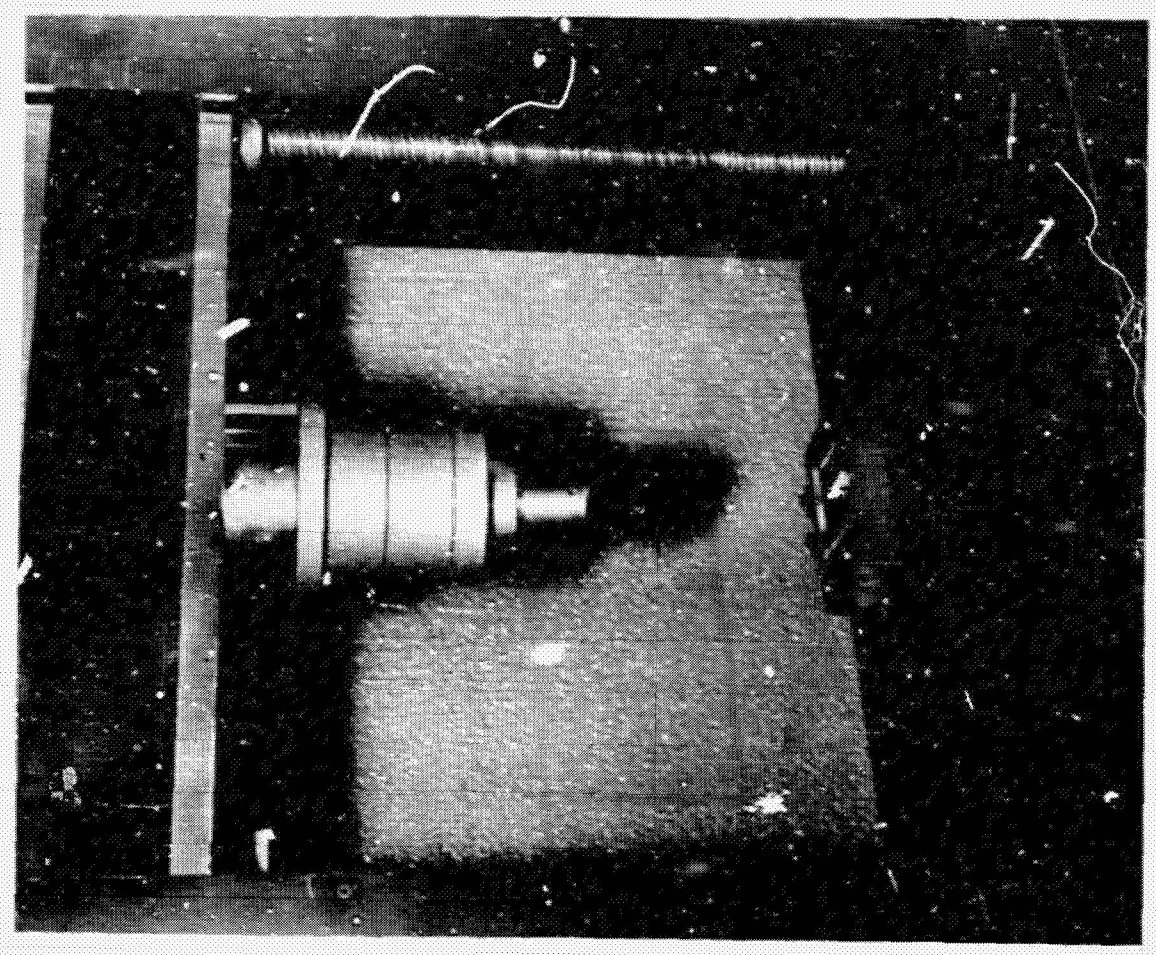

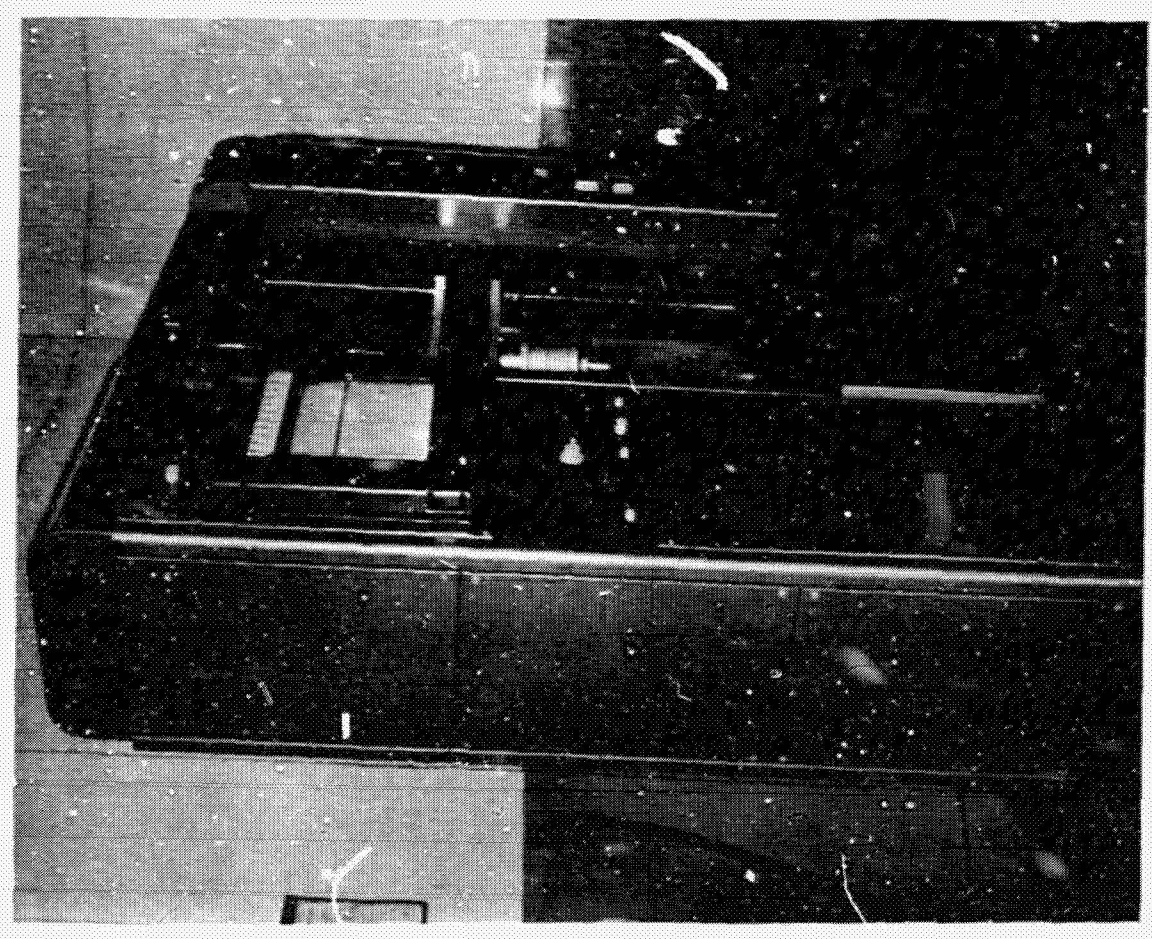

Figure 52

DETAIL WEDGE

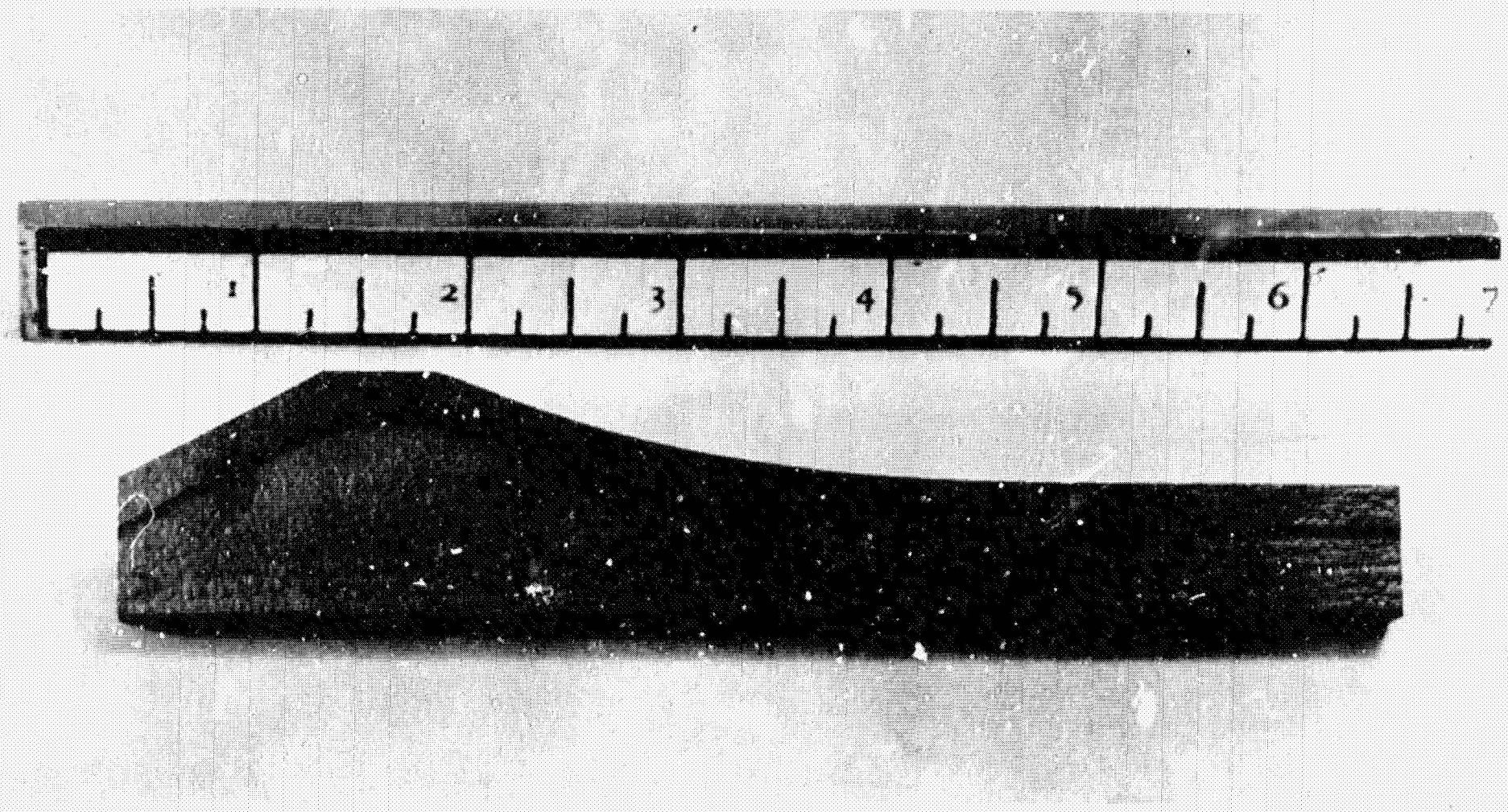

Figure 53

18-278

WEDGE ASSEMBLY FOR MACHINING ENDS AND CHAMFERS

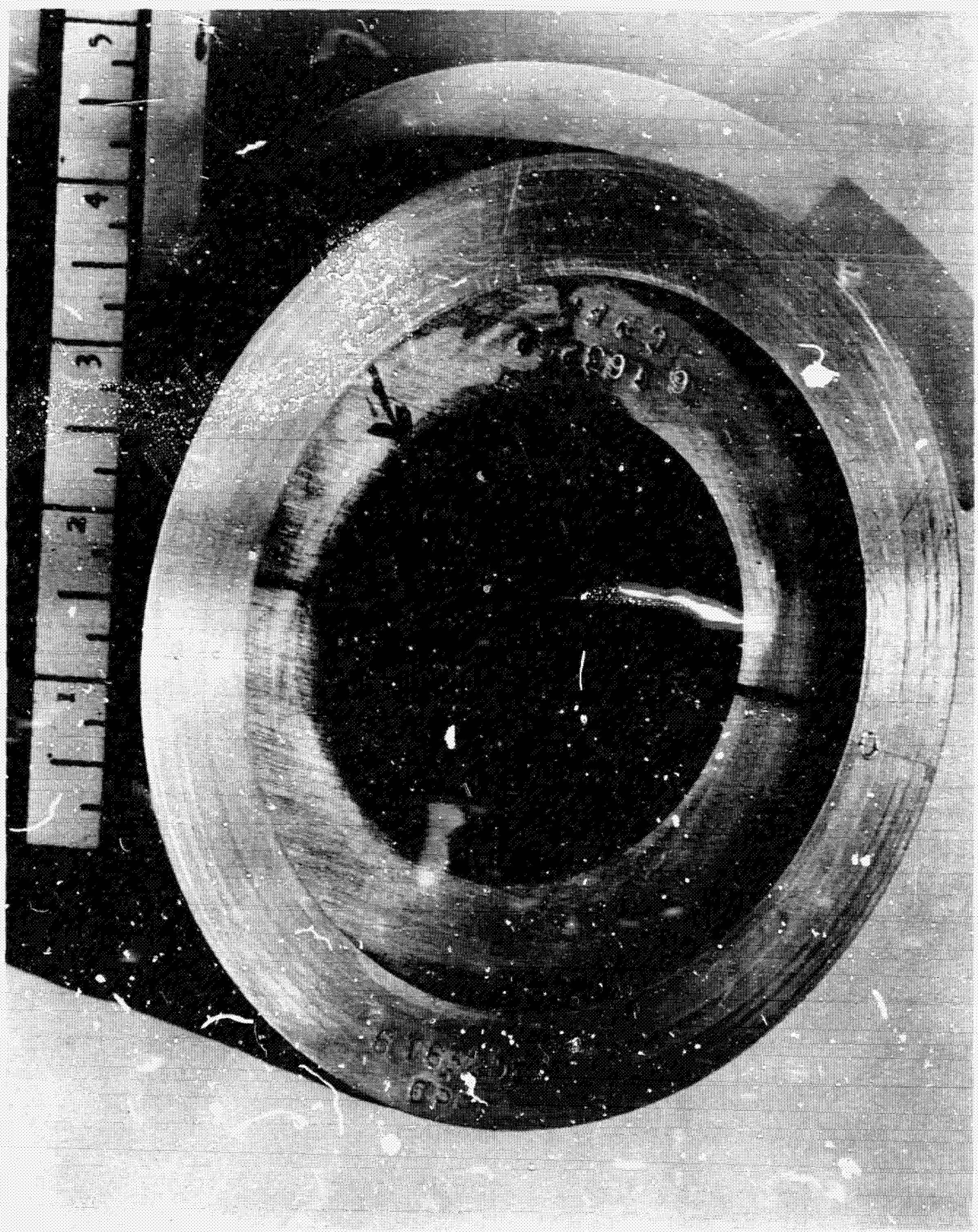

18-277

Figure 54

INJECTOR CALIBRATION USING NORMAL HEPTANE

Sixteen Port Swirl Cup Injector (ES156903N-1)

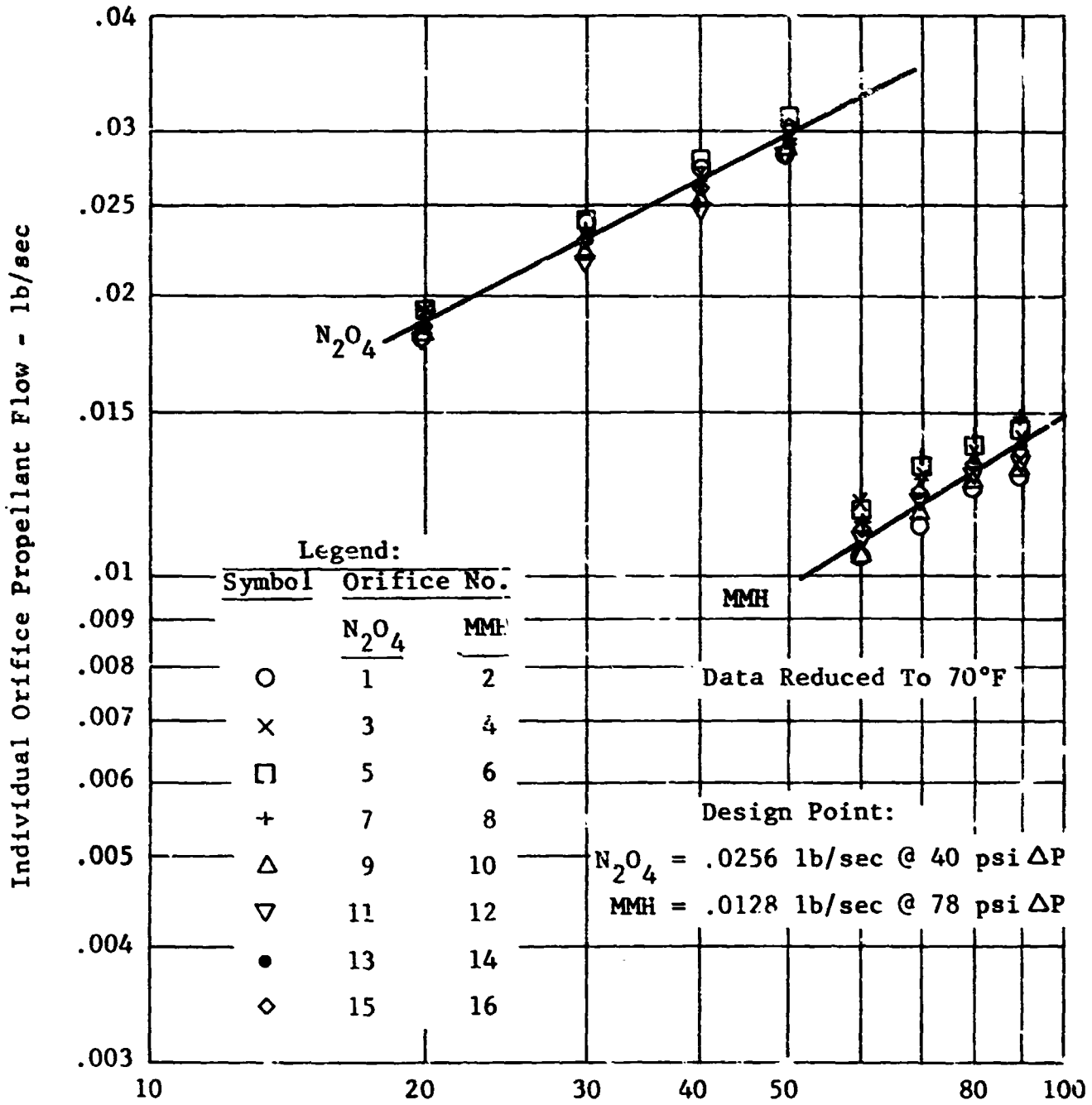

Injector Orifice Pressure Drop - psi

Figure 55

INJECTOR CALIBRATION USING NORMAL HEPTANE

Sixteen Port Swirlcup Injector (ES1[illegible]6903N-2)

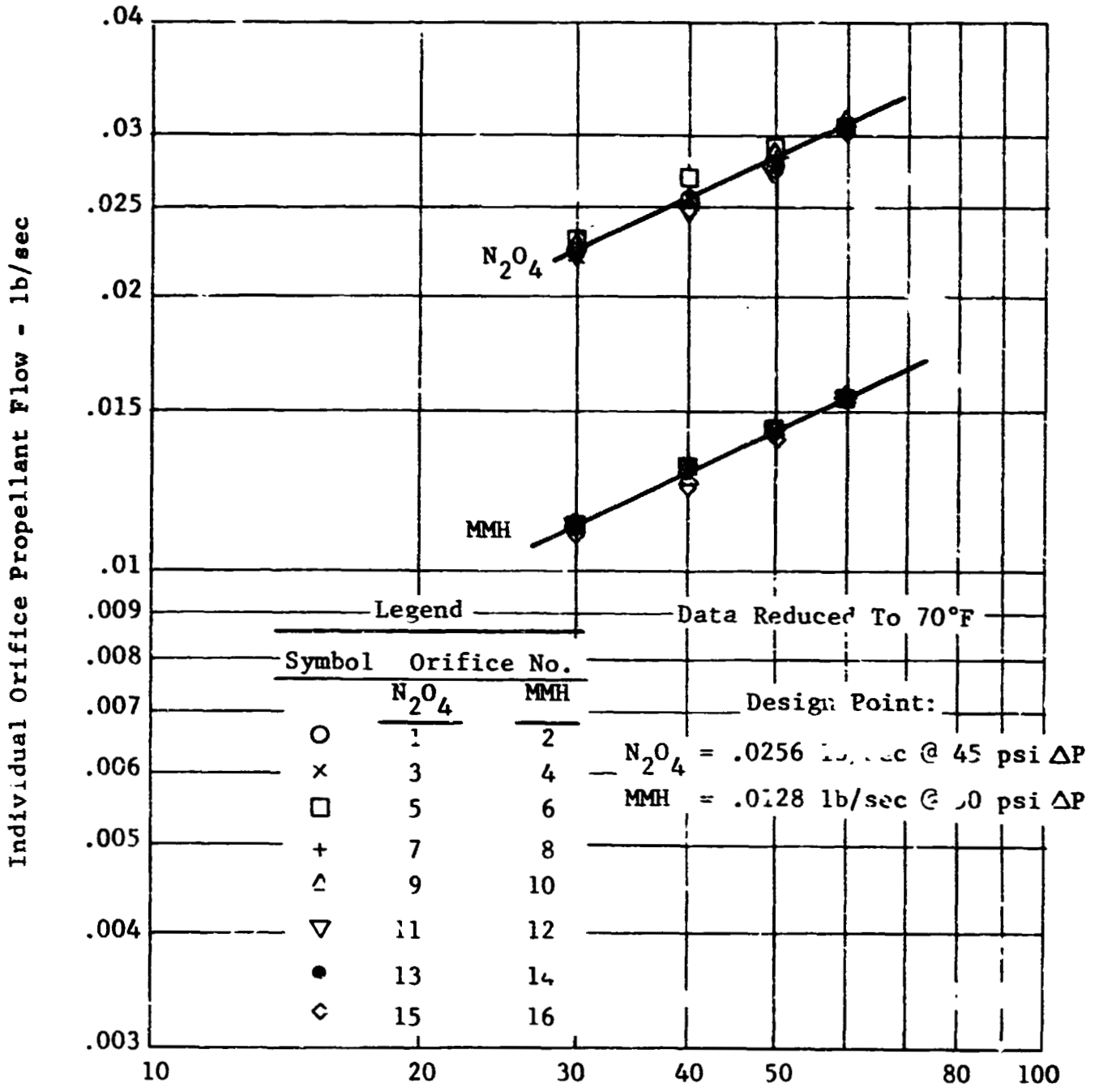

18-807

Figure 56

Test No. 23-1

Test Date 1/10/66

Duration 65 Seconds

	8 Seconds	60 Seconds
N_2O_2 System		
Tank Pressure-psig	318.3	316.0
Engine Feed Pressure-psig	194.2	193.5
Flow-lbs/sec.	0.2130	0.2096
MMH System		
Tank Pressure-psig	271.9	269.5
Engine Feed Pressure-psig	200	198.6
Flow-lbs/sec.	0.1049	0.1033
MMH Spray Cooling System		
Tank Pressure-psig	618.4	619.8
* Orifice Upstream Pressure-psig	613.8	614.6
* Orifice Downstream Pressure-psig	149.0	155.0
Flow-lbs/sec.	.0261	.0260
Swirl Cup Pressure-psia	111.0	111.3
Combustion Chamber Pressure-psia	105.4	105.7
Swirl Cup Pressure Ratio-P_{sc}/P_c	1.042	1.052
Total Propellant Weight Flow-lbs/sec.	0.3440	0.3389
Oxidizer/Fuel Ratio	1.622	1.618
C*	5390	5480
C* η %	94.6	96.4

* Calibrated fuel spray line orifice.

Table I

Test No. 23-2

Test Date 1/11/66

Duration 32 Seconds

	10 Seconds	27 Seconds
N_2O_4 System		
Tank Pressure-psig	308.2	308.2
Engine Feed Pressure-psig	186.9	183.1
Flow-lbs/sec	0.2120	0.2098
MMH System		
Tank Pressure-psig	266.0	265.2
Engine Feed Pressure-psig	194.1	192.6
Flow-lbs/sec	.1054	.1054
Swirl Cup Pressure-psia	103.2	102.3
Combustion Chamber Pressure-psia	97.8	96.9
Swirl Cup Pressure Ratio - P_{sc}/P_c	1.06	1.06
Total Propellant Weight Flow-lbs/sec	.3174	.3152
Oxidizer/Fuel ratio	2.011	1.991
C*	5401	5389
C* η %	95.0	94.6

Table II

Table

WLR-23 WEDGE LAND HOOP STRESS
.010 In. Interference Fit
Inner Land Stress/Outer Land Stress
(Minus = Compression Plus = Tension)

SECTION	0 Sec.	50 Sec.	100 Sec.	400 Sec.	500 Sec.	600 Sec. (Soak)
A	-6440/-5790	-12360/-12430	-9750/-13710	-9750/-11270	-9120/-10750	-8630/-10320
B	-6460/-5810	-12440/-12590	-13390/-13960	-10510/-12090	-9840/-11540	-8660/-10380
C	-6390/-5750	-13815/-14060	-15000/-15640	-11900/-13500	-11260/-12970	-9040/-10730
D	-6440/-5740	-14880/-15240	-15980/-16760	-12830/-14620	-12200/-14110	-8990/-10870
E	-7200/-6210	-14600/-15160	-15190/-16360	-10670/-13300	-9870/-12660	-6600/-9340
F	-10030/-8050	-13060/-14150	-11460/-13830	-1830/-7240	-480/-6240	+1740/-3860
G	-6340/-5530	-13250/-13580	-14450/-15310	-11860/-13920	-11290/-13490	-9270/-11420

All Values are in psi.

Table IV

WLR-23 WEDGE LAND HOOP STRESS
.011 In. Interference Fit
Inner Land Stress/Outer Land Stress
(Minus = Compression Plus = Tension)

SECTION	0 Sec.	50 Sec.	100 Sec.	400 Sec.	500 Sec.	600 Sec. (Soak)
A	-7120/-6410	-13000/-13010	-13830/-14250	-10270/-11740	-9630/-11210	-9130/-10770
B	-7140/-6430	-13080/-13170	-14000/-14500	-11020/-12550	-10350/-11990	-9170/-10830
C	-7060/-6350	-14440/-14620	-15580/-16160	-12400/-13950	-11750/-13410	-9530/-11180
D	-7130/-6350	-15500/-15790	-16560/-17270	-13320/-15060	-12690/-14540	-9490/-11?10
E	-7970/-6870	-15310/-15770	-15860/-16730	-11240/-13780	-10420/-13130	-7170/-9830
F	-11110/-8920	-14080/-14960	-12420/-14590	-2640/-7890	-1280/-6870	+930/-450)
G	-7010/-6110	-13880/-14130	-15050/-15820	-12350/-13920	-11780/-13920	-9760/-11850

All Values are in psi.

Table V

WLR-23 WEDGE LAND HOOP STRESS
.012 In. Interference Fit
Inner Land Stress/Outer Land Stress
(Minus = Compression Plus = Tension)

SECTION	0 Sec.	50 Sec.	100 Sec.	400 Sec.	500 Sec.	600 Sec. (Soak)
A	-7810/-7020	-13640/-13580	-14430/-14790	-10740/-12200	-10130/-11660	-9640/-11230
B	-7830/-7040	-13730/-13740	-14600/-15040	-11540/-13015	-10850/-12450	-9670/-11280
C	-7740/-6960	-15060/-15170	-16160/-16610	-12900/-14390	-12230/-13850	-10030/-11620
D	-7810/-6950	-16120/-16240	-17140/-17790	-13810/-15500	-13170/-14970	-9990/-11760
E	-7840/-7520	-16030/-16380	-16520/-17500	-11800/14270	-10970/-13600	-7750/-10320
F	-12195/-9780	-15090/-15760	-13370/-15350	-3450/-8540	-2080/-7510	+115/-5150
G	-7680/-6690	-14510/-14680	-15640/-16340	-12850/-14790	-12270/-14340	-10250/-12270

All Values are in psi.

Table VI

WLR-23 COMBINED TENSILE BENDING STRESSES
AT WEDGE OUTER LAND SURFACE
.010 In. Interference Fit

SECTION	0 Sec.	50 Sec.	100 Sec.	400 Sec.	500 Sec.	600 Sec. (Soak)
A	5810 psi	12595 psi	13840 psi	11210 psi	10675 psi	10200 psi
B	5850	12900	14220	11970	11390	10135
C	5950	13730	15080	12500	11910	9900
D	5880	14380	15810	13475	12920	10380
E	5830	14650	16150	13890	13360	10570
F	7205	14110	14420	9440	8630	6410
G	5110	13560	15605	15020	14685	12695

Table VII

WLR-23 COMBINED TENSILE BENDING STRESSES
AT WEDGE OUTER LAND SURFACE
.011 In. Interference Fit

SECTION	0 Sec.	50 Sec.	100 Sec.	400 Sec.	500 Sec.	600 Sec. (Soak)
A	6430 psi	13170 psi	14385 psi	11680 psi	11140 psi	10650 psi
B	6475	13490	14770	12430	11850	10590
C	6570	14320	15630	12970	12370	10370
D	6510	14950	16340	13930	13370	10840
E	6450	15220	16680	14340	13800	11020
F	7980	14835	15100	10020	9190	6975
G	5640	14070	16085	13425	15080	13090

WLR-23 COMBINED TENSILE BENDING STRESSES
AT WEDGE OUTER LAND SURFACE
.012 In. Interference Fit

SECTION	0 Sec.	50 Sec.	100 Sec.	400 Sec.	500 Sec.	600 Sec. (Soak)
A	7045 psi	13740 psi	14925 psi	12135 psi	11590 psi	11125 psi
B	7090	14060	15310	12905	12310	11050
C	7200	14900	16180	14440	12835	10840
D	7120	15520	16880	14390	13820	11290
E	7060	15790	17220	14800	14240	11470
F	8750	15550	15780	10595	9760	7550
G	6175	14575	16555	15015	15465	13470

Table IX

WLR-23
WATCHBAND STRESSES
$t_{W.B.}$ = .265 In.; Material: WAD 7816 (Rene' 41)

Time Sec.	W.B. Temp.	Allow. Y.S.	R_i = .010 In. Throat	Chamber	R_i = .011 In. Throat	Chamber	R_i = .012 In. Throat	Chamber
Installation	60°F	120,000 psi	56,400 psi	47,900 psi	62,900 psi	52,600 psi	67,800 psi	57,300 psi
50	125°F	120,000	94,600	84,700	100,000	87,000	102,500	89,500
100	410°F	120,000	93,600	90,300	98,600	92,400	101,000	94,800
200	880°F	120,000						
300	1180°F	120,000						
400	1350°F	110,000	59,400	75,300	63,500	77,500	65,800	79,200
500	1450°F	100,000	54,400	71,100	57,500	72,800	60,700	75,000
600 (Soak)	1500°F	95,000	36,300	61,400	39,700	63,100	42,700	65,300

WLR-23 THEORETICAL WATCHBAND RADIAL DEFLECTION HISTORY
MEASURED FROM INSTALLED POSITION
0.010 In. Interference Fit

SECTION	INSTALLED STRETCH	0 Sec.	50 Sec.	100 Sec.	400 Sec.	500 Sec.	600 Sec. (Soak)
A	+.00623	0	+.00241	+.00739	+.0211	+.0228	+.0234
B	+.00622	0	+.00304	+.00817	+.0224	+.0241	+.0237
C	+.00626	0	+.00402	+.00928	+.0236	+.0253	+.0237
D	+.00658	0	+.00462	+.00970	+.0233	+.0250	+.0226
E	+.00704	0	+.00445	+.00918	+.0218	+.0233	+.0209
F	+.00724	0	+.00401	+.00855	+.0206	+.0221	+.0201
G	+.00706	0	+.00356	+.00810	+.0202	+.0216	+.0200

All Values are in Inches

WLR-23 THEORETICAL WATCHBAND RADIAL DEFLFCTION HISTORY
MEASURED FROM INSTALLED POSITION
0.011 In. Interference Fit

SECTION	INSTALLED STRETCH	0 Sec.	50 Sec.	100 Sec.	400 Sec.	500 Sec.	600 Sec. (Soak)
A	+.00680	0	+.00195	+.00693	+.0207	+.0223	+.0229
B	+.00679	0	+.00255	+.00770	+.0220	+.0236	+.0232
C	+.00684	0	+.00356	+.00880	+.0231	+.0248	+.0232
D	+.00719	0	+.00411	+.00925	+.0229	+.0245	+.0222
E	+.00770	0	+.00406	+.00879	+.0214	+.0229	+.0206
F	+.00793	0	+.00365	+.00818	+.0203	+.0217	+.0198
G	+.00784	0	+.00321	+.00773	+.0199	+.0213	+.0197

All Values are in Inches

Table XII

WLR-23 THEORETICAL WATCHBAND RADIAL DEFLECTION HISTOR
MEASURED FROM INSTALLED POSITION
0.012 In. Interference Fit

SECTION	INSTALLED STRETCH	0 Sec.	50 Sec.	100 Sec.	400 Sec.	500 Sec.	600 Sec. (Soak)
A	+.00738	0	+.00149	+.00646	+.0202	+.0219	+.022[illegible]
B	+.00736	0	+.00211	+.00723	+.0215	+.0232	+.0228
C	+.00741	0	+.00309	+.00833	+.0226	+.0244	+.0228
D	+.00780	0	+.00375	+.00881	+.0225	+.0241	+.0218
E	+.00837	0	+.00367	+.00839	+.0210	+.0225	+.0202
F	+.00862	0	+.00328	+.00781	+.0199	+.0213	+.0194
G	+.00851	0	+.00284	+.00736	+.0195	+.0209	+.0194

All Values are in Inches

Table XIII

WLR-23 COMBINED TENSILE BENDING STRESSES
AT WEDGE OUTER LAND SURFACE
WITH REVISED WATCHBAND
.025 IN. INTERFERNCE FIT

Section	0 Sec.	50 Sec.	100 Sec.	500 Sec.	500 Sec. (Soak)
A	8990 psi	13390 psi	13963 psi	11052 psi	10680 psi
B	9070	13500	14075	11365	10560
C	9270	13710	14260	11285	10240
D	8870	13960	14730	12370	11100
E	8330	14400	15500	13780	12100
F	10180	14200	14135	9885	8715
G	7160	13830	15583	15640	14225

Table XIV

WLR-23 WEDGE LAND HOOP STRESS
WITH REVISED WATCHBAND
.025 IN. INTERFERENCE FIT
INNER LAND STRESS/OUTER LAND STRESS
(MINUS = COMPRESSION PLUS = TENSION)

Section	0 Sec.	50 Sec.	100 Sec.	500 Sec.	600 Sec. (Soak)
A	-9950/-8940	-13190/-13180	-13310/-13790	-9550/-11140	-9180/-10820
B	-9980/-8970	-12990/-13080	-13140/-13730	-9840/-11540	-9180/-10840
C	-9820/-8820	-13920/-14150	-14180/-15030	-10900/-12650	-9570/-11210
D	-9700/-8630	-14720/-15100	-15130/-16000	-11930/-13870	-9850/-11630
E	-10500/-9110	-14490/-15060	-14450/-15730	-10140/-12890	-8125/-10650
F	-14620/-11720	-13230/-14280	-10860/-13350	-1510/-7055	-810/-5885
G	-9110/-7930	-13570/-13870	-14320/-15190	-12135/-14225	-10870/-12810

All values are in psi.

WIR-23 THEORETICAL WATCHBAND RADIAL DEFLECTION HISTORY
MEASURED FROM INSTALLED POSITION
WITH REVISED WATCHBAND
.025 IN. INTERFERENCE FIT

Section	Installed Stretch	0 Sec.	50 Sec.	100 Sec.	500 Sec.	600 Sec. (Soak)
A	.01905	0	.00182	.00733	.0224	.0229
B	.01903	0	.00265	.00837	.0241	.0232
C	.01912	0	.00395	.00983	.0256	.0232
D	.01973	0	.00474	.0103	.0252	.0219
E	.02056	0	.00451	.00962	.0231	.0200
F	.02093	0	.00395	.00877	.0216	.0190
G	.02083	0	.00338	.00819	.0210	.0190

All values are in inches.

WLR-23 THEORETICAL THROAT AREA HISTORY
WITH REVISED WATCHBAND
.025 IN. INTERFERENCE FIT

Table XVI

Time - Sec.	Throat Diameter In.	Throat Area In.^{2}	Area Change %
Installation	.8340	.5463	-
50	.8457	.5617	2.82
100	.8514	.5693	4.21
500	.8659	.5889	7.80
600	.8621	.5837	6.85

WLR23 RIG ENGINE S/N 1 - BUILD 1

Wedge Sample Flexure Test Results

Sample No.	Flexure Strength
1	26,300 psi
2	24,000 psi
3	25,400 psi
4	26,900 psi
5	26,400 psi
6	23,400 psi
7	26,100 psi
8	27,700 psi
9	26,300 psi
10	24,700 psi
11	24,200 psi
12	23,200 psi
13	23,600 psi
14	24,600 psi
15	24,900 psi
16	26,100 psi
17	25,700 psi
18	25,900 psi

Table XVII

Table XVIII

ESTIMATED PRESSURE SCHEDULE

FOR HIGH PRESSURE DROP INJECTOR

Chamber Pressure 100 psia

Swirl Cup Pressure 105 psia

	Oxidizer	Fuel
- Injector Orifice	40 psi	80 psi
- Injector Manifold	5	5
- Moog Valve	35	35
Total	80	120

Feed Pressure 185 psia 225 psia